The Interaction of Water and Hydrogen with Nickel Surfaces

The Interaction of Water and Hydrogen with Nickel Surfaces

PROEFSCHRIFT

Ter verkrijging van
de graad van Doctor aan de Universiteit Leiden,
op gezag van de Rector Magnificus Prof. Mr. P.F. Van der Heijden
hoogleraar in de faculteit der Rechtsgeleerdheid,
volgens besluit van het College voor Promoties
te verdedigen op woensdag 11 November 2009
klokke 15.00 uur

door

Junjun Shan
Geboren te Zhejiang, China,
in 1979

Promotiecommissie

Promotor:	Prof. Dr. A. W. Kleyn
Co-promotor:	Dr. L. B. F. Juurlink
Overige leden:	Prof. Dr. J. W. Niemantsverdriet
	Prof. Dr. A. Hodgson
	Prof. Dr. P. Rudolf
	Prof. Dr. M. T. M. Koper
	Prof. Dr. B. E. Nieuwenhuys
	Prof. Dr. J. Brouwer

ISBN: 978-90-8570-417-1

Printed by Wöhrmann Print Service, The Netherlands

Contents

Chapter 1

Introduction

1.1 Water on surfaces

Water is life! It is a precondition for the survival of all known forms of life as well as an indispensable resource for the vast majority of industries and the global economy. It can appear in three states: the liquid state, the solid state (also called ice), and gaseous state (also called water vapor). As a chemical substance, water has a rather simple molecular structure. A single water molecule consists of two hydrogen atoms covalently bonded to an oxygen atom with a chemical formula of H_2O. The angle between the two O-H bonds is 104.45º with a distance of 0.9584 Å between the oxygen and hydrogen atoms. The oxygen atom has a slightly negative charge while the two hydrogen atoms have a slightly positive charge, which makes the water molecule a polar molecule. The different dipoles of each molecule yield an attractive interaction, which makes water molecules mutually attractive.

The hydrogen bond between water molecules is also an important factor that causes them to stick one another. The hydrogen bond is a bond between one electronegative atom and a hydrogen atom covalently bonded to another electronegative atom. A single water molecule has two hydrogen atoms covalently bonded to an oxygen atom (the electronegative atom). Therefore two water molecules can form a hydrogen bond between them. When more molecules are present, more hydrogen bonds are possible. This is because one oxygen atom of a single water molecule has two lone pairs of electrons, each of which can form a hydrogen bond with hydrogen atoms on two other water molecules. This can repeat so that each water molecule is H-bonded with up to four other molecules.

In physics and chemistry, the fundamental understanding of the properties of water has attracted considerable attention. Due to its relevance to industry, scientists in many physical or chemical fields often investigate basic questions concerning the interaction of water with solid surfaces. However, despite extensive studies of water on solid surfaces, our

understanding of how water adsorbs on a solid surface, how water desorbs, and how coadsorbates influence water adsorption or desorption still remains limited [1,2].

Depending on the precise physical circumstances, two types of adsorbed water ice exist, amorphous solid water and crystalline ice. Both types are present in nature [3]. Amorphous solid water can be obtained by vapor deposition at a substrate temperature below ~ 130 K under ultra-high vacuum (UHV) conditions [4]. Crystalline ice can be formed by direct vapor deposition above ~130 K or by crystallization of amorphous solid water [5,6]. Investigations of both types formed under UHV conditions contribute to the understanding of the properties of amorphous solid water and crystalline ice in nature.

Many investigations of water adsorbed on solid surfaces are carried out in UHV conditions. In these studies, a single metal crystal is often applied as the substrate. In his recent review, Henderson concluded that these studies generally focus on five broad categories; the electronic structure of adsorbed water, the vibrational properties, the tendency to form local or long-range order, the dynamical properties, and the water-water and water-surface interactions [2]. Research described in this thesis, falls under three of these categories. There are the vibrational properties, the tendency to form local or long-range order, and the water-water and the water-surface interactions.

1.2 Hydrogen on surfaces

Hydrogen is the most abundant chemical element in the universe, constituting roughly 75% of the normal mass. Hydrogen gas is highly flammable and it burns according to the following reaction equation: $2\ H_2(g) + O_2(g) \rightarrow 2\ H_2O(l) + 572$ kJ (286 kJ/mol). Since the only reaction product is water, hydrogen is considered as a clean energy carrier for the future, especially for mobile applications.

Significant challenges for the use of hydrogen in mobile applications are on-board storage or production of hydrogen. There are many ways to store hydrogen, for example as liquid hydrogen [7]. The method of using metal hydrides is one of the most exciting potential solutions for on-board hydrogen storage. While many metal hydrides can be formed by interaction of hydrogen with pure metals, only few may be applicable for

reasons such as the required storage capacity and weight. Thus, studies of metal-hydrogen system are crucial in hydrogen storage research.

Hydrogenation reactions play a very important role in modern industrial processes. Since hydrogenation reactions are catalyzed by metal surfaces, understanding how hydrogen interacts with metals is essential. Also for some metal catalysts, for example Raney Nickel, it is not clear that why they are such good hydrogenation catalysts.

When hydrogen is situated far from a metal surface, the H_2 molecule is considered to be in the gas phase, and there is no interaction between hydrogen and the metal surface. When the hydrogen molecule approaches the metal surface, the molecule can bounce back into the gas phase; or dissociate and a**d**sorb as atomic hydrogen on the metal surface. Dissociation and adsorption on metal surfaces has been studied using theoretical and experimental methods [see e.g. 8-10]. Hydrogen atoms can also be present in the bulk of many metals and diffuse in between interstitial sites. Hydrogen a**b**sorption and diffusion is also a well-studied topic, for example due to its importance in hydrogen embitterment [11-13].

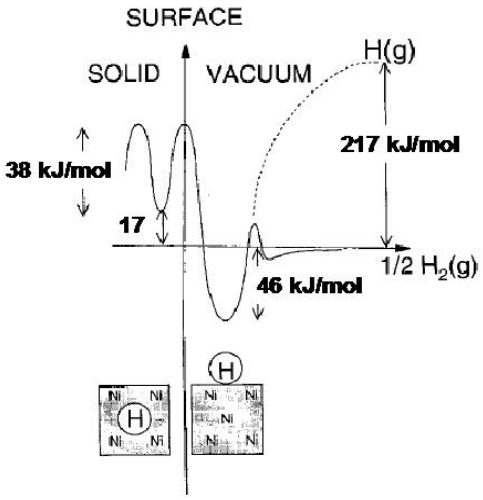

Figure 1.1 Potential energy diagram for the hydrogen-Ni(111) system. Left part of the surface represents a H atom beneath the surface. Right part of the surface represents a H atom or a H_2 molecule at or away from the surface. The figure is adopted from Ref 14.

In this thesis, we will focus on the interaction of hydrogen with the nickel surface. The potential energy diagram for the hydrogen-Ni(111) system is shown in figure 1.1. As can be seen in this diagram, a gas-phase H_2 molecule can dissociate and a**d**sorb on the nickel surface. The diagram also shows a large energy barrier, ~101kJ/mol, to continue from surface sites to subsurface sites. This large energy barrier does not allow H_2 molecules to dissociatively a**b**sorb into subsurface sites under vacuum conditions. However, as shown in figure 1.1, the initial energy level of atomic hydrogen is high enough to overcome the energy barrier to subsurface a**b**sorption. Experiments performed by Ceyer and co-workers show that subsurface hydrogen can be created under UHV conditions by impinging atomic hydrogen onto Ni(111) [14,15]. Interestingly, subsurface hydrogen has been reported to be extremely active in the hydrogenation of simple hydrocarbons [14,16].

1.3 Nickel metal surface

Nickel is a silvery-white metal with atomic number 28. It is hard, ductile, and corrosion-resistant. Nickel belongs to the transition metals and is widely used in many industrial and consumer products, such as magnets, special alloys, and stainless steel. In the laboratory or industrial catalysis, nickel based catalysts are frequently used in hydrogenation reactions.

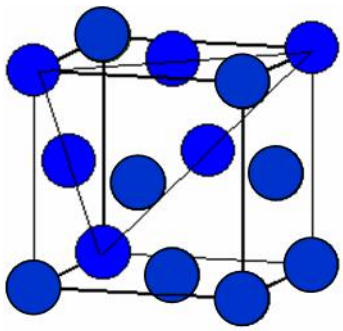

Figure 1.2 The fcc unit cell of nickel.

Nickel has a face-centered cubic (fcc) unit cell, as shown in figure 1.2. The lattice constant of the unit cell is 3.52 Å. In the laboratory, nickel single crystals, such as Ni(111), Ni(110), and Ni(100) are often used to mimic real catalyst surfaces. The most stable nickel

single crystal is Ni(111). Figure 1.3 shows the conventional birds-eye view of the Ni(111) surface. The blue circles are the first layer of nickel atoms, while the green circles represent second layer atoms. The common adsorption sites are top sites, bridge sites, and three-fold hollow sites. It is worth to note that there are two types of the three-fold hollow sites, fcc hollow sites and hcp hollows sites. The difference between these two types is that below fcc hollow site there is no second layer nickel atom, while there is a second layer nickel atom below a hcp site. In figure 1.3, sites marked with 1 are fcc hollow sites, whereas sites marked with 2 are hcp hollow sites. The octahedral subsurface sites are located just beneath the fcc hollow sites. Beneath the hcp hollow sites, the hollows are tetrahedral subsurface sites.

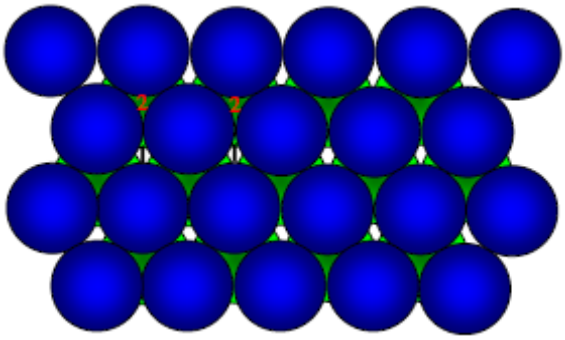

Figure 1.3 Schematic of Ni(111) .

1.4 Structure of this thesis

This thesis *"The interaction of water and hydrogen with nickel surfaces"* investigates two main areas of interest. First, the interaction of water with the bare Ni(111) surface is investigated as well as its co-adsorption behavior with hydrogen and oxygen. Second, we investigate formation and decomposition of nickel hydride (NiH_x) as an extremely thin layer formed on a Ni(111) surface.

The understanding of the interaction of water with the nickel surface is quite important for industry, due to the wide application of nickel as electrode material. However such interactions as well as co-adsorption behaviors of water with hydrogen or oxygen on nickel surfaces remain poorly understand. On the other hand, nickel hydride has found widespread

application in hydrogenation processes as Raney nickel and also as a hydrogen storage material in batteries. However, at the atomic level, the formation of nickel hydride from the pure metal and hydrogen is poorly understood. In this thesis we investigate these two areas and describe our results in following chapters.

This thesis is structured as follows: Chapter 2 describes the UHV apparatus and provides some background on the analysis techniques employed including temperature-programmed desorption, high resolution electron energy loss spectroscopy, and Auger electron spectroscopy. The first main area of interest, the interaction of water with the bare Ni(111) surface as well as its co-adsorption behaviour with hydrogen and oxygen, encompasses chapters 3, 4 and 5. Chapter 3 discusses the interaction of H_2O and D_2O with a bare and hydrogen-saturated Ni(111) surface. Surface-coverage dependencies for co-adsorption are explored in Chapter 4 and in chapter 5 we identify and characterize hydroxyl (OH) on the Ni(111) surface. The second main area of interest, formation and decomposition of nickel hydride (NiH_x) on a Ni(111) surface, encompasses chapters 6 and 7. In Chapter 6 we show that molecular hydrogen may bind to a thin film of nickel hydride prepared by impact of atomic hydrogen on the Ni(111) surface. Chapter 7 explores formation and decomposition of the film using isotopic labeling experiments. Here, we show that large isotope effects result from combined abstraction and collision-induced absorption processes when atomic H and D atoms impact on the surface.

1.5 References

[1] P. A. Thiel, and T. E. Madey, *Surf. Sci. Rep.,* 1987, **7**, 211.

[2] M. A. Henderson, *Surf. Sci. Rep.,* 2002, **46**, 5.

[3] P. Ehrenfreund, H. J. Fraser, J. Blum, J. H. E. Cartwright, J. M. Garcia-Ruiz, E. Hadamcik, A. C. Levasseur-Regourd, S. Price, F. Prodi, and A. Sarkissian, *Planet. Space Sci.,* 2003, **51**, 473.

[4] K. P. Stevenson, G. A. Kimmel, Z. Dohnálek, R. S. Smith, and B. D. Kay, *Science,* 1999, **283**, 1505.

[5] D. Chakarov, and B. Kasemo, *Phys. Rev. Lett.,* 1998, **81**, 5181.

[6] E. H. G. Backus, M. L. Grecea, A. W. Kleyn, and M. Bonn, *Phys. Rev. Lett.,* 2004, **92**, 236101.

[7] L. Schlapbach, and A. Züttel, *Nature*, 2001,**414**, 353.

[8] P. Nieto, E. Pijper, D. Barredo, G. Laurent, R. A. Olsen, E. J. Baerends, G. J. Kroes, and D. Farias, *Science*, 2006, **312**, 86.

[9] J. Q. Dai, J. Sheng, and J. Z. H. Zhang, *J. Chem. Phys.,* 1994, **101**, 1555.

[10] I. M. N. Groot, H. Ueta, M. J. T. C. Van der Niet, A. W. Kleyn, and L. B. F. Juurlink, *J. Chem. Phys.,* 2007, **127**, 244701.

[11] G. Alefeld, and J. Völkl, *Hydrogen in Metals 7-Application-Oriented Properties*, 1978, Springer-Verlag, Berlin.

[12] M. V. C. Sastri, B. Viswanathan, and S. S. Murthy, *Metal Hydrides-Fundamentals and Applications*, 1998, Narosa Publishing House, New Delhi.

[13] Y. Fukai, The metal-hydrogen system, 1993, Springer-Verlag, Berlin.

[14] S. T. Ceyer, *Acc. Chem. Res.,* 2001, **34**, 737.

[15] A. D. Johnson, K. J. Maynard, S. P. Daley, Q. Y. Yang, and S. T. Ceyer, *Phys. Rev. Lett.,* 1991, 67, 927.

[16] A. D. Johnson, S. P. Daley, A. L. Utz, and S. T. Ceyer, *Science,* 1992, **257**, 223.

Chapter 2

Experimental setup and techniques

2.1 Ultra-high vacuum system

The experiments described in this thesis are carried out in an ultra-high vacuum system. The system consists of two chambers, the top level and the lower level, separated by a gate valve. The top chamber contains a quadrupole mass spectrometer (Balzers QMS 422), an ion sputter gun, an atomic hydrogen source (tectra), a stainless steel gas doser, and a home-built capillary array doser [1]. The lower level contains an upgraded ELS22 high resolution electron energy loss spectrometer and an Auger Electron spectrometer ((Staib Instruments). A detailed description of the sample preparation and experimental procedures will be presented in subsequent chapters, hence only a brief description is given here.

The top level is also called the preparation chamber, which consists of a stainless steel cylinder with a length of 0.178 m and a diameter of 0.2 m, vertically mounted on top of the lower level. A base pressure of 3×10^{-11} mbar is achieved in this chamber by running a turbodrag pump ($230ls^{-1}$ for N_2). The turbodrag pump is backed by a rotary vane pump. The quadrupole mass spectrometer is used for analysis of the residual gas, as well as to perform temperature-programmed desorption experiments. The cleaning of the sample and the gas dosing is also performed in this chamber.

The lower level is also called the characterization chamber, which also consists of a stainless steel vessel with a nearly cylindrical shape. The length of the vessel is 0.55 m and the diameter is 0.57 m. A turbodrag pump ($230ls^{-1}$ for N_2) in combination with a rotary vane pump pumps the characterization chamber. The chamber is also equipped with a titanium sublimation pump, and an ion pump. These pumps keep the base pressure at approximately 2×10^{-10} mbar for the lower chamber with the gate valve closed. With the gate valve open, the base pressure drops to below 1×10^{-10} mbar.

The sample is mounted vertically on a manipulator allowing for sample movement. Translation along the axis of the two cylinder vessels is motorized, while translation in the

two perpendicular directions to the axis of the two cylinders can be performed manually over a range of 2.5 cm. A rotary feedthrough, pumped with a rotary vane pump, allows for a motorized rotation of 360 degree. A copper block is mounted on the manipulator, through which liquid nitrogen can be flowed. The single crystal Ni(111), cylindrical with a diameter of 10 mm and a thickness of 1 mm, is fixed to two molybdenum legs. These two legs with the sample are screwed onto the copper block. Heating is performed from the back of crystal by a tungsten filament in combination with a high voltage applied to the sample, allowing electron bombardment. The sample can be heated to 1200 K and cooled to 85 K. The crystal temperature is measured by a chromel-alumel thermocouple spot welded to the edge of the crystal.

2.2 Temperature-programmed desorption

Temperature-programmed desorption (TPD) belongs to the larger class of the thermal desorption techniques. If a metal sample is heated in a vacuum, the rate of gas evolution from the metal surface changes noticeably with temperature and, moreover, there may be several temperatures for which the evolution rate goes through a relative maximum. The rate of gas evolution increases with surface temperature, resulting in an instantaneous rise of the gas density. The rise of pressure of a certain mass or masses is detected by means of a mass analyzer. There are two approaches to thermal desorption techniques [2]. First in flash desorption, the increase in the temperature of the sample is such that the desorption rate is much higher than the rate at which gas is pumped out of the system. The data analysis is similar to that of desorption performed in a closed system with no pumping. Second, one can use a lower rate of temperature increase of the sample (between 15 seconds to several minutes). As the temperature rises, particular species are able to desorb from the surface of the sample to gas phase. Since the temperature increase is rather slow, the partial pressure due to desorption continues to increase. As the temperature increases still further the amount of species on the surface will reduce. Thus the relative pump rate increases, causing the pressure to drop again. This results in a peak in the pressure versus temperature plot. In contrast to flash desorption, the desorption of a particular binding state

results in a peak in the pressure-temperature curve rather than the rise to a plateau. Such technique is called the TPD technique.

Experimentally, TPD consists of applying a constant temperature ramp (typically in the rage of 0.5-6 Ks^{-1}) to the crystal and detecting the desorbing species in the gas phase as a function of surface temperature. The desorption temperature is related to the bond energy of bound species; a higher desorption temperature normally indicates the larger bonding energy of the adsorbate to the surface. In the case of a multilayer system, the bond energy of the first layer bonded to the substrate is generally larger than that experienced in between layers. For this reason, as described in Chapter 3, a multilayer peak usually occurs in the TPD spectrum at distinctly lower temperature than the (sub)monolayer peak. In addition, TPD measurement can also provide information about intermediate species and reaction products, in connection with a particular surface reactivity [3].

In this thesis, the TPD experiments were carried out using a quadrupole mass spectrometer together with a temperature controller (Eurotherm). The temperature controller can regulate the sample temperature by adjusting the current flowing through the filament behind the crystal. Typically, linear heating rates of 1 Ks-1 are used. With the QMS used here, 16 masses can be measured simultaneously in a mass range from 1 up to 511 atomic mass units (a.m.u.).

2.3 High resolution electron energy loss spectroscopy

In surface science, many techniques use electrons, as the probe. For example low energy electron diffraction (LEED), reflection high energy electron diffraction (RHEED), Auger electron spectroscopy (AES), and electron energy loss spectroscopy (EELS) are included in such techniques. Among these techniques, EELS employs the electrons both as the probe and the analyzed particles, which means that the electrons are used as a means of excitation, as well as the entities that carry information back from the surface. Using EELS, localized vibrational and rotational modes of adsorbed molecules can be studied as well as electronic transitions, with high resolution, which makes EELS an indispensable tool in surface science. The study of vibrations by electron energy loss is often called High Resolution

Electron Energy Loss Spectroscopy (HREELS) to differentiate it from the study of electronic transitions.

The primary energy of the electrons in HREELS is typically only between 4 and 100 eV, and the energy losses go up to a few hundred meV when only considering vibrational modes. Therefore, not only must the analyzer be capable of high-energy resolution, but also the incident beam must be highly monochromatic. Monochromators are used to obtain a narrow distribution of the electron energy. These electrons are thus within an energy window not broader than a few meV. Both hemispherical and cylindrical electrostatic electrons can be used as the monochromator. Monochromatic electrons are focused in a well defined direction onto the sample surface. The majority are elastically scattered, while, a small number of electrons will lose or gain a certain amount of energy in the interaction with the sample. Energy gain processes are very weak and can be neglected in most studies [4]. For the electrons scattered from the surface, there are two scattering mechanisms, impact scattering and dipole scattering.

In impact scattering, the electron is scattered by a local atomic potential. The electron bounces off the scatterer (adsorbate or surface phonon), experiencing a short range interaction and exchanging momentum. The momentum exchange is observed by a quasi-isotropic distribution of the scattered electrons. The scattering cross-section increases with increasing primary electron energy in impact scattering. In dipole scattering, the electron is scattered by the interaction of the electric field of the moving electron with the dipole field of the surface excitations. This is therefore a long range interaction. The momentum transfer in the dipole scattering is very small. Therefore the scattered electron pathway is very close to the specular direction. To be precise, dipole inelastically scattered electrons are distributed within a narrow lobe around the specular direction. In dipole scattering, the scattering cross-section decreases with increasing primary electron energy. It is evident that impact scattering and dipole scattering can be distinguished experimentally by the angular distribution of the inelastically scattered electrons around the specular direction. Strong peaking of the scattered intensity in this direction clearly indicates scattering in dipole fields. HREELS measurements are most often performed at or in the near vicinity of the

specular direction. These two different scattering mechanisms are shown in figure 2.1. The detailed description of the theory of HREELS can be found in Ref 4.

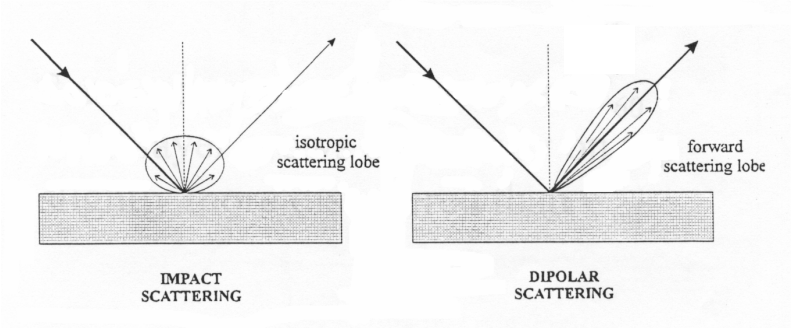

Figure 2.1 Impact scattering and dipole scattering.

A schematic drawing of the HREELS apparatus used in our studies is shown in Figure 2.2. The electron source (emission gun) and the two monochromators, pre-monochromator and main monochromator are on the right hand side. The scattering chamber is in the centre and the analyzer unit is on the left. The unit on the right side is rotatable, and the unit on the left side is fixed. The electrons are emitted from a filament and then selected and focused by the two monochromators thus allowing only electrons in a small energy range to reach the sample. Following interaction with the sample, the majority of the electrons enter the analyzer. After passing through the analyzer, electrons are directed towards the detector which is a channel electron multiplier. Data of the HREELS are acquired with the help of computer programs.

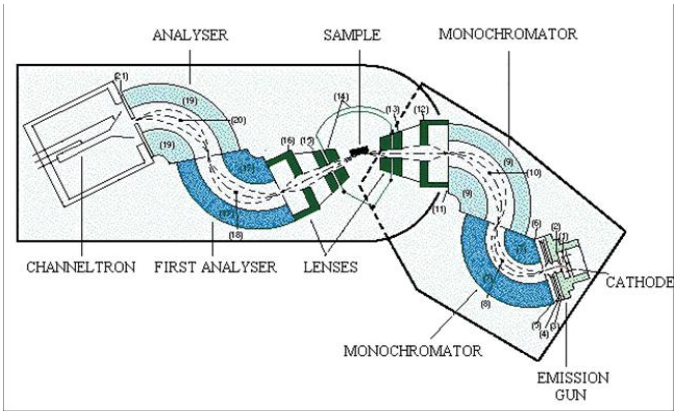

Figure 2.2 Schematic drawings of the HREELS apparatus, adopted from Ref 5.

2.4 Auger electron spectroscopy

Auger Electron Spectroscopy (AES) was developed in the late 1960's, and has become a popular technique for determining the composition of the top few layers of a surface. It cannot detect hydrogen or helium, but is sensitive to all other elements, being most sensitive to the low atomic number elements.

The theory of AES is based on the process of relaxation of the Auger electron, which is first discovered by Pierre Auger, a French physicist. In this process, electrons with energy of 3-20keV are incident upon a sample. These electrons cause core electrons from atoms contained in the sample to be ejected, which results in a photoelectron and an atom with a core hole. The atom then relaxes via electrons with a lower binding energy dropping into the core hole. The energy thus released can be converted into an X-ray or emit an electron. This electron is called an Auger electron. This scheme of this process is illustrated in Figure 2.3. After the emission of the Auger electron, the atom is left in a doubly ionized state. The energy of the Auger electron is characteristic of the element that emitted it. Thus in AES, measuring the energy of the Auger electron can identify the element in the sample.

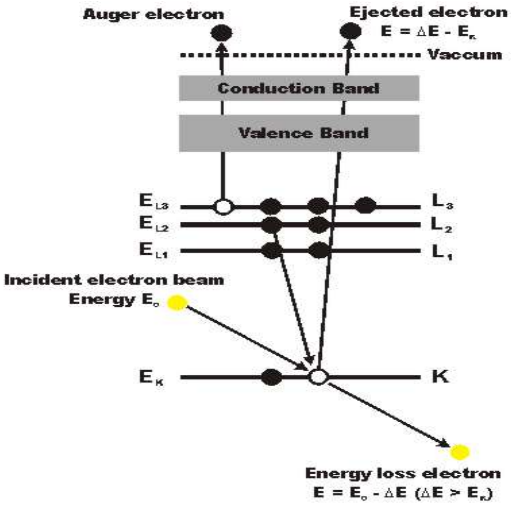

Figure 2.3 A scheme of the process of relaxation of the Auger electron.

Quantitative compositional and chemical analysis of a sample using AES is dependent on measuring the yield of Auger electrons during a probing event. Electron yield, in turn,

depends on several critical parameters such as electron-impact cross-section and fluorescence yield. Since the Auger effect is not the only mechanism available for atomic relaxation, there is a competition between radiative and non-radiative decay processes to be the primary de-excitation pathway. Generally, for heavier elements, x-ray yield becomes greater than Auger yield, indicating an increased difficulty in measuring the Auger peaks for large Z-values. Conversely, AES is sensitive to the lighter elements. For detailed descriptions of AES see Ref 6.

2.5 References

[1] C. T. Campbell, and S. M. Valone, *J. Vac. Sci. Technol. A*, 1985, **3**, 408.

[2] D. P. Woodruff, and T. A. Delchar, *Modern Techniques of Surface Science*, 2nd Edition, 1994, Cambridge University Press, Cambridge, 1994.

[3] J. W. Niemantsverdriet, *Spectroscopy in Catalysis*, 1003, Wiley, Wienheim.

[4] H. Ibach, and D. L. Mills, *Electron Energy Loss Spectroscopy and surface Vibrations*, Academic Press, New York, 1982.

[5] H. Ibach, M. Balden, D. Bruchmann, and S. Lehwald, *Surf. Sci.*, 1992, **269/270,** 94.

[6] M. Thompson, M. D. Baker, A. Christie, and J. F. Tyson, Auger Electron Spectroscopy, Chichester: John Wiley & Sons, 1985.

Chapter 3

The interaction of water with Ni(111) and H/Ni(111)

We have used temperature-programmed desorption in combination with specular and off-specular high resolution electron energy loss spectroscopy to study the interaction of H_2O and D_2O with bare and hydrogen-covered Ni(111) surface. Our results for the bare metal surface agree with previous reports and we are able to relate two prominent features in vibrational spectra to nuclear motions at the surface. Pre-covering Ni(111) with hydrogen alters both adsorption and desorption of water significantly. The strong H-Ni bond does not allow for isotopic exchange with co-adsorbed D_2O. Strong resemblance of desorption traces and vibrational spectra of submonolayer coverages on H-covered Ni(111) and multilayers on bare Ni(111) suggests that adsorption of hydrogen makes this nickel surface hydrophobic.

3.1 Introduction

The interaction of water with metal surfaces has attracted much attention in recent years [1]. This is not surprising considering the importance of water in many reactions such as corrosion, heterogeneous catalysis and electrochemistry. Despite the rather simple structure of water molecules, the understanding of the adsorbed water structure on many metal surfaces, as well as the bulk water structure, still remains limited [1,2].

Experimental studies of the interaction water with metal surfaces generally focus on close packed metal surfaces, e.g. Pd(111) [3,4], Pt(111) [5-11], Ru(0001) [12-14], and Ni(111) [15-17]. Recently, STM studies on Pd(111)[3] and helium-scattering investigations on Pt(111)[5] have shown that below 40 K, water initially adsorbs as isolated molecules (monomers). With increasing coverage and temperature, they form dimers, trimers, tetramers and so on. For the saturated monolayer, low-energy electron diffraction (LEED) studies show various structures on close-packed surfaces. On Pd(111) and Ru(0001), the $(\sqrt{3}\times\sqrt{3})R30^{o}$ structure has been observed [3,12], whereas on Pt(111) a $(\sqrt{39}\times\sqrt{39})R16^{o}$ structure develops [7-10]. Recently, Hodgson *et al.* observed a "labile" $(2\sqrt{7}\times2\sqrt{7})R19^{o}$ structure on Ni(111) that changed into the previously reported $(\sqrt{3}\times\sqrt{3})R30^{o}$ structure [15] due to impact of the electron beam. Formation of the incommensurate structure was related to the small lattice constant of Ni(111) in comparison to Pd(111), Pt(111) and Ru(0001).

Vibrational spectroscopy of water layers also yields information on water adsorption. Jacobi *et al.* recently performed a high-resolution electron energy loss (HREELS) study of water on Pt(111) and observed, with unprecedented resolution, the OH stretching vibration near 425 meV, H-O-H bending vibration near 200 meV, various librations between 50 and 100 meV, and frustrated translations below 50 meV [18]. High resolution studies employing IR spectroscopy can provide additional insight. For example, results of a recent study of water adsorption implied the presence of a ring hexamer structure over a wide coverage range on Ni(111) [17].

Desorption of water from, among others, Pt(111) and Ni(111) has been characterized in terms of (sub)monolayer desorption and multilayer desorption [11,15]**.** A temperature-programmed desorption (TPD) feature near 170 K saturates whereas a feature near 160 K does not saturate with increased exposure to water. In addition, the 160 K feature shows

zero-order desorption characteristics and is therefore believed to be due to the multilayer desorption. The feature at 170 K is attributed to (sub)monolayer desorption.

Besides studies of pure water adsorption, several studies have probed co-adsorption with other molecules and atoms. Considerable attention has focused on co-adsorption with oxygen on platinum, nickel and their alloys, since reactions at the cathode in low-temperature fuel cells are rate limiting [19,20]. A fuel cell is an electrochemical conversion device. It produces electricity by a chemical reaction. Every fuel cell has two electrodes, one positive and one negative, called, respectively, the anode and cathode. The reactions that produce electricity take place at the electrodes. On the other hand, co-adsorption with hydrogen has received much less attention and is currently poorly understood. Of the few co-adsorption studies with hydrogen, some claim formation of H_3O^+ (or hydrated forms of the hydronium ion) under UHV conditions on platinum surfaces [21]. A quick survey of the literature, however, indicates many inconsistencies. For example, for Pt(111) co-adsorption of hydrogen and water has been described to results in “strong changes” in TPD spectra[18] and was found to have “little if any effect”[21].

In the present study, we use TPD and HREELS to investigate the interaction of (sub)monolayer and multilayers of water with the bare and hydrogen-covered nickel surface. This co-adsorbed system is of particular interest due to the simultaneous presence of hydrogen and water in alkaline fuel cells that use nickel as its catalyst and electrode material. After presenting our data, we discuss our results and compare them to similar results found previously in UHV studies employing comparable nickel and platinum surfaces. Our analysis allows us to assign several features observed in HREEL spectra and suggests how hydrogen changes the chemical nature of Ni(111) with respect to water adsorption.

3.2 Experiment

Experiments are carried using an UHV system, which consists of two chambers. The upper level and the lower level are separated by a gate valve. The top chamber contains a quadrupole mass spectrometer (QMS) used for TPD measurements and residual gas analysis, an ion sputter gun, an atomic hydrogen source, a stainless steel gas doser, and a

home-built capillary array doser [22]. The lower chamber contains an upgraded ELS22 high resolution electron energy loss spectrometer and an Auger Electron spectrometer. The base pressure of the system is less than 1×10^{-10} mbar.

The Ni(111) single crystal, cut and polished to <0.1º of a low Miller-index plane (Surface Preparation Laboratories, Zaandam, the Netherlands), can be heated to 1200 K by electron bombardment and cooled to 85 K. The sample temperature is measured by a chromel-alumel thermocouple spot-welded to the edge of the crystal. The crystal is cleaned by Ar^+ sputtering, annealing at 1100 K, followed by oxidation in 10^{-7} mbar of O_2 and reduction in 10^{-6} mbar of H_2. Auger electron spectroscopy verifies surface cleanliness. H_2O (18.2 MΩ resistance) and D_2O (99.96% isotopic purity, Aldrich Chemical company) are cleaned by repeated freeze-pump-thaw cycles. Both are dosed through the capillary array doser. During dosing, the sample is placed 15 mm in front of the doser. Water coverages are estimated from integrated TPD traces. We have also determined the obtained hydrogen coverage as a function of dose using integrated TPD traces. All TPD measurements were performed with a heating rate of 1.0 K/s. The HREEL spectra were recorded at 5 to 9 meV resolution (FWHM) with typical 1×10^4 cps for the scattered elastic peak.

3.3 Results

3.3.1 H_2O and D_2O on bare Ni(111)

Figure 3.1 displays a set of TPD spectra of H_2O and D_2O on bare Ni(111) at various initial coverages. The sample temperature was kept at 85 K while dosing water through the capillary array doser. As observed previously [15,16,23,24], there are two distinct desorption features. At low coverage, spectra show a single feature at ~170 K. With increasing coverage, this feature reaches saturation, and a second feature appears at ~155 K. This low temperature feature does not saturate with increasing exposure and shows zero-order desorption kinetics at high coverages. For clarity, we only show lower coverages here. We have deconvoluted the TPD traces using two Gaussian profiles and observe that the feature at low temperature appears slightly before saturation of the feature at high temperature. For the water coverage, we define 1 ML as the integration of the deconvoluted, saturated high temperature feature. For example, the total desorption of 1

ML D_2O in figure 3.1 consists of 0.15 and 0.85 ML of the two individual features. We note that the similarity of H_2O and D_2O in the TPD spectra indicates no isotope effects in desorption. However, in agreement with previous study on Pt(111) [25], isotopic scrambling in TPD traces after dosing mixed layers of H_2O and D_2O are also observed in our study.

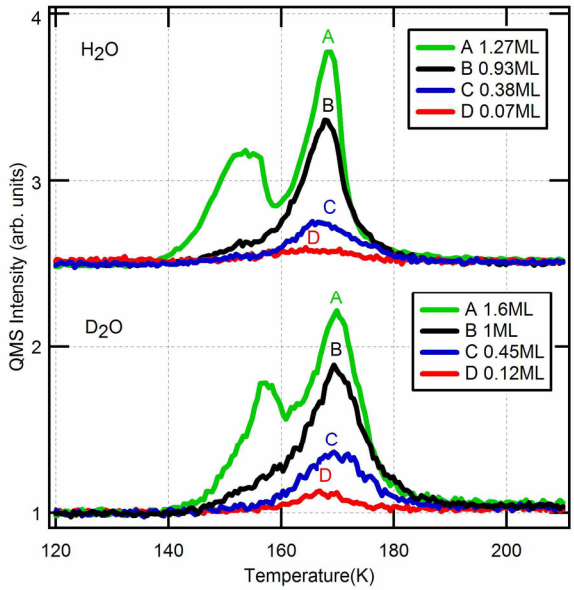

Figure 3.1 TPD of various exposures of H_2O and D_2O on Ni(111) at 85 K.

HREEL spectra of various coverages of H_2O and D_2O, adsorbed at 85 K, are shown in Figure 3.2. These spectra are taken in the specular direction with an incident angle of 60º and an impact energy of 5 eV. The indicated water coverage was determined by integration of the TPD spectrum after obtaining the vibrational spectrum. In the sub-monolayer regime, we observe five main regions. For D_2O, they are centered at 315, 145, 80, 45 and 28 meV. The weak 315 and 145 meV features increase in intensity with coverage and are most clearly distinguished in the multilayer spectrum. The frequency of the strong feature appearing at 80 meV appears coverage-independent. The 45 meV broad feature shifts to higher frequencies with increasing coverage, which is much more pronounced for H_2O. The latter also increases in intensity and broadens. It dominates the region centered at 75 meV

in the multilayer spectrum. Finally, a weak feature at 28 meV is only clearly observed in the shoulder of the specular peak for multilayers (see also the top trace in figure 3.5). The H_2O spectra show similar features with the same dependencies around 420 (see inset), 200, 105, 50, and 30 meV. The feature around 50 meV shifts to higher frequencies with increasing coverage as does the 45 meV feature for D_2O. We believe that variations in intensity and resolution in the comparison of H_2O and D_2O spectra are primarily due to variations in experimental conditions and signal averaging. We also observe a feature at 175 meV in HREEL spectra after combined dosing of H_2O and D_2O. This feature has been observed in similar experiments on Pt(111) and was assigned to the HOD bending vibration [25]. This observation indicates that isotopic scrambling observed in TPD experiments has already occurred at 85 K. Finally, we have taken HREEL spectra of D_2O layers that were formed at 85 K and subsequently annealed at 140 K. These spectra show no differences to the ones presented in figure 3.2.

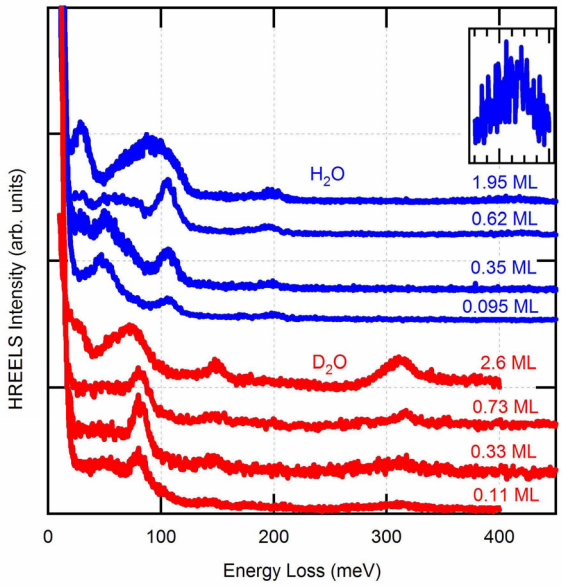

Figure 3.2 HREEL spectra of H_2O and D_2O on Ni(111) at 85 K for various coverages. The inset shows the spectrum for 1.95 ML H_2O in the 380 to 440 meV region.

Figure 3.3 compares HREEL spectra of H_2O and D_2O taken at the specular angle and 10º off-specular. Comparison of spectra taken at specular and off-specular angles can be used to differentiate between dipole and impact scattering mechanisms in vibrational excitation [26]. For H_2O, we only show spectra for a multilayer, whereas for D_2O we show spectra ranging from 0.11 to 2.6 ML. Noteworthy are the strongly angle-dependent intensities for the 30 meV feature in the multilayer spectra (28 meV for D_2O) and the 80 meV feature in the sub-monolayer regime of D_2O.

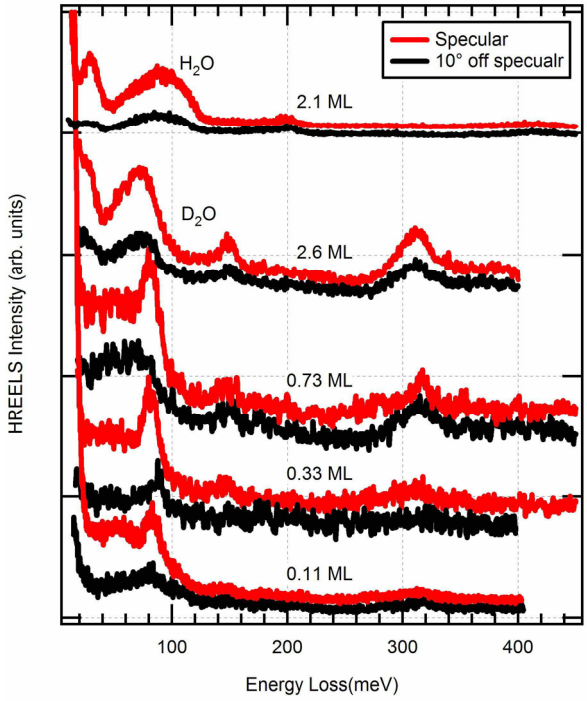

Figure 3.3 Comparison of HREEL spectra taken at the specular and off-specular angle for H_2O and D_2O on Ni(111).

3.3.2 D_2O on hydrogen-covered Ni(111)

In order to examine the influence of co-adsorbed hydrogen on the binding of water on Ni(111), we have performed similar experiments to those mentioned above for the H-precovered surface. Hydrogen is known to dissociatively adsorb on Ni(111) with a low barrier to reaction, although large exposures are necessary to (nearly) complete saturation

[27,28]. Comparison of our integrated TPD traces for a large range of H_2 doses up to 2×10^{-2} mbar*s indicates that a dose of 2×10^{-3} mbar*s H_2 at 85 K nearly saturates the surface. Figure 3.4 shows TPD spectra taken after an H_2 exposure of 2×10^{-3} mbar*s at 85 K with consecutive exposure to D_2O. For comparison, Figure 3.4 also shows the D_2O TPD spectra from the bare Ni(111) surface. At a D_2O coverage of 1.8 ML, desorption from a hydrogen covered surface shows a single peak that traces the zero-order desorption onset exactly. No separation of this peak is observed. Also, at the low D_2O coverage of 0.18 ML, we only observe desorption near 155 K. The inset shows the difference between 0.11 ML of D_2O for the bare and hydrogen-covered surface in detail. The D_2O desorption peak has shifted 10 K downward by prior adsorption of hydrogen. Associative desorption of H_2 occurs in two peaks at 320 K and 360 K and is not affected by the D_2O overlayer. By also monitoring m/z 3 (3, M – HD) and 19 (19, M – HOD) in these experiments, we find no evidence of isotopic mixing between H_{ads} and the D_2O.

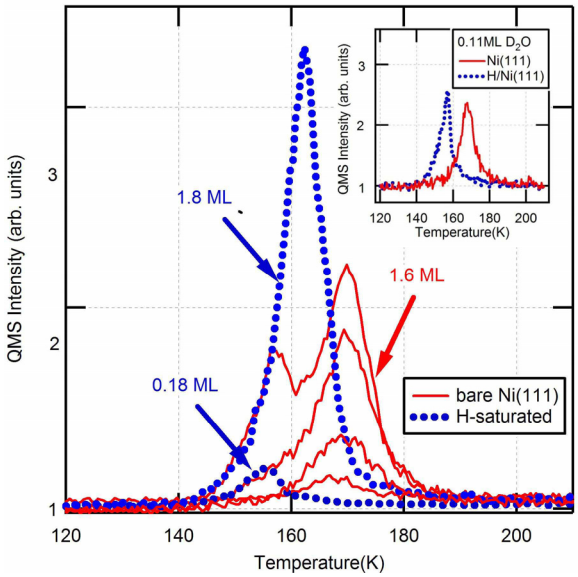

Figure 3.4 TPD of various amounts of D_2O from H-saturated and bare Ni(111). The inset shows the same comparison for 0.11 ML D_2O. For coverages, see also figure 3.1.

Figure 4.5 compares HREEL spectra of D_2O on the H-covered and bare surface. The middle and bottom spectra are taken after dosing 0.11 ML of D_2O, whereas the top spectrum was taken after dosing a multilayer of D_2O on the bare surface. The spectra for the sub-monolayer coverages show various differences. The strong 80 meV feature is either obscured or has disappeared upon pre-adsorption of hydrogen. Also, the 45 meV feature is replaced by a feature centered around 70 meV, which resembles the broad feature observed in this regime for multilayers. Finally, the 28 meV feature, observed clearly for multilayers on the bare surface, is already distinguishable for 0.11 ML on the hydrogen-covered surface. In HREEL spectra we again find no evidence of isotopic exchange between the saturated H-layer and D_2O.

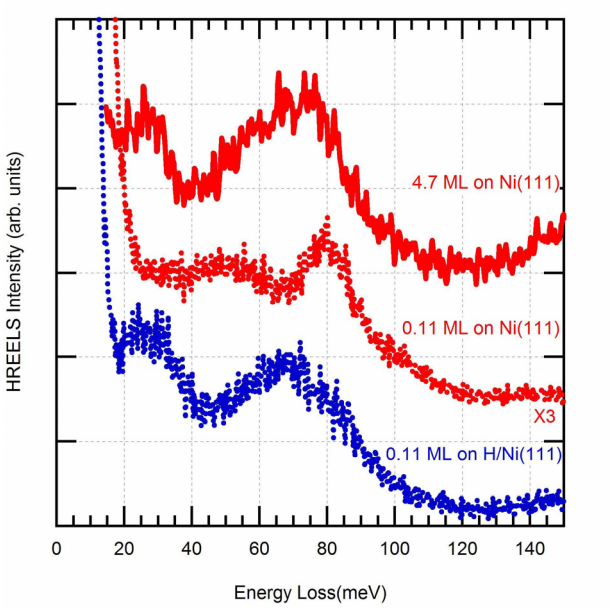

Figure 3.5 HREEL spectra of 0.11 ML D_2O on hydrogen-saturated Ni(111) compared to 4.7 ML and 0.11 ML D_2O on bare Ni(111).

3.4 Discussion

First, we turn our attention to the TPD spectra in figure 3.1. Our spectra are in excellent agreement with recently published spectra by Gallagher *et al.* who deposited water layers from exposure to a molecular beam at 135 K [15]. They are also in good agreement with

other previous studies [16,23,24]. It is generally agreed that the peak at ~170 K is due to (sub)monolayer adsorption of water, whereas the peak developing near 155 K is due to consecutive multilayer growth. Our TPD spectra show no evidence of the presence of steps or other defects on our surface, which would result in desorption of H_2O at higher temperatures. Since dissociation of H_2O at such defects also leads to H_2 associative desorption at higher temperatures [24], we have traced m/z 2 (2, M – H_2) in these TPD experiments and find no evidence for H_2O dissociation. Although our results do not provide information whether water layers grown at 85 K are amorphous or crystalline, we can conclude that our experimental procedures form layers of non-dissociated H_2O molecules. Combined with the absence of the 127 meV vibrational signature of adsorbed hydroxyl groups in HREEL spectra [18], the TPD experiments that indicate formation of HOD in mixed H_2O/D_2O layers allow us to conclude that at 85 K isotopic scrambling takes place without dissociation of water at the surface.

In the literature, several reports discuss adsorption of water in terms of a bilayer structure [1,2]. For example, Jo *et al.* interpreted a double maximum in the high temperature TPD features of water desorbing from Pt(111) [29] as a result of such a bilayer structure. More recent results for Pt(111) both confirm [18] and dispute the experimental results and interpretation [6]. Our TPD spectra for Ni(111) show only a single feature in the high temperature region, as was found by Gallagher *et al.* [15]. Therefore, these results yield no basis for a more detailed interpretation of the structure of adsorbed water.

Next, we attribute the features of our HREELS results shown in figure 3.2 by comparison to results from IR and HREELS studies of water adsorbed on Ni(111) [17], Pt(111) [18,25], and Ni(100) [30]. From the five main regions in the sub-monolayer D_2O spectra, the features centered at 315 and 145 meV have consistently been attributed to the O-D stretch and D-O-D bend. In HREEL spectra of H_2O these vibrational modes appear at 420 and 200 meV, in agreement with the expected isotopic frequency ratio between 1.3 and 1.4. The similarity in frequency of the stretching and bending modes of water on Pt(111) and Ni(111) and of water in the gas phase [1,17,18,25], indicate that these modes are not strongly affected by the metal substrate. Although the bending and stretching modes increase in intensity with coverage, the intensities observed here are too weak to use a

change between specular and off-specular intensity (figure 3.3) for commenting on possible molecular orientation with respect to the surface normal. We note that it is commonly assumed that water bonds through the oxygen atom to the metal surface. We also note that we do not observe a clear feature that could be attributed to the free OH or OD stretch, which has been reported for a bilayer structure [1,2]. This feature would be expected around 460 meV for OH and 340 meV for OD [17,18].

Two of the three remaining features in the spectra for D_2O submonolayer coverages fall within the frequency range generally attributed to librations, namely the peaks around 80 and 45 meV. For the latter, the intensity increases and the frequency shifts with increasing dose, resembling librations observed on Pt(111) [18,25] and Ni(100) [30]. The apparent decrease in off-specular intensity suggests that this feature at 45 meV is, at least in part, due to dipole scattering.

For the dominant libration at 80 meV, both the intensity at low coverage and its strongly decreased off-specular intensity suggest a dipole scattering mechanism. The same feature appears in the H_2O spectra at 105 meV, yielding an isotopic frequency ratio of 1.31. Our spectra at much higher coverages suggest that this mode is obscured by formation of multilayers. Although an unspecified libration appears with similar frequency in deconvoluted spectra of H_2O and D_2O on Ni(100) [30], it is much less pronounced. For Pt(111), two narrow features at comparable frequencies are observed, but only for bilayers and also not nearly as dominant [18]. A DFT study of gas phase $(H_2O)_n$ clusters finds vibrational frequencies of similar energy for $n\geq3$ [31]. However, this study does not specify the accompanying nuclear motions. Since an assignment can not be based on this previous work, we consider the possible librations: wag, rock and twist. We note that when water is bound through the oxygen atom, only the rocking and the wagging librations become dipole active when the site symmetry is reduced from C_{2v} to C_S. We also note that frequencies of these librations are not expected to vary much between monomers and weakly bound structures, such as clusters [3,5,6] and hexamer rings [17]. Finally, we find that, in comparison to IR spectra of nickel aquocomplexes, e.g. $Ni(H_2O)_6SiF_6$, the frequency of the rock agrees well with our observed feature at 80 meV [32], whereas the wag and twist have lower frequencies. We therefore suggest that the broad librations at lower frequencies

consists of nuclear motions resembling the twist and wag, whereas the higher libration resembles the rock for (sub-)monolayer coverages. Additionally, we note that Gallagher *et al.* showed that the delicate balance between interaction of water molecules with the surface and the lateral hydrogen-bonded network is easily disrupted by multilayer formation [15]. The 80 meV peak seems characteristic of (patches of) this (2√7x2√7)R19° structure as it remains clearly distinguishable after annealing at 140 K, but is not observed when forming multilayers.

We are left with one discernable feature at 28 meV for D_2O (30 meV for H_2O). The rather small isotopic frequency ratio of ~1.05 is characteristic for a vibration which involves the whole water molecule. Indeed, features in this regime are generally attributed to frustrated translations and a mode at the same frequency has been observed on Pt(111) [18,25]. Strong weakening in the off-specular intensity for both H_2O and D_2O suggests that this translation mode is dipole active. Although it was first assigned by Sexton [25] to a motion parallel to the metal surface, Jacobi *et al.* recently proposed it to be the frustrated translation normal to the surface [18]. Our data support the latter assignment. In addition, since this mode is only clearly observable for both Pt(111) and Ni(111) in the multilayer regime, we believe it corresponds to the frustrated translation normal to the surface of hydrogen-bonded water molecules in multilayers, i.e. the D_2O···DOD stretch. The D_2O···M stretch in the submonolayer regime has been connected by Jacobi *et al.* [18] to an energy loss feature around 15 meV, which is unobservable in our spectra.

Figure 3.4 and 3.5 provide clear evidence that pre-covering the surface with hydrogen affects the interaction of water with Ni(111). Hydrogen atoms are known to adsorb to the Ni(111) surface on three-fold hollow sites forming a (1x1) overlayer [27]. Contrary, water on the bare nickel surface has been shown to form a labile, incommensurate (2√7x2√7)R19° layer that has water molecules residing above various sites [15]. We consider whether our results from figure 3.4 and 3.5 indicate how water molecules bind to the H-covered surface and whether the first layer of water wets this surface. In this respect we recall that previous experiments using co-adsorption of H and H_2O on Pt(111) indicate shifts in TPD features that may be compared to those shown in figure 3.4. Jacobi *et al.* mention that very small amounts of hydrogen affect TPD features of H_2O such that the two

desorption peaks merge [18]. Contrary, Wagner and Moylan note that they observe little if any effect [21] for the same system. Instead, they observe changes in HREEL spectra that are ascribed to formation of H_3O^+. This (hydrated) hydronium ion was also proposed to be formed in co-adsorption studies on Pt(100) [33] and Pt(110) [34].

Our data in figure 3.4 clearly indicate weakened bonding of water with the surface when pre-covering it with hydrogen. For 0.11 ML of D_2O, the desorption temperature shifts downward by 10 K upon pre-adsorption of a full monolayer of H, corresponding to the temperature regime for desorption from multilayers. Additionally, our HREELS data for the same small quantity of water clearly features the peak around 28 meV, which we assigned, in agreement with a HREELS study at higher resolution [18], to the frustrated translation of hydrogen-bound D_2O normal to a D_2O layer. This suggests that a small amount of water already forms multilayered islands on hydrogen-covered Ni(111). This behavior resembles the hydrophobic character observed for the first layer of water on Pt(111) [11,35]. This suggestion of a hydrophobic character of hydrogen-saturated Ni(111) is strengthened by the absence of the pronounced feature around 80 meV, which we suggest to be characteristic of the labile (sub)monolayer structure observed in a low-intensity LEED study [15].

Contrary to the presented interpretation, we observe that the leading edge of the 0.18 ML trace does not follow the same zero-order desorption for 1.8 ML D_2O on the hydrogen-saturated surface or the 1.6 ML desorption from the bare surface. This causes some doubt regarding the proposed multilayered island formation. Therefore, we also consider another bonding geometry that does not imply multilayered island formation. One could imagine that individual D_2O molecules preferentially bind to H_{ads}. The observed frequency at 28 meV could then be due to a similar frustrated translation normal to the surface, whereas the 80 meV feature characteristic of (patches of the) incommensurate $(2\sqrt{7}x2\sqrt{7})R19°$ layer has disappeared since the lateral ordering of water molecules is now dominated by interaction with the H-lattice. For this bonding geometry, desorption from submonolayer coverages would resemble multilayer desorption since it also requires breaking of the $D_2O\cdots H$ hydrogen-bond. However, we would expect at least some frequency shift for the 28 meV feature since it is unlikely that the dipole-dipole interaction between water molecules strongly resembles the interaction between a water molecule and a hydrogen atom adsorbed

onto Ni(111). In addition, we note that, if these hydrogen bonds were comparable, this bonding geometry would also require overlap of the onset in the TPD traces for 0.18 and 1.8 ML. We therefore conclude that, although we can not exclude the latter bonding geometry, the multilayered island formation due to a hydrophobic character of hydrogen-covered Ni(111) is more plausible. We note that adsorption-desorption techniques using rare gases, chloroform, and bromoform, which have been shown to be sensitive to the local topography of the surface (see e.g. Ref. 11, 15 and 36) may provide more conclusive evidence of the proposed hydrophobicity.

Finally, we consider whether we have reason to believe that hydronium-ions are formed on the Ni(111) surface, as has been suggested for co-adsorption of hydrogen with water on platinum surfaces [21,33,34]. For Pt(111), the existence of this ion was based on the appearance of an additional peak around 143 meV in HREEL spectra after flashing hydrogen and water, co-adsorbed at 95 K, to 150 K. We do not observe such a peak nor any other significant changes in our HREEL spectra upon flashing to 140 K. In addition, we find no isotope exchange between H_{ads} and D_2O, which would be expected if a transiently formed H_3O-moiety decomposed prior to water desorption. The Ni-H bond has considerable strength and an activation barrier may be preventing such species to form. Therefore, we conclude that our data show no evidence of formation of a hydronium ion or hydronium-like species. In this regard, we stress that the hydrogen-bonding between D_2O and H_{ads} considered in the previous paragraph is very different from a chemical bond between these species. The HREEL feature at 28 meV is only indicative of an O···H hydrogen-bond and not of an O-H intramolecular chemical bond.

3.5 Conclusions

Based on TPD and HREEL spectra we conclude that hydrogen, atomically bound to Ni(111), affects the interaction between this metal surface and water significantly. Whereas a hydrogen-bonded network of water multilayers shows isotopic scrambling without water dissociation at 85 K on the surface, the H-Ni bond is too strong to allow isotope exchange with co-adsorbed water. We expect that the same H-Ni bond strength prevents formation of H_3O^+ or similar species. In contrast, our data actually suggest that saturating the Ni(111)

surface with hydrogen makes the surface hydrophobic, and that multilayered islands of water molecules form at submonolayer coverages.

3.6 Rererences

[1] P. A. Thiel, and T. E. Madey, *Surf. Sci. Rep.*, 1987, **7**, 211.

[2] M. A. Henderson, *Surf. Sci. Rep.*, 2002, **46**, 5.

[3] T. Mitsui, M. Rose, E. Fomin, D. Ogletree, and M. Salmeron, *Science*, 2002, **297**, 1850.

[4] X. Zhu, J. White, M. Wolf, E. Hasselbrink, and G. Ertl, *J. Phys. Chem.*, 1991, **95**, 8393.

[5] A. L. Glebov, A. P. Graham, and A. Menzel, *Surf. Sci.*, 1999, **428,** 22.

[6] J. Daschbach, B. Peden, R. Smith, and B. D. Kay, *J. Chem. Phys.*, 2004, **120**, 1516.

[7] M. Morgenstern, J. Muller, T. Michely, and *G. Comsa, Z. Phys. Chem.*, 1997, **198**, 43.

[8] A. Glebov, A. P. Graham, A. Menzel, and J. P. Toennies, *J. Chem. Phys.*, 1997, **106**, 9382.

[9] S. Haq, J. Harnett, and A. Hodgson, *Surf. Sci.*, 2002, **505**, 171.

[10] G. Zimbitas, S. Haq, and A. Hodgson, *J. Chem. Phys.*, 2005, **123**, 174701.

[11] G. A. Kimmel, N. G. Petrik, Z. Dohnalek, and B.D. Kay, *Phys. Rev. Lett.*, 2005, **95**, 166102.

[12] S. Haq, C. Clay, G. R. Darling, G. Zimbitas, and A. Hodgson, *Phys. Rev. B*, 2006, **73**, 115414.

[13] C. Clay, S. Haq, and A. Hodgson, *Chem. Phys. Lett.*, 2004, **388**, 89.

[14] P. J. Feibelman, *Science*, 2002, **295**, 99.

[15] M. E. Gallagher, S. Haq, A. Omer, and A. Hodgson, *Surf. Sci.*, 2007, **601**, 268.

[16] R. H. Stulen, and P. A. Thiel, *Surf. Sci.*, 1985, **157**, 99.

[17] M. Nakamura, and M. Ito, *Chem. Phys. Lett.*, 2004, **384**, 256.

[18] K. Jacobi, K. Bedurftig, Y. Wang, and G. Ertl, *Surf. Sci.*, 2001, **472**, 9.

[19] M. Nakamura, M. Tanaka, M. Ito, and O. Sakata, *J. Chem. Phys.*, 2005, **122**, 224703.

[20] V. R. Stamenkovic, B. Fowler, B. S. Mun, G. Wang, P. N. Ross, C. A. Lucas, and N. M. Markovic, *Science*, 2007, **315**, 493.

[21] F. T. Wagner, and T. E. Moylan, *Surf. Sci.*, 1988, **206**, 187.

[22] C. T. Campbell, and S. M. Valone, *J. Vac. Sci. Technol. A*, 1985, **3**, 408.

[23] T. E. Madey, and F. P. Netzer, *Surf. Sci.*, 1982, **117**, 549.

[24] C. Mundt, and C. Benndorf, *Surf. Sci.*, 1993, **287/288**, 119.

[25] B. A. Sexton, *Surf. Sci.*, 1980, **94**, 435.

[26] H. Ibach, and D. L. Mills, *Electron Energy Loss Spectroscopy and surface Vibrations*, Academic Press, New York, 1982.

[27] K. Christmann, O. Schober, and G. Ertl *et al*., *J. Chem. Phys.*, 1974, **60**, 4528.

[28] H. P. Steinruck, A. Winkler, and K. D. Rendulic, *Surf. Sci.*, 1985, **152**, 323.

[29] S. K. Jo, J. Kiss, J. A. Polanco, and J. M. White, *Surf. Sci.*, 1991, **253**, 233.

[30] R. Brosseau, M. R. Brustein, and T. H. Ellis, *Surf. Sci.*, 1993, **280**, 23.

[31] S. S. Xantheas, *J. Chem. Phys.*, 1994, **100**, 7523.

[32] Kazuo Nakamoto, *Infrared and Raman Spectra of Inorganic and Coordination Compounds, Part B*, 5th Edition, John Wiley & Sons Inc., New York, 1997, pp. 53–56.

[33] N. Kizhakevariam, and E. M. Stuve, *Surf. Sci.*, 1992, **275**, 223.

[34] N. Chen, P. Blowers, and R. I. Masel, *Surf. Sci.*, 1999, **419**, 150.

[35] G. Zimbitas, and A. Hodgson, *Chem. Phys. Lett.*, 2006, **417**, 1.

[36] M. L. Grecea, E. H. G. Backus, H. J. Fraser, T. Pradeep, A. W. Kleyn, and M. Bonn, *Chem. Phys. Lett.*, 2004, **385**, 244.

Chapter 4

Co-adsorption of water and hydrogen on Ni(111)

We have studied the surface coverage dependence of the co-adsorption of D and D_2O on the Ni(111) surface under UHV conditions. We use detailed temperature-programmed desorption studies and high resolution electron energy loss spectroscopy to show how pre-covering the surface with various amounts of D affects adsorption and desorption of D_2O. Our results show that the effects of co-adsorption are strongly dependent on D-coverage. In the deuterium pre-coverage range of 0 - 0.3 ML, adsorption of deuterium leaves a fraction of the available surface area bare for D_2O adsorption, which shows no significant changes compared to adsorption on the bare surface. Our data indicates phase segregation of hydrogen and water into islands. At low post-coverages, D_2O forms a two-phase system on the remaining bare surface that shows zero-order desorption kinetics. This two phase system likely consists of a two-dimensional (2D) solid phase of extended islands of hexamer rings and a 2D water gas phase. Increasing the water post-dose leads at first to 'freezing' of the 2D gas and is followed by formation of ordered, multilayered water islands in between the deuterium islands. For deuterium pre-coverages between 0.3 and 0.5 ML, our data may be interpreted that the water hexamer ring structure, $(D_2O)_6$, required for formation of an ordered multilayer, does not form anymore. Instead, more disordered linear and branched chains of water molecules grow in between the extended, hydrophobic deuterium islands. These deuterium islands have a D-atom density in agreement with a (2x2)-2D structure. The disordered water structures adsorbed in between form nucleation sites for growth of 3D water structures, which (partially) spill over the deuterium islands. Loss of regular lateral hydrogen bonding and weakened interaction with the substrate reduces the binding energy of water significantly in this regime and results in lowering of the desorption temperature. At deuterium pre-coverages greater than 0.5 ML, the saturated (2x2)-2D structure mixes with (1x1)-1D patches. The mixed structures are also hydrophobic. On such surfaces, submonolayer doses of water lead to formation of 3D water structures well before wetting the entire hydrogen-covered surface.

4.1 Introduction

Although the simultaneous interaction of water and hydrogen with various metal surfaces has been studied and reviewed [1-10], the nature of the interaction between these species remains poorly understood. Co-adsorption of hydrogen and water on nickel is of particular interest due to their simultaneous presence on the anode of alkaline fuel cells. Also in many industrial processes, such as steam reforming, hydrogen and water co-exist on the catalyst surface. Steam reforming is the chemical process, where at high temperatures (700-1100ºC) and pressure and in the presence of a metal-based catalyst (nickel), steam reacts with methane to yield CO and hydrogen.

For the Ni(111) surface, several studies have investigated adsorption of either H_2 [11-14] or H_2O [15-19]. Hydrogen is known to dissociately adsorb on Ni(111) with a low barrier to reaction, although large exposures are necessary to (nearly) complete saturation [11-14]. The saturation coverage is generally agreed to be 1.0 monolayer (ML) [12-14]. Hydrogen is known to adsorb into fcc three-fold hollow sites from both experimental and theoretical studies [12,14,20-22]. Around 0.25 ML, an IV-LEED study suggests formation of p(2x2) islands at ~150 K [12], whereas a more recent HREELS study claims formation of (2x2)-2H islands already at much lower coverages and at 100 K [23]. At 0.5 ML, a (2x2)-2H structure exists which develops with increasing coverage into the (1x1)-H saturated structure [14,23]. Adsorption using molecular beam techniques shows that there is no isotopic dependencies in reactivity [24]. Also for desorption, no isotopic dependencies have been observed [25]. Hydrogen mobility has been studied using laser-induced desorption and optical diffraction techniques [26]. The diffusion rate is found to be 10^{-15} cm^2/s at 65 K and 10^{-7} cm^2/s at 240 K. At ~ 100 K, the rate increases monotonically from 3 x 10^{-13} cm^2/s at $\theta \approx 0.02$ to 1.3 x 10^{-12} cm^2/s at $\theta \approx 0.5$.

Experimental studies find water adsorption to be non-dissociative [15]. DFT calculations agree that an H_2O molecule preferentially binds on-top and experiences a large barrier to dissociation into H + OH, although calculated binding energies vary significantly [27,28]. A temperature-programmed desorption (TPD) spectrum of water from Ni(111) shows a feature near 170 K that saturates whereas a feature originating around 155 K does not saturate with increasing exposure. The latter shows zero-order desorption

characteristics. The 170 K feature is attributed to (sub)monolayer desorption, whereas the 155 K feature is believed to be due to multilayer desorption [15-19]. Previous investigations of the structure of water at (sub)monolayer coverages reported a (√3×√3)R30º pattern at θ~1 [16]. However, Gallagher *et al.* recently observed a labile (2√7×2√7)R19º structure using low-current LEED for a single water layer grown at 135 K. This structure was affected by prolonged exposure to the electron beam resulting in increased intensity near the √3 positions [15]. A second layer of water was reported to wet the first layer, but destroyed the (2√7×2√7)R19º structure. Only thicker layers formed an incommensurate ice structure, closely oriented to the Ni(111) surface. Recently, Nakamura *et al.* used infrared reflection absorption spectroscopy to study water adsorption on Ni(111) and suggested that hexamer water clusters with a ring-like shape dominate on the Ni(111) surface at wide (sub)monolayer water coverages at 20 K [29].

Although we are not aware of any UHV co-adsorption studies of H_2 and H_2O on Ni(111) to date, co-adsorption on Pt(111) has been studied and provides a reference for H_2O/H/Ni(111). An early co-adsorption study employing high resolution electron energy loss spectroscopy (HREELS) claimed formation of H_3O^+ (or hydrated forms of the hydronium ion) under UHV conditions on Pt(111) [3]. Such H_3O^+ formation was also reported on other Pt surfaces [7,8]. For adsorption and desorption of a co-adsorbed layer, a survey of the literature up to recent years indicates several inconsistencies. For example, for Pt(111) co-adsorption has been described to results in “strong changes” in TPD spectra [2] and was found to have “little if any effect” [3]. Although these conflicting observations had both been made before [4,5], results from a recent study by Petrik and Kimmel [9] provide a tentative explanation for the older claims. In a study that focused on electron-stimulated desorption and reactions occurring in water adsorbed to Pt(111), they also investigated the influence of adsorbing deuterium prior to dosing ~2 ML D_2O. They find that, at low coverages, D atoms stabilize D_2O. This is indicated by the appearance of a separate TPD peak at higher desorption temperature (~175 K) at the expense of the ~168 K desorption feature from the water monolayer interacting with the bare Pt(111) surface. However, at a D-coverage of ~0.25 ML (assuming a saturation coverage for deuterium of 1.0 ML), the same peak shifts back to below 170 K and reduces in size. Apparently, changes in

desorption features on Pt(111) are strongly dependent on deuterium pre-coverage and, at different pre-coverages, TPD spectra can appear both different and similar to spectra taken for water desorbing from the bare metal.

Recently, we have initiated a combined TPD-HREELS study to elucidate how adsorbed hydrogen affects the metal-water interaction on Ni(111) [30]. For the hydrogen-saturated surface, we have suggested that atomically-bound hydrogen increases hydrophobicity and that multilayered water islands form at submonolayer coverages. Using isotopic labeling we have identified various vibrations and showed that there are no isotopic effects in adsorption or desorption. We also found no evidence for isotope exchange between atomically-bound hydrogen and deuterated water nor did we find evidence for formation of H_3O^+ or similar species. We attributed this to the H-Ni bond strength preventing such reactions. See Chapter 3 for detail description.

In the this chapter, we use detailed TPD studies in combination with HREELS to investigate how much smaller amounts of pre-adsorbed hydrogen affect adsorption of water at (sub)monolayer coverages on Ni(111). Since no isotopic effects have been reported in adsorption or desorption for both hydrogen and water, we use D_2 and D_2O in our studies and expect our results and conclusions to hold generally for hydrogen-water co-adsorption on Ni(111). After presenting our data, we discuss and compare our results in combination with conclusions from previous studies. Our analysis allows us to suggest in detail how pre-adsorbed hydrogen affects the bonding between water molecules on Ni(111) and what causes differences observed between Pt(111) and Ni(111) for this system.

4.2 Experiment

Experiments are performed in an UHV apparatus. This apparatus consists of two chambers, which are separated by a gate valve. The top level is equipped with an ion sputter gun, an atomic hydrogen source, a stainless steel leak valve, a home-built capillary array doser [31], and a quadrupole mass spectrometer (Balzers QMS 422) used for TPD measurements and residual gas analysis. The lower level is equipped with an upgraded ELS22 high resolution electron energy loss spectrometer and a double-CMA Auger Electron spectrometer (Staib Instruments). The base pressure of the system is less than 1×10^{-10} mbar.

The Ni(111) single crystal is cut and polished to less than 0.1º of the low Miller-index plane (Surface Preparation Laboratories, Zaandam, the Netherlands). It can be heated to 1200 K by electron bombardment and cooled to 85 K. The sample temperature is measured by a chromel-alumel thermocouple spot-welded to the edge of the crystal. Sample preparation and verification of cleanliness were described in detail in chapter 3 or Ref. 30. D_2O (99.96% isotopic purity, Aldrich Chemical company) is cleaned by repeated freeze-pump-thaw cycles after which helium (Messer, 99.999%) is introduced to the glass container to a total pressure of approximately 1 bar. When dosing water, monitoring the helium partial pressure in our vacuum apparatus allows for increased dosing accuracy.

After cleaning, the sample is kept at 85 K while dosing D_2 (Linde, 99.9%) through a stainless steel leak valve, followed by dosing D_2O with the sample placed 15 mm in front of the capillary array doser. The deuterium coverage, θ_D, is estimated from integrating the TPD feature in separate experiments in which only D_2 is introduced. The latter is required since dosing water is accompanied by dosing helium, which lingers in the vacuum system and distorts the baseline of the TPD traces for *m/z* 4 (4, M – D_2). The TPD integral of D_2 is converted to an absolute coverage using a separately determined calibration curve based on D_2 doses ranging from $1x10^{-6}$ to $20{,}000x10^{-6}$ mbar*s. HREEL spectra were recorded at 5 to 9 meV resolution (FWHM) with typical 1×10^4 cps for the scattered elastic peak.

All TPD measurements were performed with a heating rate of 1.0 K/s. Desorption of water from a single crystal at this rate may result in complex changes in the baseline due to non-equilibrated conditions between vacuum and chamber walls during the experiment. In particular, we notice a pump tail in TPD spectra that seems related to the water coverage on the crystal. In order to accurately quantify the amount of adsorbed water that desorbs either in a single or two partially overlapping peaks, we have used various functional forms to fit desorption traces. We describe this here in detail since it is of some consequence to the analysis of our data and we find such discussion lacking in the literature for water desorption.

Water desorption from metal surfaces is often described in terms of mono- and multilayer desorption as indicated by two separate desorption peaks and in terms of zero- and first-order desorption kinetics. Initially, we used two Gaussian profiles to fit the low

and high temperature peaks also observed in our TPD traces, although neither zero- or first-order desorption kinetics result in truly Gaussian peak shapes. The differential equations describing such desorption can not be solved without assumptions or simplifications [32]. Therefore, we used more elaborate deconvolution functions to improve the fitting procedure. In particular, we fit each main peak with a function that combines a distorted Gaussian line shape with an exponential decay to account for the pump tail. The distorted Gaussian line shape is a multiplication of an inverted tangent hyperbolic with a Gaussian profile, both centered at the same peak value, T_p. The pump tail consists of an exponential decay multiplied by a regular tangent hyperbolic, centered at the same peak value, T_p. Enforcing the same value ensures that the pump tail has no variable delay relative to the original desorption from the single crystal. The tangent hyperbolic in the pump tail contribution accounts for the rate at which desorption from chamber walls is 'turned on'.

Figure 4.1 shows the best fitting results for a single experiment where we dosed 0.05 ML D followed by approximately 0.8 ML D_2O. The inset in figure 4.1a shows the raw data for a large temperature regime, whereas the figure 4.1a and 4.1b zoom in on the relevant temperature regime. For figure 4.1a, we used the elaborate fitting procedure. It shows the four contributions for the two main peaks observed in the spectrum as dotted lines (LT, LTP, HT, and HTP). The raw data is shown as a dashed line and the total fit is shown as a solid line. To reduce uncertainty in this fitting procedure, the ratio of peak heights of the low temperature peak (LT) with its pump tail (LTP) was fixed after determining this ratio for the more intense high temperature peak (HT, HTP). Also, the decay rate of the pump tail was determined for the high temperature peak and fixed accordingly for the low temperature peak in every experiment. Inspection of figure 4.1a shows that this procedure accurately reproduces the experimental trace. We also observe that the pump tail of the low temperature peak around 158 K completely overlaps with the main desorption trace of the high temperatures peak at 170 K. Although the example shown here results in fairly unambiguous decomposition, we note that the ambiguity increases when the low and high temperature peaks are closer in size and/or peak desorption temperature. Figure 4.1b shows the fit using partially overlapping Gaussians. The fit is obviously less accurate. However, when converting the integrated peaks to absolute coverages, where the reference for 1 ML

equals the maximum size of the decomposed high temperature peak, the simple fitting procedure yields the same results as the more elaborate fitting procedure within 10%. This is likely due to the proportionality of the desorption peak and its pump tail. Since the differences are small, we use the simple fitting procedure throughout this chapter to analyze TPD traces and determine absolute coverages, except when otherwise stated.

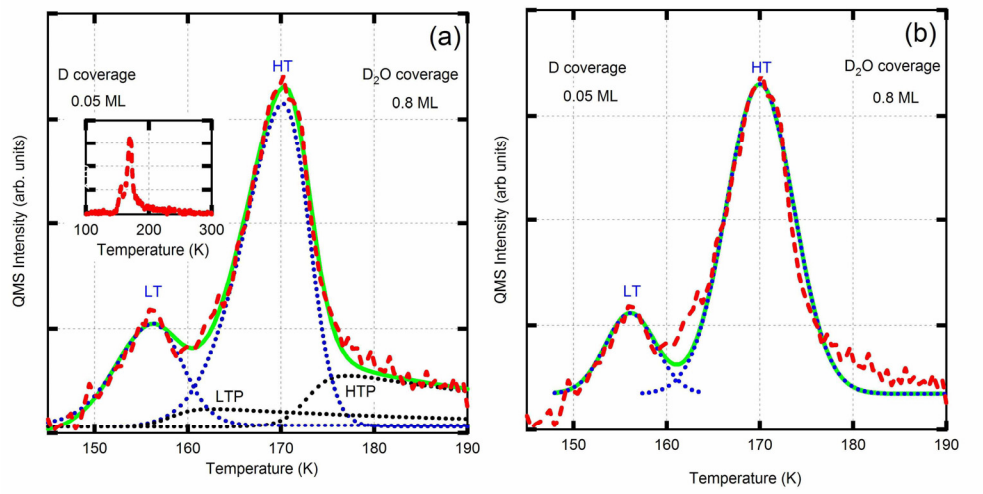

Figure 4.1 The fitting of D_2O TPD spectra from 0.8 ML deposited on 0.05 ML D pre-covered Ni(111) at 85 K. (a) Using the elaborate fitting procedure. (b) Using the simple fitting procedure with two Gaussian profiles. The inset shows the same TPD trace with temperature range from 100 K to 300 K. See text for abbreviations.

4.3 Results

Figure 4.2 displays six sets of TPD spectra of D_2O desorbing from various pre-coverages of deuterium on Ni(111). For $\theta_D = 0$ ML (Figure 4.2a), we only show water traces for $\theta_{D2O} \leq 1$ ML for clarity. Similar traces for $\theta_{D2O} > 1$ ML can be found in Chapter 3 and in reference [30]. For the bare Ni(111) surface, the D_2O desorption spectra show a single feature that initiates at ~166 K and shifts to ~170 K upon reaching saturation. Just before saturation, we observe a second feature at ~155 K. This low temperature feature has previously been shown not to reach saturation with increased dosing and shows zero-order desorption characteristics [15-19,30]. In figure 4.2a, this low temperature feature is just discernable as

a deviation from the baseline below 160 K for the 1 ML D_2O trace. It becomes more pronounced with larger dose or pre-covering with D (Figure 4.2b and 4.2c). We observe in our experiment that on the bare surface a 1.0 ML D_2O coverage consists of at most 0.15 and at least 0.85 ML of the low and high temperature features, respectively.

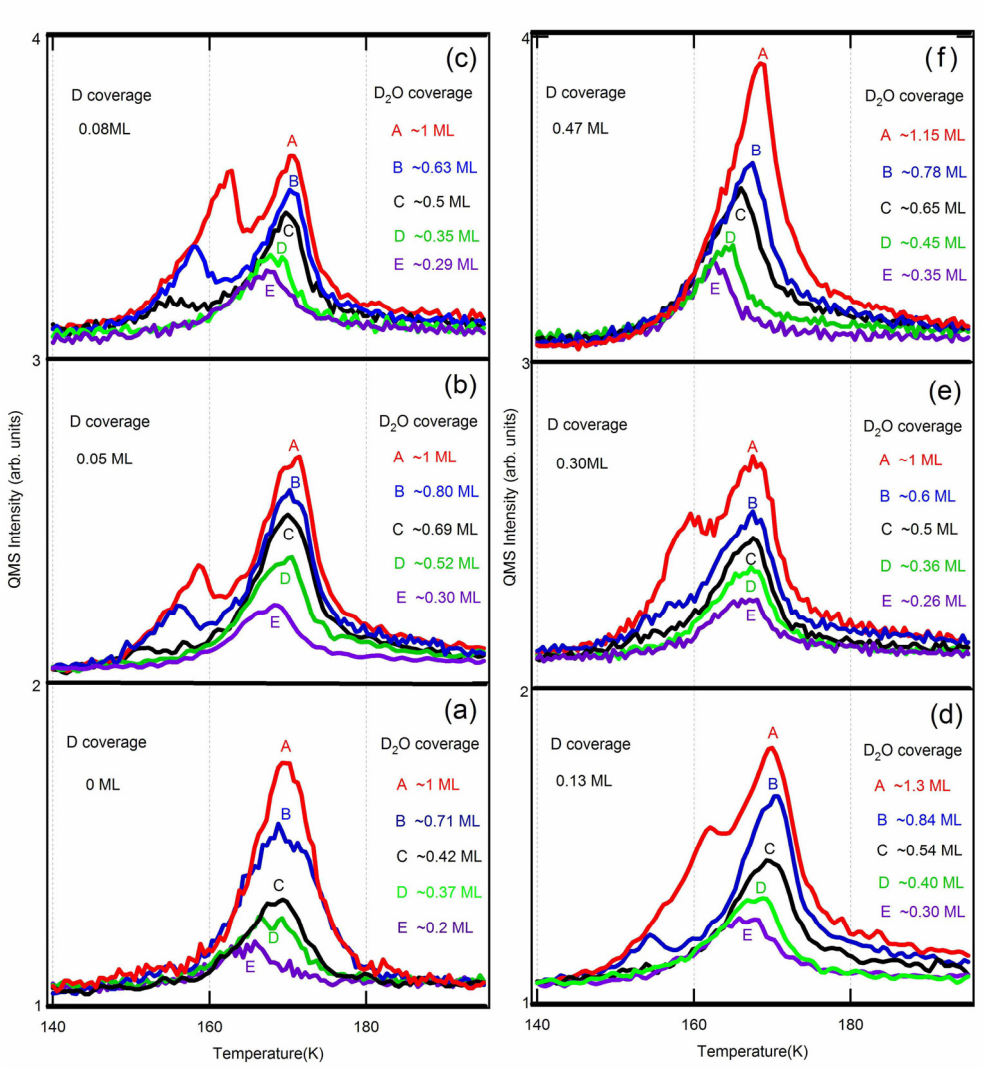

Figure 4.2 TPD of various amount of D_2O deposited on various D pre-coverages at 85 K.

Upon close inspection, figure 4.2 reveals detailed information on the influence of pre-adsorbed hydrogen on water adsorption. First, we notice that for θ_D = 0 ML (Figure 4.2a)

traces C-E show typical characteristics of zero-order desorption kinetics: overlapping leading edges and desorption maxima shifting to higher temperature with increased dose [32]. However, for traces A and B the desorption maximum does not shift anymore and the leading edges do not coincide with the leading edge of trace C. This behavior is typical of first-order desorption kinetics. Upon inspection of previously published TPD spectra of water desorption from the bare Ni(111) surface we notice similar behavior, although it was not commented on by the authors [15-19]. In experiments using θ_D = 0.05, 0.08 ML and 0.13 ML (Figure 4.2b, 2c, and 2d) we observe the same behavior for water desorption. At low θ_{D2O}, characteristics of zero-order desorption kinetics are apparent for the high temperature desorption peak, whereas it switches to first-order desorption kinetics with increasing θ_{D2O}. In the same figures we also observe that the low temperature peak around 155 K develops at lower D_2O coverages with increasing D coverage. For θ_D = 0.05 ML, the low temperature peak appears near θ_{D2O} = 0.7 ML whereas for θ_D = 0.08 ML it is already observable around $\theta_{D2O} \approx$ 0.5 ML. We note that, for $\theta_D \approx$ 0.13 ML, its appearance seems delayed to $\theta_{D2O} \approx$ 0.8 ML. This low temperature peak, starting at 155 K as a well defined peak and shifting upward with increased dose, shows typical zero-order desorption characteristics.

In contrast, at θ_D = 0.30 ML (Figure 4.2e), the lack of overlapping leading edges for the high temperature peak and the steadiness of the peak desorption temperature imply first-order desorption kinetics only. Whereas in figure 4.2a-d the peak temperature shifted to 170 K, it only reaches ~ 168 K here. Also, the low temperature peak grows in simultaneous with the high temperature peak in traces E, D, C and B. In figure 4.2b-d growth of the low and high temperature peaks are much more clearly separated.

For θ_D = 0.47 ML and $\theta_D \geq$ 0.35 ML (Figure 4.2f), we observe only a single desorption feature with a peak temperature that smoothly shifts to higher values. Decomposition into a low and high temperature features is obviously not applicable here. Close inspection of the leading edges in figure 4.2f indicates that desorption resembles, but does not strictly follow, zero-order kinetics. For example, traces A and B share a leading edge only up to approximately half of the maximum desorption rate. The same is true for traces C and D.

Figure 4.3 shows additional water TPD spectra for θ_D = 0.47 ML with water coverages ranging from 0.11 ML to 0.18 ML. Traces F, G and H, are off-set to show their first-order desorption characteristics more clearly. The leading edge of these traces deviates from the leading edges of traces D and E and the peak maximum does not shift between θ_{D2O} = 0.11 and 0.18 ML. Apparently, the characteristics of zero-order desorption as shown in figure 4.2f only appear after a minimum coverage of water on the surface is exceeded.

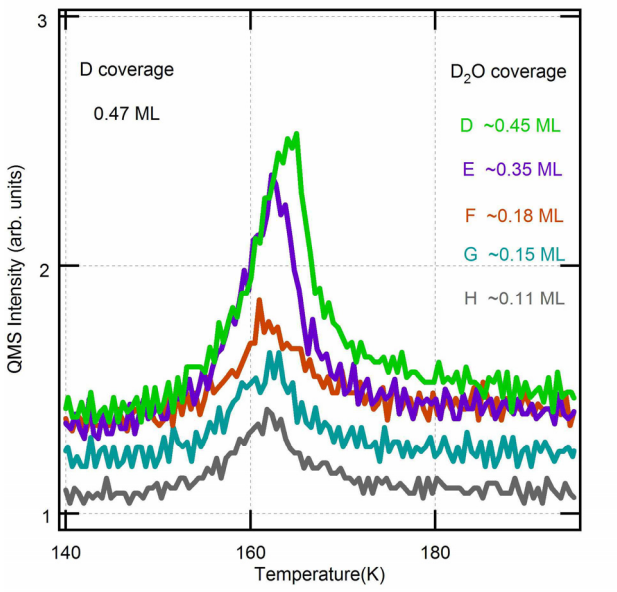

Figure 4.3 TPD of various amounts of D_2O deposited onto 0.47 ML D/Ni(111) at 85 K.

Using the simple decomposition scheme discussed in the experimental section, we have quantified the partitioning of water desorbing in the low and high temperature peaks. Figure 4.4 presents this partitioning for a fixed post-dose of ~1.0 ML D_2O in the range of θ_D = 0 - 0.35 ML. With increasing θ_D, the fraction of D_2O molecules desorbing in the low temperature component increases at the expense of the fraction in the high temperature component. The shape of the curve shows two changes in slope near θ_D = 0.08 ML and 0.3 ML creating three regions. For θ_D = 0 - 0.08 ML, the slope for the high temperature partition equals ~2.5 ML D_2O/ML D. Between θ_D = 0.08 and 0.30 ML it reduces to 0.3 ML D_2O/ML D. Beyond θ_D = 0.30, the slope rapidly increases. Here, we can not determine a

slope since we can not decompose the high and low temperature features accurately beyond $\theta_D = 0.35$.

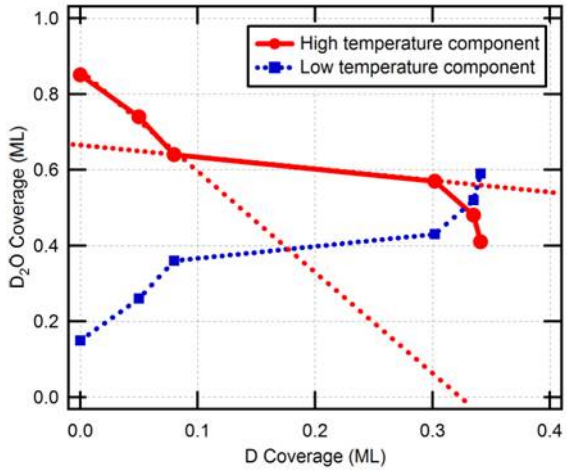

Figure 4.4 The partitioning of 1ML D_2O on various D pre-coverages on Ni(111).

In our previous study of $H_2O(D_2O)$/Ni(111) and D_2O/H/Ni(111) at Chapter 3, we have shown that HREEL spectra provide additional information regarding the bonding of water molecules adsorbed on Ni(111). In figure 4.5, we present such data for a $\theta_D = 0.3$ ML with varying θ_{D2O}. Figure 4.2e shows TPD spectra for the same deuterium pre-coverage where we noticed a deviation from water desorption behavior compared to lower D pre-coverages. For the bottom spectrum in figure 4.5, no D_2O was dosed. This spectrum was taken using an impact energy of the primary electron beam (E_p) of 9.6 eV with specular angle and shows a single feature at 90 meV. This feature is known to be caused by the Ni-D stretch vibration [23]. It is no longer observed when lowering E_p to 5 eV, as shown in the subsequent spectra in figure 4.5. This effect has been observed before for hydrogen adsorption on Ni(111) [33] and was attributed to resonance scattering [33,34]. Resonance scattering may be viewed as a special form of impact scattering. It involves transient formation of a negative ion and shows an energy-dependent scattering cross-section [35]. All other spectra shown in figure 4.5 were taken at $E_p = 5$ eV to ensure that observed energy losses in the same energy range cannot be attributed the to Ni-D stretch. The other three spectra shown in figure 4.5 for co-adsorption of D_2O and D all show the peak

attributed to the D-O-D bending vibration around 150 meV [2,30,36], and a broad feature between 50 and 100 meV generally attributed to D_2O librations [2,30,36]. We also observe the O-D stretch vibration at 310 meV. The intensity of the librations strongly increases with D_2O coverage. For θ_{D2O} = 0.90 ML, the 28 meV peak attributed to D_2O-D_2O hydrogen-bonded translation normal to the (111) plane [2,30] is also clearly observable. In the 0.73 ML trace the same peak appears less pronounced as a shoulder on the elastic peak.

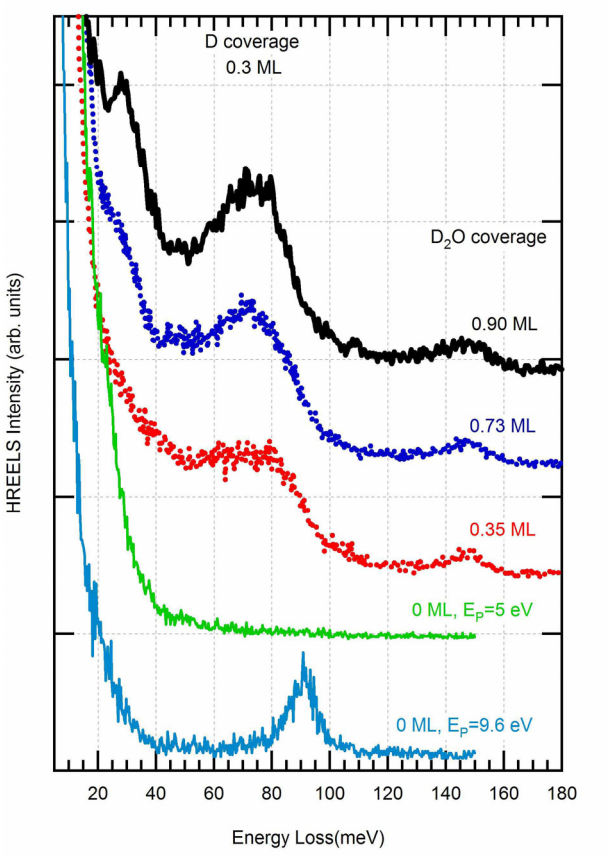

Figure 4.5 HREEL spectra of various D_2O coverages deposited onto 0.3 ML D/Ni(111).

Taking a different perspective, we have also investigated the influence of θ_D on desorption of a fixed post-coverage of 0.35 ML D_2O. Figure 4.6a plots TPD spectra of D_2O. We observe that the peak center shifts to lower temperatures with increasing θ_D. Figure

4.6b displays the center value of a Gaussian line shape fitted to the D_2O desorption traces from figure 4.6a as a function of θ_D. For this small D_2O post-coverage, the center value accurately matches the temperature at which the desorption rate is highest. For $0 < \theta_D < 0.3$ ML, the peak temperature shifts to lower values gradually at a rate of 2 K/ML D. Beyond $\theta_D = 0.3$ ML, the shift suddenly increases to ~25 K/ML D. Beyond $\theta_D = 0.50$ the shift of the peak center seems more gradual again and the slope is similar to the slope observed in the first section. The arrows in figure 4.6b point toward combinations of D and D_2O coverages for which also HREEL spectra were taken.

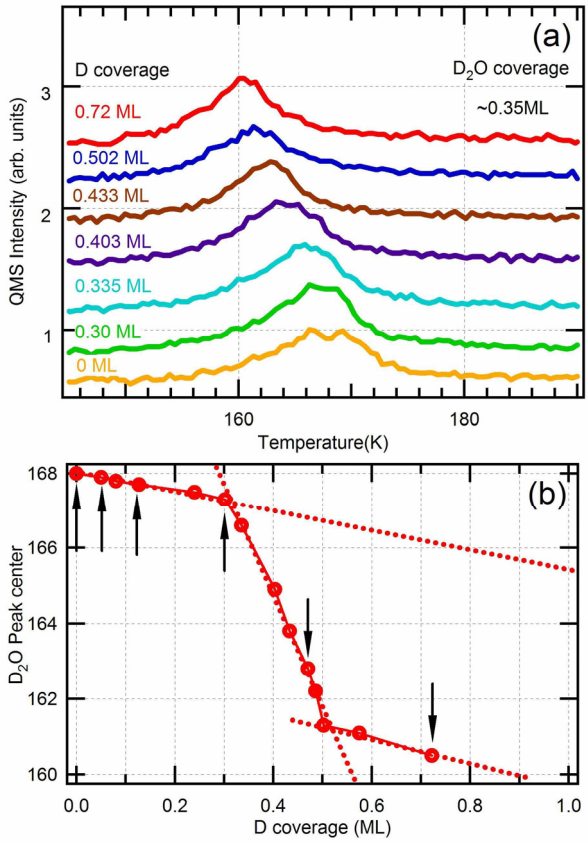

Figure 4.6 (a) TPD spectra of 0.35 ML D_2O on various D coverages. (b) D_2O peak center versus various D coverages.

Figure 4.7 shows the HREEL spectra corresponding to the D and D_2O coverages indicated in figure 4.6b by arrows. The HREEL spectrum for θ_D = 0 ML shows an intense and relatively sharp feature at 80 meV. In addition, the background signal toward lower energy does not show the expected exponential decay from the elastic peak, indicating a very broad loss of low intensity centered near 50 meV. This broad loss develops into a distinct feature with increased D_2 dose and shifts up to ~75 meV at the highest coverage as shown here. The distinct peak at 80 meV does not shift and is still clearly observable in the HREEL spectra for θ_D = 0.05 and 0.13 ML, although its intensity decreases relative to the upcoming feature at lower energy. The peaks merge completely for $\theta_D \geq 0.30$ ML. In relation to the TPD spectra for the same coverages in figure 4.6b, the loss of the distinct peak at 80 meV seems to coincide with the sharp turn at θ_D = 0.30 ML in figure 4.6b. Only at the highest D coverage, we clearly observe the multilayer peak at 28 meV.

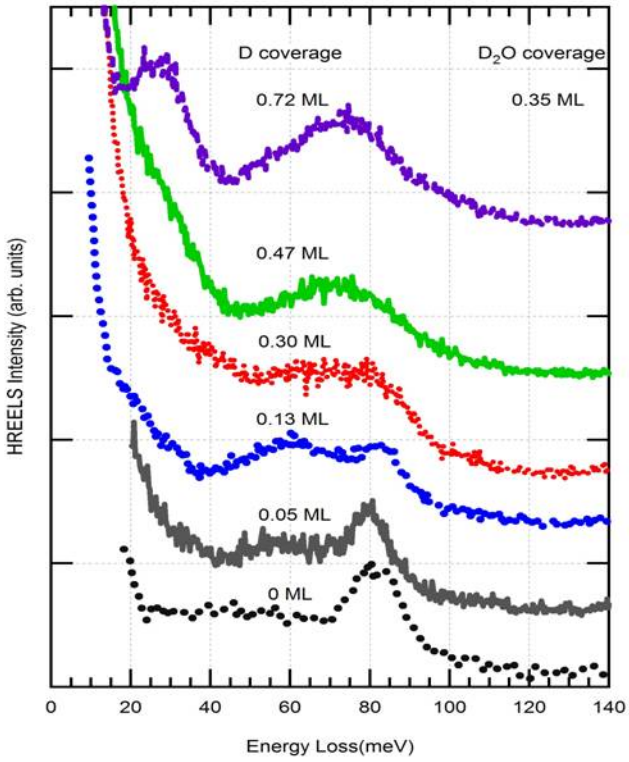

Figure 4.7 HREEL spectra of 0.35 ML D_2O deposited on various D coverages.

4.4 Discussion

First, we focus our attention on the TPD spectra in figure 4.2a. Our spectra are in excellent agreement with previously published spectra of water desorbing from bare Ni(111) [15-19]. It is generally agreed that the high temperature feature at ~170 K is attributed to the (sub)monolayer water desorption from the bare Ni(111) surface. The low temperature feature, starting at ~155 K, is ascribed to multilayer desorption. In our spectra, we observe that the high temperature feature shows zero-order desorption kinetics for lower coverages and first-order desorption kinetics at higher coverages. Observation of zero-order desorption kinetics is usually attributed to multilayer desorption, e.g. from multilayers of physisorbed noble gases or ice. Here, however, it is unlikely that water shows these characteristics at coverages far below 1 ML due to formation of multilayers. First, a separate desorption peak for multilayers 155 K has been identified [15-19]. Second, the 28 meV feature, which is indicative of multilayer formation [2,30,36], is absent [30]. To explain a similar observation for water desorption from Pt(111), Kay and co-workers recently suggested that water forms a two-phase system on the surface, consisting of a condensed phase and a 2-D gas-like phase, at thermodynamic equilibrium [37,38]. They argue that, under conditions present in their study, the rate of desorption is governed only by the temperature and thus zero-order kinetic behavior is observed. Since the same conditions also apply in our experiments, our TPD spectra for $\theta_D = 0$ and $\theta_{D2O} < 0.7$ ML can therefore be explained if water adsorbs as such a two-phase system onto the Ni(111) surface. The presence of at least the condensed phase on Ni(111) is in accordance with results from a previous RAIRS study that indicates formation of $(D_2O)_6$ clusters at both lower temperatures and much lower coverages [29].

Upward from $\theta_{D2O} = 0.7$ ML, desorption traces in figure 4.2a show first-order characteristics. Recent LEED experiments on water adsorption on Ni(111) show that a $(2\sqrt{7}x2\sqrt{7})R19°$ LEED pattern is observable after dosing more than 0.67 layer of water on Ni(111), although here water was adsorbed at 135 K [15]. Below 0.67 layer, absence of LEED patterns indicated that water did not have a tendency to form extended islands of any structure. Our observed change from zero-order to first order desorption kinetics then suggests that initial adsorption into co-existing condensed and gas-like phases has been

reduced to adsorption as a single phase at larger exposures. Summarizing, the results from these three combined studies suggest that, prior to desorption and up to ~ 0.7 ML, water forms a two-phase system consisting of a condensed phase of (extended) hexamer rings in equilibrium with a 2-D water gas. Beyond 0.7 ML, the entire system "freezes" into a single condensed phase with (2√7x2√7)R19° structure from which first-order desorption is observed.

Following this line of reasoning, enough bare nickel surface remains to accommodate the two-phase water system at low total coverages up until, at least, a deuterium pre-coverage of 0.13 ML. TPD traces in figure 2b, 2c, and 2d attest to this by the unchanged transition from zero-order to first-order desorption kinetics in the high temperature peak prior to the appearance of the low temperature peak around 155 K. It seems that the presence of such small amounts of deuterium mostly results in reducing available surface area for water adsorption without modifying the interaction of water with either the surface or itself significantly. Both experimental and theoretical studies have addressed how hydrogen adsorbs at such low coverages. A HREELS study suggests that the (2x2)-2H structure, which saturates the surface at θ_D = 0.5 ML and which has also been observed with LEED [12], is likely also the dominant adsorption structure at much lower coverages and at a substrate temperature of 100 K [23]. Vibrational features of this structure remained visible down to θ_{D2O} = 0.05 ML. Theoretical studies [21,39] support that this (2x2)-2H structure is more stable than the previously claimed p(2x2) structure [12], which could also exist in the range $0 < \theta_D < 0.25$ ML. Regardless, deuterium must obviously forms islands if it retains any of these structures at low coverages. With this in mind, it seems plausible that at the pre-coverages used in Figure 4.2b-2d, atomically-bound deuterium and water are not mixed on the surface but are adsorbed in separate islands. If they were mixed, the delicate balance between hydrogen bonding and the water-metal interaction [15] would be affected and result in measurable changes in TPD spectra. Therefore, we propose that water and atomically-bound hydrogen are phase segregated while both interact directly with the Ni(111) surface for these co-adsorption coverages. It may be that post-adsorption of water actually limits the mobility of atomic deuterium on the surface and enforces complete coalescence of a 2D atomic deuterium gas into deuterium islands.

If phase separation takes place, one may expect that it should be possible to use water as a titrant for the remaining bare nickel surface area after partial hydrogen adsorption. Indeed, this could provide a quantitative value for the hydrogen surface density at very low coverages, from which adsorption structures may be deducted or ruled out. A plot of the amount of water desorbing in the high temperature TPD feature as a function of deuterium pre-coverage, yields a slope that represents the area blocked for water adsorption by deuterium. If both axes are expressed in terms of their maximum coverage (here 1 ML), island formation of deuterium in a p(2x2) structure would yield a slope of 4, since at θ_D = 0.25 ML the entire surface would be covered by this structure and no bare nickel surface remains for water adsorption. For a (2x2)-2D structure, it would result in a value of 2. Figure 4.4 is such a plot for a post-dose of ~1.0 ML D_2O. The upper trace represents the integrated area for water interacting with bare patches of the nickel surface as a function of D-coverage. The slope in the range θ_D = 0 - 0.1 ML equals ~2.5, whereas it flattens to 0.3 up to θ_D = 0.3 ML. Although the initial slope seems to agree reasonably well with a (2x2)-2D structure, we caution for qualifying this as strong evidence, since we have noticed partitioning between the low and high temperature peaks at θ_D = 0. Partitioning here is likely a result of the experimental method and apparatus used to deposit water onto the surface. The interpolation in figure 4.4 may underestimate the slope at very low values of θ_D since the high temperature peak has not reached its maximum value for, at least, the data shown for θ_D = 0 ML. Partitioning due to experimental procedures without being a consequence of hydrogen co-adsorption may also be present in data at slightly higher deuterium coverages. To check whether we can circumvent this complication, we have also performed the TPD decomposition for a wide range of θ_D using $\theta_{D2O} > 1.0$ ML with the more elaborate TPD fitting procedure mentioned in the experimental section. As mentioned before, results are more ambiguous at larger water coverages due to overlap of the TPD peaks, the required assumption of a particular analytical form to fit data, and the presence of pump tails. However, in all attempts to determine the slope using water as a titrant, we find values between 2 and 4 for $\theta_D < 0.1$ ML. Although these values are not inconsistent with hydrogen adsorbing in (mixed) islands of above mentioned structures, and perhaps

also without island formation, we do not feel that our analysis here is conclusive and attribute the scatter to the above mentioned assumptions in the TPD fitting procedure.

Returning to figure 4.4, we find another aspect noteworthy. In the range $0.1 < \theta_D < 0.3$ ML, the amount of water that desorbs in the high temperature peak diminishes only modestly. At $\theta_D = 0.3$ ML, we find $\theta_{D2O} = 0.6$ ML for the high temperature peak. This is significantly more (and beyond the uncertainty of our fitting procedure) than would fit onto the remaining bare surface if deuterium adsorbed as the more dense (2x2)-2D islands. We offer two possible explanations for this observation. First, growth of water islands may compress (2x2)-2D islands into partial (1x1)-D structures. Coexistence of the (2x2)-2D and (1x1)-1D structures has been observed for $0.5 < \theta_D < 1.0$ ML [12]. DFT calculations indicate that there is an energetic penalty for creation of (1x1)-1H from (2x2)-2H of 50 meV/H atom [21]. Energy differences between hydrogen-bonding and water-metal bonding for Ni(111) may be similar, although theoretical studies do not agree on the binding energy of a water molecule to the surface [27,28]. A recent LEED study suggests that energy differences between various structures that water may assume on the surface are likely small [15]. A second explanation for the almost unchanged partitioning in figure 4.4 for $0.1 < \theta_D < 0.3$ ML may be provided if water islands spill over onto hydrogen islands. The binding energy of such spill-over water molecules may only be diminished modestly in order for these to desorb as part of the high temperature TPD feature. This could be the case if the lateral hydrogen bonding is mostly retained.

The results shown in figure 4.6 can be interpreted to support either explanation. For a fixed amount of 0.35 ML D_2O, figure 4.6b shows that water desorption is not strongly affected by a deuterium pre-coverage up to approximately $\theta_D = 0.30$ ML. Beyond $\theta_D = 0.30$ ML, the rate of decline of the peak desorption temperature increases almost 10-fold. A second sharp turn in figure 4.6b occurs at $\theta_D = 0.5$ ML. Picking up the original idea that deuterium adsorbs as (2x2)-2D islands, it is logical that phase-separated hydrogen and water islands show no strong effects up to $\theta_D = 0.30$ ML, since, combined, they cover 95% of the surface. If deuterium remains adsorbed in this structure there is no bare nickel surface left at $\theta_D = 0.5$ ML. In the 'compression' scenario, the second inflection in figure 4.6b is then a result of not having any of the post-dosed water interacting with the bare

nickel surface to initiate compression of the deuterium layer. In the 'spill-over' scenario, an increasing fraction of the 0.35 ML post-dosed water is adsorbed by extending water islands over deuterium-covered regions.

However, when considering the size of the available patches of bare nickel surface left over when 0.3 ML deuterium adsorb as randomly distributed (2x2)-2D islands, it seems related to the size of hexamer ring structures, $(D_2O)_6$, which were deducted from RAIRS spectra [29]. The number of hydrogen bonds per water molecule is higher for ring structures (up to 1.5 per H_2O) than for linear chains (up to 1.0 per H_2O). A random distribution of (2x2)-2D islands at θ_D = 0.3 ML leaves almost no bare nickel patches large enough to grow single ring structures and extensions from it, let alone for θ_D closer to 0.5. Therefore, we find that our observations are most easily explained if deuterium remains adsorbed mostly in a (2x2)-2D structure up to 0.5 ML with water molecules forming smaller and more disordered structures (e.g. short linear and branched chains) in between. The disordered water clusters are increasingly destabilized as a result of having fewer hydrogen bonds with increasing deuterium pre-coverage. This causes an increasingly lowered binding energy and lowered desorption temperature.

Two different observations suggest that water does not initially form a multilayered structure when a larger amount of water is dosed than which 'fits' into the empty nickel surface area in the range $0.1 < \theta_D < 0.3$ ML. First, the 155 K feature known to represent multilayer formation of water in TPD spectra does not appear in figure 4.6a as it does in figure 4.2b-2e. Instead we see a gradual shift to lower desorption temperatures, indicative of a gradual change in binding energy. Second, we do not observe the 28 meV feature indicative of multilayer formation in figure 4.7 up to $\theta_D > 0.5$ ML. The peak just appears as a shoulder on the elastic peak for θ_{D2O} = 0.35 ML with θ_D = 0.47 ML. Therefore, some spill-over seems to occur prior to formation of a multilayer in this regime.

With this description of water adsorption at the metal interface with deuterium pre-coverage ranging from 0 to 0.3 ML, we can now revisit the TPD features observed in figure 4.2b-2e. For low total coverages, separate deuterium and water islands are formed. When the remaining bare nickel surface area is large enough, water assumes a two-phase system at equilibrium. With increasing water dose, a point is reached where the additional water

cannot be accommodated on the bare metal surface. Depending on the size of the deuterium islands, water either adsorbs as a multilayer or spills over onto deuterium islands. The shapes and shifts of traces in figure 4.2e (and to some extent in 2d) suggest that spill over is also followed by growth of a (disordered) multilayer for higher doses. The two HREEL spectra for the larger total coverages in figure 4.5 confirm this suggestion through the appearance of the 28 meV feature.

Having discussed water adsorption on lower pre-coverages, we turn to deuterium pre-coverages of ~0.5 ML and higher. Figure 4.2f and 4.3 suggest that initially a small amount of water adsorb as water clusters onto a (mostly) saturated (2x2)-2D structure. These clusters grow laterally up to ~0.2 ML before acting as nucleation sites for 3D growth of disordered 'snowballs' that show approximate zero-order desorption kinetics. The increase in surface area with increasing radius of such, roughly, hemispherical structures would, at least qualitatively, result in the deviation of zero-order desorption kinetics as observed in figure 4.2f. The observed sudden changes in the leading edges may even suggest layer-by-layer growth of such 3D structures. Beyond $\theta_D > 0.5$ ML the peak desorption temperature (figure 4.6b) continues to drop slowly indicating that mixed (1x1)-1D and (2x2)-2D structures are also hydrophobic. When extrapolated to $\theta_D = 1.0$ ML we obtain from figure 4.6b the same desorption temperature as expected for 0.35 ML D_2O from our previous study in Chapter 3. Also, the typical 28 meV feature in HREEL spectra appears at very low water coverages as shown in the top trace in figure 4.7. A rough estimate based on relative intensities of HREEL features for the librations and the D_2O-D_2O normal translation suggests that for $\theta_D = 0.72$ ML and $\theta_{D2O} = 0.35$ ML, the hemispherical 'snowballs' are similar in thickness as the flatter structure created at $\theta_D = 0.30$ ML and $\theta_{D2O} = 0.90$ ML.

In Chapter 3 we attributed the 80 meV peak in D_2O HREEL spectra, as shown in figure 4.7, to the rocking motion of water molecules. We had found this feature to result from dipole scattering and suggested that this mode could be characteristic of the $(2\sqrt{7}x2\sqrt{7})R19^\circ$ structure. The other libration feature around 50 meV was attributed to the wag and twist motions of water molecules. However in figure 4.7, for $\theta_{D2O} = 0.35$ ML and $\theta_D = 0.13$ ML the 80 meV peak is still clearly observable, whereas in such case the formation of the 'frozen' $(2\sqrt{7}x2\sqrt{7})R19^\circ$ structure is not yet expected. Our data actually show that, with

increasing θ_D, the relative intensity of this peak decreases while the relative intensity of the wag and twist feature increases. This seems at odds with a description that attributes these features to a single species on the surface. As we discussed earlier, with increasing θ_D, we expect the mobility of free water molecules (2D gas) to be reduced up to a point where the entire system freezes. With the same increase, the relative number of free gas-like water molecules is decreased compared to the number in the condensed phase. At θ_D = 0.30 ML, the whole system seems frozen, and almost no free gas-like molecules are left. These considerations lead us to speculate that the 80 meV peak is actually related to librations of water molecules in a 2D gas, whereas the 50-75 meV peak results from librations in the condensed phase. We are aware of only one theoretical study that has addressed vibrational frequencies for single H_2O molecules on Ni(111). This study has predicted that the H_2O-Ni stretch, which may be expected to show strong dipole scattering, appears at 75 meV [28], in reasonable agreement with the strong loss observed at 80 meV.

Finally, we compare our results obtained for co-adsorption of D and D_2O on Ni(111) to similar data for Pt(111). For the latter, the most recent and detailed desorption spectra [9] indicates that post-dosing 2 ML D_2O on top of varying pre-doses of D initially results in stabilization of the water layer closest to the metal. Petrik and Kimmel show that, up to a D-atom density of 3.5×10^{14} cm^{-2} (which corresponds to ~0.25 ML when assuming a 1.0 ML D/Pt saturation coverage) a separate desorption peak with a maximum desorption temperature of ~5 K higher than the monolayer desorption peak, appears in TPD spectra. The new, higher temperature peak grows in at the expense of the original peak. At pre-coverages exceeding $\theta_D = 3.5 \times 10^{14}$ cm^{-2}, the D_2O desorption peak shifts back to lower temperatures (to ~170 K) and reduces in size. We distinguish two main differences between the effect of hydrogen pre-adsorption on water adsorption for Pt(111) and Ni(111). First, stabilization of water by atomic deuterium does not occur on Ni(111). On Pt(111), stabilization may be related to formation of H_3O^+ species [3]. No evidence was found for formation of such species on Ni(111) by TPD and HREELS as we discussed in Chapter 3. Second, at very large deuterium doses, water desorption from Pt(111) shows no reduction in binding energy of D_2O compared to the bare surface. On Ni(111), the drop in desorption temperature for small amounts of water adsorbed on a hydrogen overlayer reaches ~10 K.

Apparently, conversion of bare Ni(111) to H-covered Ni(111) makes the surface considerably more hydrophobic, whereas it does not on Pt(111).

The difference in the observed sign of the work function change upon dissociatively adsorbing hydrogen on these surfaces provides a possible explanation for this difference. On Pt(111), the work function decreases by 230 mV by adsorption of ~0.8 ML of the saturation coverage of hydrogen [40,41]. On Ni(111) a work function increase of 195 meV was observed upon adsorbing hydrogen [11]. The difference in hydrophobic character may therefore be a result of repelling (Ni) or attracting (Pt) local fields between D_2O_{ads} and D_{ads}.

A second explanation for the difference between the effect of hydrogen adsorption at large doses may be provided by analogy to the observed hydrophobic character of a monolayer of crystalline ice on Pt(111) grown at substrate temperatures above 135 K [38]. Here, hydrophobicity was argued to result from a lack of dangling OH bonds and lone pairs to interact with a second layer of water molecules. Water molecules in the first layer had previously been shown to bond alternatively through an oxygen lone pair and a hydrogen atom [42]. If a water (sub)monolayer grown at 85 K on Ni(111) also orders itself using Ni-HO bonds, pre-adsorption of hydrogen likely makes this type of bonding unfavorable, enforcing a different bonding structure. Experiments using rare gas [38], chloroform [43], or bromoform [44] adsorption may assist in judging whether the first layer of water on Ni(111) resembles the first crystalline ice layer grown on Pt(111).

4.5 Summary

Figure 4.8 summarizes our results regarding water adsorption onto a partially deuterium-covered Ni(111) surface. For $0 < \theta_D < 0.1$ ML and low θ_{D2O}, deuterium and water segregate into islands. Our data does not provide information on possible adsorption structures of D atoms, but strongly suggests that D_2O forms a two-phase system at equilibrium. We propose that it consists of a condensed phase, likely based on a hexamer ring structure ("hex", red), and a 2D gas phase (marked by single D_2O molecules, although this may not be the dominant species in that phase). This two-phase system is characterized by zero-order desorption kinetics and a distinct 80 meV feature in HREEL spectra. The latter may be related to the 2D gas phase. For $0 < \theta_D < 0.1$ ML and high θ_{D2O}, deuterium and water

islands are still phase segregated. D_2O has 'frozen' into a single phase prior to formation of a multilayer ("ML", purple). The multilayer gives rise to the 155 K desorption feature and a 28 meV loss in HREEL spectra. For $0.1 < \theta_D < 0.3$ ML, D atoms are most likely forming (2x2)-2D islands. At low θ_{D2O}, water and deuterium still phase segregate and D_2O forms the two-phase system as described before. For higher θ_{D2O}, additional D_2O spills over onto D-islands forming more disordered structures ("dis", orange) and/or multilayers. Spill-over versus multilayer formation is governed by the size of water and deuterium islands. In this range, desorption spectra show less discriminate increases in the high and low temperatures features. For $0.3 < \theta_D < 0.5$ ML, we suggest that water can no longer form hexagonally-based structures in direct contact with the nickel surface and that smaller water clusters in between deuterium islands form nucleation sites for growth of disordered 3D structures. For $\theta_D > 0.5$ ML, D_2O molecules initially cluster on a mixed (1x1)-1D / (2x2)-2D surface before growing 3D structures. The underlying deuterium layer is increasingly hydrophobic upon approaching saturation.

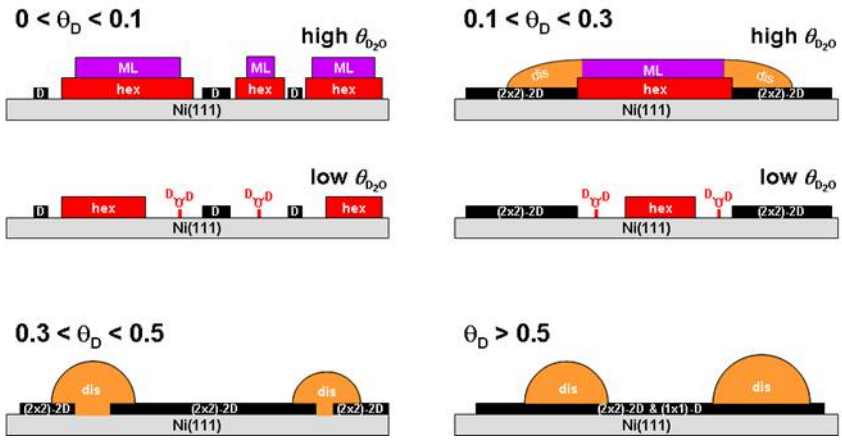

Figure 4.8 Schematic representations of adsorbed structures for water and deuterium. See text for details on color coding and abbreviations.

4.6 References

[1] M. A. Henderson, *Surf. Sci. Rep.*, 2002, **46**, 5.

[2] K. Jacobi, K. Bedurftig, Y. Wang, and G. Ertl, *Surf. Sci.*, 2001, **472**, 9.

[3] F. T. Wagner, and T. E. Moylan, *Surf. Sci.*, 1988, **206**, 187.

[4] S. K. Jo, J. A. Polanco, and J. M. White, *Surf. Sci.*, 1988, **253**, 233.

[5] G. B. Fisher, and J. L. Gland, *Surf. Sci.*, 1980, **94**, 446.

[6] J. Schott, D. Lackey, and J. K. Sass, *Surf. Sci.*, 1990, **238**, L478.

[7] N. Chen, P. Blowers, and R. I. Masel, *Surf. Sci.*, 1999, **419**, 150.

[8] N. Kizhakevariam, and E. M. Stuve, *Surf. Sci.*, 1992, **275**, 223.

[9] N. G. Petrik, and G. A. Kimmel, *J. Chem. Phys.*, 2004, **121**, 3727.

[10] C. D. Taylor, R. G. Kelly, and M. Neurock, *J. Electrochem. Soc.*, 2007, **154**, F55.

[11] K. Christmann, O. Schober, G. Ertl, and M. Neumann, *J. Chem. Phys.*, 1974, **60**, 4528.

[12] K. Christmann, R. J. Behm, G. Ertl, M. A. Van Hove, and W. H. Weinberg, *J. Chem. Phys.*, 1979, **70**, 4168.

[13] A. Winkler, and K. D. Rendulic, *Surf. Sci.*, 1982, **118**, 19.

[14] K. Mortensen, F. Besenbacher, I. Stensgaard, and W. R. Wampler, *Surf. Sci.*, 1988, **205**, 433.

[15] M. E. Gallagher, S. Haq, A. Omer, and A. Hodgson, *Surf. Sci.*, 2007, **601**, 268.

[16] T. E. Madey, and F. P. Netzer,, *Surf. Sci.*, 1982, **117**, 549.

[17] R. H. Stulen, and P. A. Thiel, *Surf. Sci.*, 1985, **157**, 99.

[18] T. Pache, H. P. Steinruck, W. Huber, and D. Menzel, *Surf. Sci.*, 1989, **224**, 195.

[19] C. Mundt, and C. Benndorf, *Surf. Sci.*, 1993, **287/288**, 119.

[20] B. Bhatia, and D. S. Sholl, *J. Chem. Phys.*, 2005, **122**, 204707.

[21] J. Greeley, and M. Mavrikakis, *Surf. Sci.*, 2003, **540**, 215.

[22] R. Baer, Y. Zeiri, and R. Kosloff, *Phys. Rev. B*, 1997, **55**, 10952.

[23] H. Yanagita, J. Sakai, T. Aruga, N. Takagi, and M. Nishijima, *Phys. Rev. B*, 1997, **56**, 14952.

[24] A. C. Luntz, J. K. Brown, and M. D. Williams, J. Chem. Phys., 1990, **93**, 5240.

[25] K. Christmann, *Surf. Sci. Rep.*, 1988, **9**, 1.

[26] G. X. Cao, E. Nabighian, and X. D. Zhu, *Phys. Rev. lett.*, 1997, **79**, 3696.

[27] M. Pozzo, G. Carlini, R. Rosei, and D. Alfè, *J. Chem. Phys*., 2007, **126**, 164706.

[28] H. Yang, and J. L. Whitten, *Surf. Sci.*, 1989, **223**, 131.

[29] M. Nakamura, and M. Ito, *Chem. Phys. Lett.*, 2004, **384**, 256.

[30] J. Shan, J. F. M. Aarts, A. W. Kleyn, and L. B. F. Juurlink, *Phys. Chem. Chem. Phys.*, 2008, **10**, 2227; this thesis chapter 3.

[31] C. T. Campbell, and S. M. Valone, *J. Vac. Sci. Technol. A.*, 1985, **3**, 408.

[32] A. M. Dejong, and J. W. Niemantsverdriet, *Surf. Sci.*, 1990, **233**, 355.

[33] A. D. Johnson, K. J. Maynard, S. P. Daley, Q. Y. Yang, and S. T. Ceyer, *Phys. Rev. lett.*, 1991, **67**, 927.

[34] H. Ibach, and D. L. Mills, *Electron Energy Loss Spectroscopy and surface Vibrations*, Academic Press, New York, 1982.

[35] G. J. Schulz, *Rev. Mod. Phys.*, 1973, **45**, 423.

[36] B.A. Sexton, *Surf. Sci.*, 1980, **94**, 435.

[37] J. L. Daschbach, B. M. Peden, R. S. Smith, and B. D. Kay, *J. Chem. Phys.*, 2004, **120**, 1516.

[38] G. A. Kimmel, N. G. Petrik, Z. Dohnalek, and B. D. Kay, *Phys. Rev. Lett.*, 2005, **95**, 166102.

[39] G. Kresse, and J. Hafner, *Surf. Sci.*, 2000, **459**, 287.

[40] K. Christmann, G. Ertl, and T.Pignet, *Surf. Sci.*, 1976, **54**, 365.

[41] K. Christmann, and G. Ertl, *Surf. Sci.*, 1976, **60**, 365.

[42] H. Ogasawara, B. Brenda, D. Nordlund, M. Nyberg, A. Permenschikov, L. G. M. Pettersson, and A. Nilsson, *Phys. Rev. Lett.*, 2002, **89**, 276102.

[43] G. Zimbitas, and A. Hodgson, *Chem. Phys. Lett.*, 2006, **417**, 1.

[44] M. L. Grecea, E. H. G. Backus, H. J. Fraser, T. Pradeep, A. W. Kleyn, and M., Bonn, *Chem. Phys. Lett.*, 2004, **385**, 244.

Chapter 5

Identification of Hydroxyl on Ni(111)

Hydroxyl (OH) is identified and characterized on the Ni(111) surface with high resolution electron energy loss spectroscopy. We find clear evidence of stretching, bending and translational modes that differ significantly from modes observed for H_2O and O on Ni(111). Hydroxyl may be produced from water using two different methods. Annealing of water co-adsorbed with atomic oxygen at 85 K to above 170 K leads to creation of OH with simultaneous desorption of excess water. Pure water layers treated in the same fashion show no dissociation. However, exposure of pure water to 20 eV electrons below 120 K produces OH in the presence of adsorbed H_2O. In combination with temperature-programmed desorption studies, we show that OH groups recombine between 180 and 240 K to form O and immediately desorbing H_2O. The lack of influence of co-adsorbed H_2O at 85 K on the hydroxyl's O-H stretching mode indicates that OH does not participate in a hydrogen-bond network.

5.1 Introduction

Hydroxyl adsorbed on metal surfaces (OH) has attracted much attention in recent years [1-10]. This is not surprising considering the central role of OH as a reaction intermediate in many heterogeneously catalyzed and electrochemical reactions. Despite considerable efforts, understanding of the formation and reaction pathways and the geometry of adsorbed OH, including its dependence on surface structure and co-adsorbates, remains limited.

Fisher and Sexton were the first to demonstrate formation of OH on a metal single crystal by means of high resolution electron energy loss spectroscopy (HREELS) and ultraviolet photoelectron spectroscopy (UPS) [1]. Annealing of water molecules adsorbed on oxygen pre-covered Pt(111) produced OH above 155 K. Formation of OH from the H_2O + O reaction on this surface was confirmed later by other groups employing various techniques [2,3], whereas water adsorption on clean Pt(111) is non-dissociative [11,12]. Besides the possibility of creating OH from co-adsorbed water and atomic oxygen, Mitchell and White reported OH production in an intermediate stage of the catalytic H_2 oxidation by O_2 on Pt(111) [4], although they noticed differences when comparing their HREEL spectra with Fisher and Sexton's. Later, Germer and Ho also observed OH during the H_2 oxidation by means of time-resolved EELS [5]. Their EEL spectra were more consistent with Fisher and Sexton's. Recently, discrepancies between these studies were explained by Ertl and co-authors [2]. They investigated the properties of OH on Pt(111) by means of HREELS and scanning tunneling microscopy (STM). In their studies, the properties and formation of OH under these two different reaction conditions were both studied and compared. Discrepancies between earlier studies were explained by the different degree of order under the different reaction conditions used to produce OH. Although such studies have shed light on the formation of OH on Pt(111), controversies persist. For example, HREELS studies have suggested that the adsorption site of OH is the three-fold hollow site [4,13], while STM, HREELS, low energy electron diffraction (LEED), and density functional theory (DFT) studies suggest preference for the top site [2,3].

Since the early studies by Fisher and Sexton, adsorbed OH has been identified on several other metal surfaces, e.g. Pd(100) [14], Si(100) [15], Ni(110) [16,17] most often by HREELS. Oddly, OH has not yet been identified on Ni(111), which is the dominating

surface structure on nickel catalyst particles. Adsorbed OH on this surface is therefore expected to be relevant to large industrial processes, such as methane steam reforming, but also to small scale applications, such as alkaline fuel cells. To date, spectroscopic studies for co-adsorption of H_2O with O on Ni(111) are inconsistent. From temperature programmed desorption (TPD) studies, Madey and Netzer suggested formation of OH as a result of annealing co-adsorbed H_2O+O above 120 K [6], whereas UPS studies by Pache *et al.* conclude that no OH forms under the same conditions [18]. Both suggestions were supported by later studies using reflection-adsorption infrared spectroscopy (RAIRS) [10], combined TPD and UPS [19], and TPD and X-ray photoelectron spectroscopy (XPS) [20]. Clear and unambiguous identification of OH on Ni(111) is currently lacking. Theoretical studies for OH on Ni(111) have so far focused on adsorption energy, site and geometry, concluding that OH is preferentially adsorbed on the three-fold hollow site with its O-H axis almost perpendicular to the surface [7,9,21].

In this Chapter, we use HREELS, Auger Electron Spectroscopy (AES) and TPD to study a single H_2O layer and H_2O co-adsorbed with O on Ni(111). We focus our attention on spectroscopic identification of species that are present before and after annealing these systems to various temperatures. Additionally, we have used electron bombardment of the pure H_2O layer to help us identify reaction products.

5.2 Experimental

Experiments are carried out in an UHV system, which consists of two chambers. The top chamber is equipped with an ion sputter gun, an atomic hydrogen source, a bakeable UHV leak valve, a movable tungsten filament, a home-built capillary array doser [22], and a quadrupole mass spectrometer (Balzers QMS 422) used for TPD measurement and residual gas analysis. The lower chamber contains an upgraded ELS 22 high resolution electron energy loss spectrometer and a double-pass CMA Auger electron spectrometer (Staib Instruments). The top and lower chambers are separated by a gate valve. The typical base pressure of the system is less than 1×10^{-10} mbar.

The Ni(111) single crystal, cut and polished to less than 0.1º of the low Miller-index plane (Surface Preparation Laboratories, Zaandam, the Netherlands), can be heated to 1200

K by electron bombardment and cooled to 85 K. The crystal temperature is measured by a chromel-alumel thermocouple spot-welded to the edge of the crystal. The crystal is cleaned by Ar^+ sputtering, annealing at 1100 K, followed by oxidation in 10^{-7} mbar of O_2 and reduction in 10^{-6} mbar of H_2. After cleaning, the surface cleanliness is verified by AES. H_2O (18.2 MΩ/cm resistance) is cleaned by repeated freeze-pump-thaw cycles after which helium (Messer, 99.999%) is introduced to the glass water container to a total pressure of approximately 1 bar. To increase water dosing accuracy, we monitor the helium partial pressure in the vacuum chamber when dosing water. H_2O is dosed through the capillary array doser, which is placed 15 mm in front of the sample. Water coverages are estimated from integrated TPD traces. A detailed description of our conversion of a TPD integral to absolute water coverage is presented in Chapter 3 or Ref 23. Atomic oxygen on the surface is produced from dissociative adsorption of O_2 [24], which we dose through the leak valve. The oxygen coverage is estimated using AES. In particular, we use the integrated AES feature near 513 eV for a 0.25 ML O-coverage from O_2 dissociation as a reference [10,25,26] when determining smaller O-coverages for the same integrated feature. All TPD measurements were performed with a heating rate of 1.0 K/s. The HREEL spectra were recorded at 5 to 9 meV resolution (FWHM) with typical 1×10^4 cps for the scattered elastic peak.

5.3 Results and Discussion

5.3.1 TPD Spectra

Figure 5.1 displays a set of TPD spectra of H_2O on clean and oxygen pre-dosed Ni(111). The sample temperature was kept at 85 K while dosing H_2O through the capillary array doser. Trace 5.1A is a TPD spectrum of H_2O desorption from clean Ni(111) without additional treatment. Trace 5.1B shows the TPD spectrum of H_2O desorption from the ~0.05 ML atomic oxygen pre-covered surface. In trace 5.1C, H_2O is adsorbed on the clean surface at 85 K before exposing the front of the crystal to 20 eV electrons for 100 s. Electrons are created by heating the moveable tungsten filament while acceleration of electrons toward the crystal is achieved by applying a potential of +20 eV to the crystal relative to the grounded filament. During electron bombardment, the crystal temperature

increases to ~120 K. The electron beam current is ~0.1 mA. After exposure to electrons, the crystal is cooled to 85 K before taking a TPD spectrum.

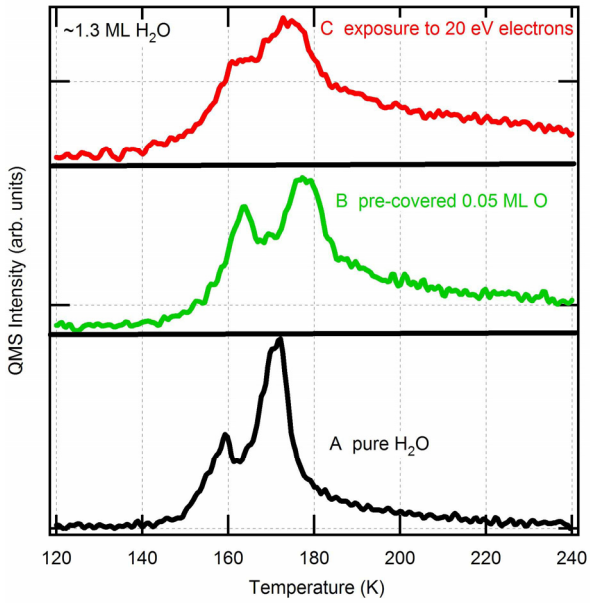

Figure 5.1 TPD of ~ 1.3 ML H_2O on clean and atomic oxygen pre-covered Ni(111) surface.

First, we focus on the trace 5.1A. The spectrum clearly shows two distinct desorption features: a high temperature peak at ~ 170 K and a low temperature peak at ~ 160 K. Such spectra corresponding to water desorption from clean Ni(111) have already been studied in detail before [6,18,19,23,27,28]. It is generally agreed that the high temperature peak is due to desorption from a (sub-)monolayer coverage of water interacting directly with the Ni(111) surface. The low temperature peak is due to desorption of multilayers of water. With increasing coverage, the (sub-)monolayer peak reaches saturation, while the multilayer peak does not saturate. For clarity, we only show a desorption trace of ~1.3 ML H_2O here. More traces with a wide coverage range can be found in Chapter 3 and 4.

In trace 5.1B desorption of H_2O from oxygen pre-covered Ni(111) shows two clear desorption features and a broad tail at higher temperatures, as observed previously by other groups [6,18,20]. These early studies ascribe the feature at ~ 162 K to desorption of water multilayers, while the feature at ~ 176 K is attributed to the (sub)monolayer desorption. The

observed shift from 170 to 176 K for this peak has generally been attributed to an increase in bond energy for water adsorbed to the surface when co-adsorbed with atomic oxygen. We observe a third, broad feature reaching up to above 240 K. It is generally described as occurring between ~ 180 K and ~ 240 K [6,18,20]. Two interpretations have been proposed for the appearance of this broad peak. The first interpretation suggests initial OH formation from reaction of H_2O + O with, at higher temperatures, reaction in the reverse direction [6,19]. The second interpretation attributes this feature to intact H_2O molecules directly chemisorbed on the Ni(111) surface [16,20]. Here, the new higher temperature feature was suggested to result from varying bond energies and differing H_2O-H_2O interactions.

Trace 5.1C shows three features which are very similar to those in the middle spectrum. Most prominently, the impact of electrons on the pure H_2O surface results in the same additional high temperature desorption feature between 180 and 240 K observed when co-adsorbing the same amount of water with ~0.05 ML atomic oxygen.

It is well known that energetic electrons impacting onto adsorbed water molecules may lead to dissociation of water into OH_{ads} and H_{ads} [29,30]. Also, TPD studies of recombination of OH on metal surfaces e.g. Pt(111) [1], Pt(110) [31], Pd(110) [32], show an additional high temperature desorption feature above 200 K [11,12]. The presence of the high temperature feature in TPD spectra 5.1B and 5.1C then suggests which of the two proposed origins for the broad high temperature feature is most likely: Co-adsorption with atomic oxygen, similar to impacting electrons, leads to formation of OH with consecutive recombination of OH to form H_2O and O between 180 and 240 K. To test this suggestion more stringently, we study the changes in vibrational features observed at various conditions and treatments in the next section. In this study, we do not pay particular attention to the H_{ads} created by electron impact. It may desorb instantaneously, recombine with OH_{ads} to form H_2O in competition with reaction between two adsorbed hydroxyl groups to form H_2O + O_{ads}, recombine with O_{ads} if the latter is formed from reaction between hydroxyl groups, or desorb as H_2 at higher temperatures.

5.3.3 Vibrational Spectra

HREEL spectra of ~1.1 ML H_2O adsorbed on Ni(111) pre-covered by ~0.05 ML atomic oxygen are shown in Figure 5.2 with various amplified regions. All spectra were recorded

at the specular angle with an impact energy of 5.0 eV. Trace 5.2A is a spectrum taken directly after preparing the system at 85 K. For trace 5.2B, we have annealed the system to 150 K for 100 s, followed by cooling to 85 K prior to collecting the spectrum. For trace 5.2C, we again annealed the same system for 100 s, but at the increased temperature of 170 K, followed by cooling to 85 K. Finally, for trace 5.2D, we have annealed the sample to 250 K for 100 s, followed by cooling. Annealing to 155 K in the first step leads to no changes compared to annealing to 150 K. When omitting the first annealing step and proceeding directly to annealing the system to 170 K, the same HREEL spectrum appears as shown in trace 5.2C. Changing the atomic oxygen pre-coverage to approximately 0.25 ML, while keeping the water coverage and annealing-cooling procedures the same, does also not result in any significant changes when compared to the HREEL spectra shown in Figure 5.2.

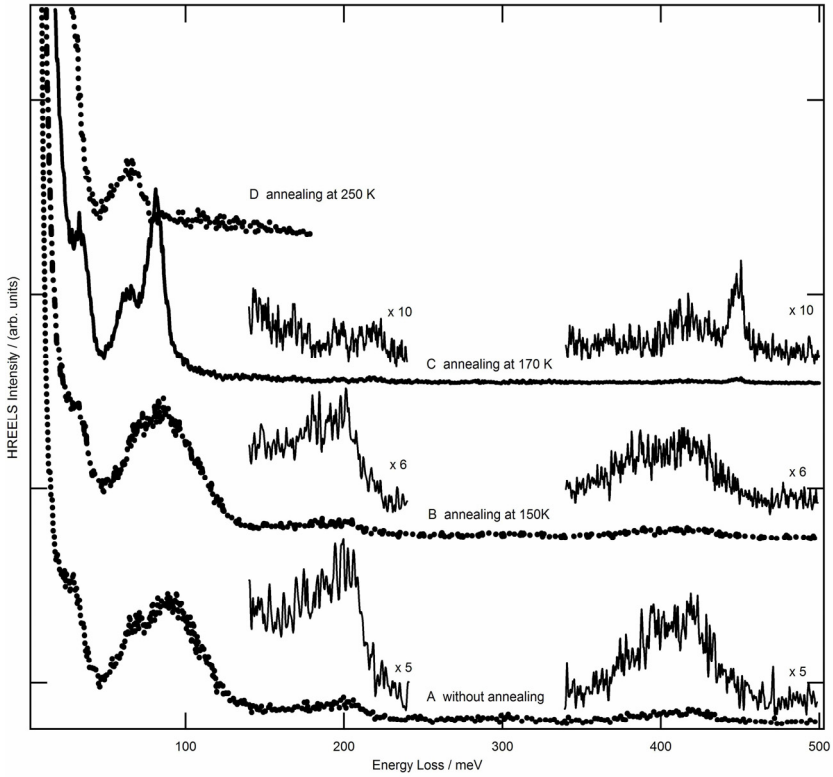

Figure 5.2 HREEL spectra of 1.1 ML H_2O co-adsorbed with ~0.05 ML atomic oxygen on Ni(111), followed by various annealing procedures.

In trace 5.2A, there are four distinct features, centered near 30, 90, 200, and 420 meV. The spectrum strongly resembles the spectrum of a comparable amount of H_2O adsorbed on clean Ni(111), showing the same positions and shapes of these features. A detailed analysis of the HREEL spectrum for H_2O/Ni(111) can be found in Chapter 3 and 4. In accordance with earlier assignments, we ascribe the 30 meV feature to H_2O's frustrated translation normal to the surface in a second or higher water layer. These H_2O molecules are hydrogen-bound to water molecules in lower layers, resulting in a (nearly) surface-independent frequency. The broad feature centered at 90 meV is ascribed to the librational modes of H_2O, which we can not resolve. The 200 meV feature is ascribed to the H-O-H bending mode. Finally, the 420 meV feature results from the O-H stretch mode in a hydrogen-bonded network. The shoulder near 70 meV on the low energy side of the 90 meV feature is most likely due to the Ni-O stretch. HREEL spectra of atomic oxygen on Ni(111) have previously identified this vibration at 70 meV [26,30]. We therefore conclude that spectrum A is the combined spectrum of O_{ads} and H_2O_{ads} and shows no additional features that may be related to formation of OH or other new species on the surface resulting from co-adsorption at 85 K. On Pt(111), the same conclusion was drawn for a similarly prepared system [1].

Trace 5.2B shows that annealing the O + H_2O layer on Ni(111) to 150 K (not shown is the same trace at lower resolution for 155 K) does not result in any significant changes. The four peaks described previously still occur at the same energies and with the same relative intensities. No new features appear. In contradiction to previous investigations that claim formation of OH near 120 K from H_2O + O on the basis of TPD and electron simulated desorption ion angular distribution (ESDIAD) techniques [6], we find no vibrational spectroscopic evidence for such reaction up to 155 K.

Trace 5.2C indicates that annealing to 170 K does result in significant changes in the species present on the Ni(111) surface. First, we find that features at 420 and 200 meV have (almost) entirely disappeared. A new, sharp feature appears at 450 meV. Also, the broad feature centered at 90 meV has been replaced by a much sharper and more intense feature centered at 83 meV. The shoulder peak observed near 70 meV in traces 5.2A and 5.2B now

appears more pronounced at 65 meV. Finally, careful inspection of the peak at the lowest energy indicates a shift from 30 meV in trace A and B to 34 meV in trace 5.2C.

Annealing to 250 K leads to a loss of all characteristic vibrational features except the feature around 65-70 meV, previously identified as the Ni-O stretch. We only show the highest resolution spectrum, which focuses on the regime up to 180 meV. Spectra taken at lower resolution over the entire energy range show no vibrational losses at higher energy.

First, we discuss the presence of water on the surface using both TPD and HREEL spectra from figures 5.1 and 5.2. In the vibrational spectra 5.2A and 5.2B, H_2O's characteristic stretching and bending frequencies at 420 and 200 meV are clearly present. TPD trace 5.1B shows that H_2O multilayers are not expected to desorb rapidly at 150 K and the continued presence of some multilayered water is confirmed by the H_2O-H_2O frustrated translational mode at 30 meV in trace 5.2B. In short, annealing to 150 K for 100 s does not affect the system as prepared.

Desorption of water occurs when annealing at higher temperatures. Multilayered water desorbs most rapidly near 160 K for this coverage. Monolayer desorption likely has an onset near the same temperature, but the convolution of desorption peaks in trace 5.1B renders us unable to identify a unique onset for such desorption. The large differences in the vibrational spectra shown in 5.2B and 5.2C strongly suggest that the chemical identity of species on the surface has also changed after annealing to 170 K. However, trace 5.1B shows that H_2O is still being produced at much higher temperatures. It appears that annealing ~1 ML H_2O co-adsorbed with ~0.05 ML O_{ads} to 170 K results in partial desorption of H_2O with a simultaneous chemical change at the surface that continues to yield water desorption at higher temperatures. From trace 5.2D, we conclude that, upon complete desorption of H_2O, adsorbed oxygen atoms remain.

The vibrational features in trace 5.2C shed light on the identity of the species present after annealing to 170 K. Starting with the highest energy loss, we note that the narrow peak appearing at 450 meV on Ni(111) is very close to the non-hydrogen-bonded O-H stretching frequency generally observed in a water network (around 458 meV) [34,35]. However, two arguments contest the assignment of this feature to non-hydrogen-bonded water. First, the appearance of this feature is not accompanied by an energy loss in the

regime for H-O-H bending vibrations. It seems very unlikely that the significant intensity of the stretch vibration could be associated with little or negilible intensity for the accompanying bending vibration. Second, in Chapter 4 we have found that in a regime where water coexist on the Ni(111) surface as a condensed phase and a lattice gas, the lattice gas shows a very strong and characteristic energy loss at 105 meV. This feature is clearly present in all spectra when non-hydrogen-bonded water molecules can coexist with hydrogen-bonded colleagues, but is not present in trace 5.2C. For these reasons we find it unlikely that the sharp feature at 450 meV results from intact water molecules bound in some way to the nickel lattice with an additional presence of 0.05 ML oxygen.

Adsorbed OH is a more likely the origin of the observed energy loss at 450 meV and the other changes observed between spectra 5.2B and 5.2C. First, the O-H stretching frequency is reported at 450 meV for free OH radicals [36]. As non-hydrogen-bonded OH, hydroxyl's stretch frequency appears at similar frequencies on Si(100) (463 meV) [15], and Pt(111) (456 meV) [37]. We note that the stretch frequency for OH in $\beta Ni(OH)_2$ has also been observed around 460 meV by inelastic neutron scattering (INS) [38]. Second, a bending frequency in the vicinity of 200 meV would not be expected for OH. We also do not observe a feature near this frequency. Instead, we observe a strong feature at 83 meV, which is reminiscent of the OH-bending frequency reported for OH on Ni(110) at 84 meV [17]. Finally, the appearance of a feature at 34 meV is consistent with the hindered translational modes of OH. On Pt(111) two separate features appear at 43 and 29 meV [2]. In trace 5.2C, this particular feature cannot result from multilayered water as TPD trace 5.1B indicates that multilayers have desorbed after annealing to 170 K. Our observation of a single mode instead of two on Pt(111) may result from our poorer resolution.

Considering the possible geometries for OH on a surface, a number of point groups and corresponding dipole active modes may be identified [39]. For an OH molecule adsorbed with its axis strictly along the surface normal point groups e.g. C_{6v}, C_{3v} and C_{2v} may be possible. However, such geometries are not very likely as OH is known to strongly tilt away from the surface normal on Pt(111) [2,3], and theoretical investigations for OH on Ni(111) predict a tilted geometry [7, 9, 21] with a 10º difference between the O-H bond axis and surface normal [7]. The reduced symmetry leads to point group C_S for OH

adsorbed on the three-fold hollow, the bridge and top sites if the symmetry plane for the O-H group is also a symmetry plane of the bare surface. For C_S, four dipole active modes and two impact scattering modes are expected. The dipole active modes may be described as the O-H stretch, Ni-OH stretch, OH rotation within the symmetry plane and OH translation within the symmetry plane. The impact scattering modes are the OH rotation and OH translation normal to the symmetry plane and are expected to be considerably less intense than the dipole active modes. Figure 5.3 presents an HREEL spectrum (C') taken at 10º from the specular angle. The spectrum was taken after the same treatment of the H_2O + O overlayer corresponding to spectrum C in figure 5.2. For comparison we repeat this spectrum in figure 5.3. We notice that all four peaks located near 450, 83, 65, and 34 meV, which only appear after annealing this overlayer, are dipole active. This observation strongly supports our attribution of the new peaks to hydroxyl groups. Considering the previous comparison to published spectra, the observed dipole activity allows us to identify the 450 meV feature as the dipole active O-H stretch, the 83 meV feature as the dipole active Ni-O-H bending motion in the symmetry plane, and the 34 meV feature as the dipole active OH translational mode within the symmetry plane. The feature at 65 meV must then correspond to the dipole active Ni-OH stretch, representing only a small shift from the frequency observed for the Ni-O stretch [26,33]. On Pt(111) a similar small frequency shift has been observed for hydrogenation of Pt-O [1,2]. We can not observe or unambiguously identify the two non-dipole active modes, which are expected to have significantly less intensity.

To further exclude other possible origins for our spectral features, we finally consider other O and H containing molecules and groups. We do not observe any feature around 106 meV, which is reported to be the O-O stretch mode for hydrogen polyoxides molecules [40,41]. Thus the formation of species in our experiments, e.g. HO_2 and H_2O_2 is not supported by our EELS data in 5.2C. Due to a lack of other potential intermediates, we conclude that the frequencies observed in trace 5.2C are due to the formation of OH from annealing H_2O and O on Ni(111) above 170 K. The continued formation of H_2O from this surface to much higher temperatures in TPD experiments implies that these hydroxyl fragments recombine to form H_2O which, above 170 K, immediately desorbs.

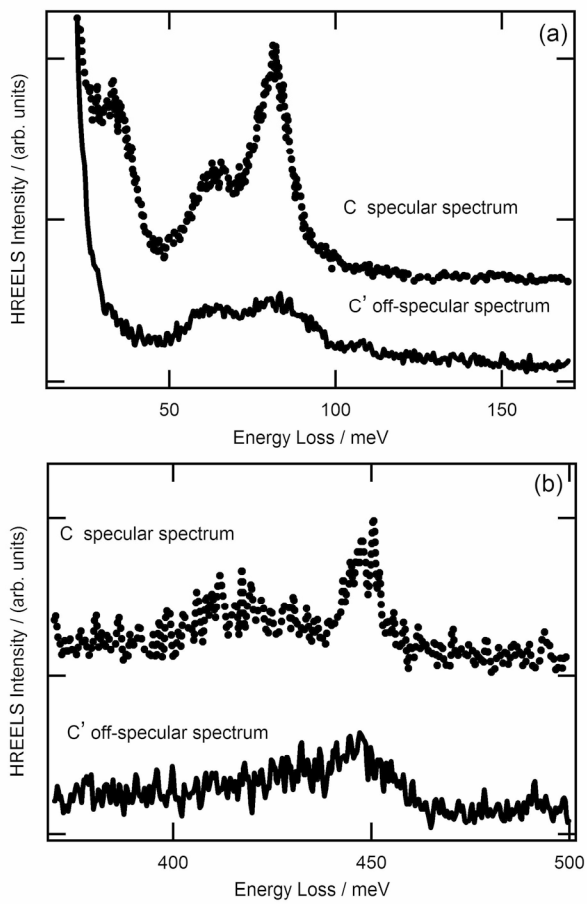

Figure 5.3 Off-specular (C') and specular (C) HREEL spectra in the range of a) 10 to 175 meV and b) 370 to 500 meV of ~1 ML H_2O co-adsorbed with ~0.05 ML atomic oxygen on Ni(111), followed by annealing to 170 K.

5.3.3 Hydroxyl co-adsorbed with water

Figure 5.4 shows HREEL spectra for the O-H stretching region for OH and H_2O under various conditions. Note that we use non-alphabetical numbering in this graph. Traces 5.4A and 5.4C are parts of the same spectra shown in figure 5.2 as traces 5.2A and 5.2C. For trace 5.4E, the Ni(111) crystal is first covered by ~ 1.1 ML H_2O at 85 K before exposing the front of the sample to 20 eV electrons for 100 s. After electron bombardment, a HREEL spectrum is recorded at 85 K. For trace 5.4F, the same treatment is applied, but after

exposure to electrons, we anneal the sample at 170 K for 100 s prior to acquiring the HREEL spectrum at 85 K.

Two features are observable in trace 5.4E: a broad feature centered at 420 meV and a sharp peak at 450 meV. As we noted before, impact of energetic electrons on adsorbed water has been shown to lead to dissociation and formation of hydroxyl species on various surfaces. The appearance of the 450 meV peak in trace 5.4E confirms that the same occurs on Ni(111). The 420 meV feature is most likely due to water molecules remaining on the surface after exposure the electrons, indicating that electron bombardment has only fragmented a fraction of the initially adsorbed water molecules. The absence of the broad feature at 420 meV in trace 4F confirms this assignment, since annealing the sample to 170 K for 100 s leads to complete desorption of molecularly-bound H_2O. The remaining feature at 450 meV in trace 5.4F results from adsorbed OH that has not yet reacted back to form H_2O.

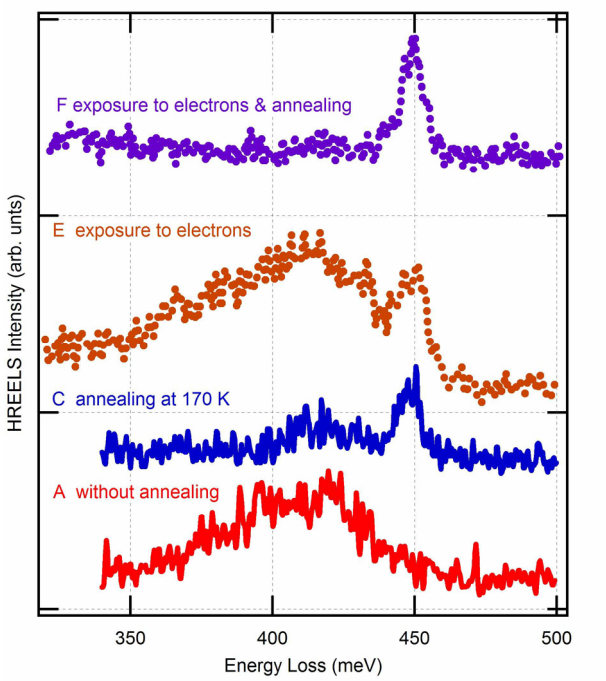

Figure 5.4 HREEL spectra of the O-H stretching range for OH and H_2O adsorbed on Ni(111) under various conditions.

Interestingly, the presence of water on the surface seems not to affect co-adsorbed OH. As discussed, OH in trace 5.4F is produced by exposure of a pure water layer to electrons, while in trace 5.4C it is produced by annealing H_2O + O to 170 K. In the latter case, very little water remains on the surface, whereas in the first case the OH is immersed in a layer of water, which we can remove by an additional annealing step. Comparing the energy loss of the hydroxyl's O-H stretching mode in traces 5.4C, 5.4E and 5.4F, we find that the center frequency and width are not affected by the presence water or the procedure employed to produce OH. We find this noteworthy for two reasons. First, the lack of change in this energy loss suggests that, even in the presence of ~1 ML of water, OH_{ads} is not involved in a hydrogen-bonded network of water molecules. Participation in such a network would have affected the O-H stretch frequency and width significantly. In addition, for Pt(111), the procedure for producing OH has been suggested to affect observed vibrational features. For OH on Ni(111) this is clearly not the case and OH can be identified unambiguously by a single set of frequencies.

The tendency of OH to participate in a hydrogen-bonded network or lack there-of may be related to the adsorption geometry of OH on the surface. For Pt(111), OH is suggested to bond with the O-H axis tilted toward to the surface on top sites [1-3]. In various relative concentrations to H_2O on Pt(111), LEED experiments suggest that OH simply replaces H_2O in hexagonal structures, creating a hydrogen-deficient water network. The deficiencies are present as missing H atoms above or below the network plane [42,43]. On Ni(111), the first water layer does wet the metal, as it does on Pt(111) [44,45], but the water structure is significantly different [27]. It has been suggested that differences are, at least in part, caused by the smaller lattice constant of Ni. Also, theoretical studies for OH on Ni(111) suggest that bonding of hydroxyl is more stable on three-fold hollow sites than on top or other sites [7,9,21]. The bond energy is calculated to be 8 times larger that the bond energy of H_2O to this surface (~80 vs. 10 kJ/mol) [7], and the O-H axis is predicted to be slightly tilted from the surface normal when adsorbed in absence of water. A continued preference for this bonding geometry in the presence of water would explain our observed results since this geometry does not allow for participation in hydrogen-bond networks which are oriented more parallel to the surface. The large bond energy of OH on the three-fold hollow site

strengthens this suggestion, since it significantly exceeds energies generally associated with hydrogen bond formation.

5.4 Conclusions

Based on HREEL and TPD spectra we identify the adsorbed hydroxyl species on the Ni(111) surface. Annealing of water on atomic oxygen pre-covered Ni(111) at 170 K or exposure of electrons to pure water on Ni(111) both lead to the hydroxyl formation. Recombination of hydroxyl is observed from ~ 180 K to ~ 240 K, leaving O_{ads} on the surface. The lack of a dependence of the O-H stretching mode to co-adsorbed water suggests that there is no hydrogen-bonding between OH and H_2O. This is in agreement with the prediction of an almost vertically bound OH on Ni(111).

5.5 References

[1] G. B. Fisher, and B. A. Sexton, *Phys. Rev. Lett.,* 1980, **44**, 683.

[2] K. Bedurftig, S. Volkening, Y. Wang, J. Wintterlin, K. Jacobi, and G. Ertl, *J. Chem. Phys.,* 1999, **111**, 11147.

[3] A. P. Seitsonen, Y. Zhu, K. Bedurftig, and H. Over, *J. Am. Chem. Soc.,* 2001,**123**, 7347.

[4] G. E. Mitchell, and J. M. White, *Chem. Phys. Lett*., 1987, **135**, 84.

[5] T. A. Germer, and W. Ho, *Chem. Phys. Lett*., 1989, **163**, 449.

[6] T. E. Madey, and F. P. Netzer, *Surf. Sci*., 1982, **117**, 549.

[7] H. Yang, and J. L. Whitten, *Surf. Sci*., 1989, **223**, 131.

[8] C. D. Roux, H. Bu, and J. W. Rabalais, *Surf. Sci*., 1992, **279**, 1.

[9] H. Yang, and J. L. Whitten, *Surf. Sci*., 1997, **370**, 136.

[10] M. Nakamura, M. Tanaka, M. Ito, and O. Sakata, *J. Chem. Phys.,* 2005, **122**, 224703.

[11] P. A. Thiel, and T. E. Madey, *Surf. Sci. Rep.,* 1987, **7**, 211.

[12] M. A. Henderson, *Surf. Sci. Rep.,* 2002, **46**, 5.

[13] G. Gilarowski, W. Erley, and H. Ibach, *Surf. Sci*., 1996, **351**, 156.

[14] E. M. Stuve, S. W. Jorgensen, and R. J. Madix, *Surf. Sci*., 1984, **146**, 179.

[15] H. Ibach, H. Wagner, and D. Bruchmann, *Solid State Commun.,* 1982. **42**, 457.

[16] L. Ollé, M. Salmeron, and A. M Baró, *J. Vacuum Sci. Technol. A,* 1985, **3**, 1866.

[17] M. Hock, U. Seip, I. Bassignana, K. Wagemann, and J. Küppers, *Surf. Sci., 1*986, **177**, L978.

[18] T. Pache, H.-P. Steinruck, W. Huber, and D. Menzel, *Surf. Sci*., 1989, **224**, 195.

[19] R. H. Stulen, and P. A. Thiel, *Surf. Sci*., 1985, **157**, 99.

[20] M. Schulze, R. Reißner, K. Bolwin, and W. Kuch, Fresenius. *J. Anal. Chem.*, 1995, **353**, 661.

[21] M. Pozzo, G. Carlini, R. Rosei, and D. Alfè, *J. Chem. Phys.,* 2007, **126**, 164706.

[22] C. T. Campbell, and S. M. Valone, *J. Vac. Sci. Technol. A,* 1985, **3**, 408.

[23] J. Shan, J. F. M. Aarts, A. W. Kleyn, and L. B. F. Juurlink, *Phys. Chem. Chem. Phys.,* 2008, **10**, 4994; this thesis chapter 4.

[24] K. Wandelt, *Surf. Sci. Rep.,* 1982, **2**, 1.

[25] P. H. Holloway, and J. B. Hudson, *Surf. Sci*., 1974, **43**, 141.

[26] G. T. Tyuliev, and K. L. Kostov, *Phys. Rev.* B, 1999, **60**, 2900.

[27] M. E. Gallagher, S. Haq, A. Omer, and A. Hodgson, *Surf. Sci*., 2007, **601**, 268.

[28] J. Shan, J. F. M. Aarts, A. W. Kleyn, and L. B. F. Juurlink, *Phys. Chem. Chem. Phys.,* 2008, **10**, 2227; this thesis chapter 3.

[29] T. Harb, W. Kedzierski, and J. W. McConkey, *J. Chem. Phys.,* 2001, **115**, 5507.

[30] C. D. Lane, N. G. Petrik, T. M. Orlando, and G. A. Kimmel, *J. Phys. Chem. C,* 2007, **111**, 16319.

[31] J. Fusy, and R. Ducros, *Surf. Sci*., 1990, **237**, 53.

[32] J. W. He, and P. R. Norton, *Surf. Sci*., 1990, **238**, 95.

[33] G. Chiarello, A. Cupolillo, C. Giallombardo, R. G. Agostino, V. Formoso, D. Pacile, L. Papagno, and E. Colavita, *Surf. Sci*., 2003, **536**, 33.

[34] M. Nakamura, and M. Ito, *Chem. Phys. Lett.,* 2004, **384**, 256.

[35] K. Jacobi, K. Bedurftig, Y. Wang, and G. Ertl, *Surf. Sci*., 2001, **472**, 9.

[36] M. W. Urban, *Vibrational Spectroscopy of Molecules and Macromolecules on Surface.* 1993, Wiley Inc, New York, p. 138.

[37] C. Klünker, C. Steimer, J. B. Hannon, M. Giesen, and H. Ibach. *Surf. Sci*., 1999, **420**, 25.

[38] R. Baddour-Hadjean, F. Fillaux, and J. Tomkinson, *Physica. B,* 1995, **213&214**, 637.

[39] H. Ibach, and D. L. Mills, *Electron Energy Loss Spectroscopy and surface vibrations.* 1982, Academic Press, New York.

[40] J. L. Arnau, and P. Giguère, *J. Chem. Phys.,* 1974, **60**, 270.

[41] C. F. Jackels, *J. Chem. Phys.,* 1993, **99**, 5768.

[42] C. Clay, S. Haq, and A. Hodgson, *Phys. Rev. Lett.,* 2004, **92**, 046102.

[43] G. Zimbitas, M. E. Gallagher, G. R. Darling, and A. Hodgson, *J. Chem. Phys.,* 2008, **128**, 074701.

[44] G. A. Kimmel, N. G. Petrik, Z. Dohnálek, and B. D. Kay, *Phys. Rev. Lett.,* 2005, **95**, 166102.

[45] G. Zimbitas, and A. Hodgson, *Chem. Phys. Lett.,* 2006, **417**, 1.

Chapter 6

Adsorption of molecular hydrogen on an ultrathin layer of Ni(111) hydride

We have used high resolution electron energy loss spectroscopy and temperature-programmed desorption to study the interaction of atomic hydrogen with Ni(111). Our results agree mostly with previous reports. We find that exposing Ni(111) to atomic hydrogen below 90 K leads to a 125 K TPD feature and two additional HREELS losses. Isotopic exchange studies lead us to attribute these features to molecular hydrogen bound to an ultrahin nickel hydride layer formed on the surface. We suggest that such binding is induced by reversible surface roughening that accompanies the phase change between the metallic nickel and the ultrathin nickel hydride layer.

6.1 Introduction

Chemisorbed molecular states for H_2 on metal surfaces are rare and mostly associated with considerable surface roughness. In recent years, theoretical studies have indicated that H_2 may bind chemically, but without dissociation, near steps at otherwise well-ordered metal surfaces, e.g. Pd(210) [1], Pt(211) [2] and even on Pd(110) [3]. Direct experimental evidence for chemisorbed molecular states has emerged from HREELS and TPD studies for H_2 adsorption on Ni(510) [4] and Pd(210) [5]. Such a molecular state may act as a precursor state and thus be of crucial importance to the dynamics of hydrogen dissociation. For example, results from experimental and theoretical studies for H_2 dissociation on Pt(211) [2,6] indicate that molecular chemisorption wells in the potential energy surface dominate dissociation at low impact energies.

The interaction of H_2 with Ni(111) has attracted attention as nickel has found widespread application in hydrogenation processes. Hydrogen dissociates on this surface with a low reaction barrier, although large exposures are necessary for (nearly) complete saturation [7-10]. The saturation coverage is generally agreed to be 1.0 monolayer (ML) [8-10], with hydrogen atoms adsorbing, especially at higher coverages, into fcc three-fold hollow sites [8,10,11-15]. Supersonic molecular beam [15] and temperature programmed desorption (TPD) studies [16] report no isotopic dependence in dissociative adsorption or associative desorption. Desorption generally occurs in two peaks near 330 K and 370 K and is very sensitive to contamination and defects [17]. A well-ordered, clean and defect-free Ni(111) surface is characterized by a ~40 K difference between the two desorption maxima.

Although surface-bound H does not diffuse into subsurface sites, Ceyer and co-workers showed that subsurface hydrogen atoms can be created under UHV conditions by impinging atomic hydrogen onto Ni(111) [18,19]. We refer to such a surface filled by subsurface hydrogen as an *ultrathin nickel hydride layer*. Formation of bulk nickel hydride is endothermic by 0.17 eV per H atom in the low concentration limit [20] and, consequently, an ultrathin nickel hydride layer is expected to decompose well below room temperature under vacuum conditions. In their TPD spectra, Ceyer and coworkers indeed observe two additional TPD features at 185 and 215 K. Using atomic hydrogen or ion sources, other groups have also observed TPD features well below the surface desorption

temperatures and attributed them to recombinative desorption of interstitial hydrogen [21-23].

HREEL spectra of such ultrathin nickel hydride layers show a feature centered at ~100 meV, in addition to features resulting from surface-bound hydrogen at 145 and 119 meV [18,24]. Subsurface hydrogen has been reported to be extremely active in hydrogenation of simple hydrocarbons [19,23,25-29] and it has found use as a titrant in experiments showing that mode-selected vibrational excitation of the C-H bond in gas-phase CHD_3 prior to impact with a thin nickel deuteride film leads primarily to C-H bond cleavage [30]. Recent debate focuses on the mechanism by which interstitial hydrogen reacts with surface-bound species to form gaseous products [12,13,19,31-34].

Hydrogen has also been reported to bind molecularly to nickel, although significant surface corrugation is required. Andersson and coworkers reported an additional H_2 TPD feature at 125 K after exposing a clean Ni(510) surface to molecular hydrogen [4]. They attributed this TPD feature to molecularly bound hydrogen based on the observation of HREELS features at 28 and 398 meV for H_2 and corresponding features at 23 and 345 for HD and 21 and 289 meV for D_2. These features were attributed to correspond to a bending mode and the H-H stretch, respectively.

In this chapter, we report that molecular hydrogen binds to an ultrathin nickel hydride layer prepared from Ni(111). TPD experiments indicate recombinative desorption of subsurface H and surface H, and molecularly bound H_2. HREEL spectra at 85 K show losses at energies previously reported for interstitial atomic hydrogen, surface-bound atomic H, and surface-bound molecular H_2. When using mixed atomic hydrogen and deuterium beams to prepare the thin nickel hydride layer, we find an additional energy loss indicative of molecular HD. Combined with the observation of the disappearance and reappearance of the elastically scattered electron beam from our HREEL spectrometer, we interpret our results to indicate that formation of the thin nickel hydride film at 85 K leads to enough corrugation for this surface to bind molecular hydrogen.

6.2 Experiment

Experiments are carried out in an UHV system, which consists of two chambers. The top chamber is used for preparation of the Ni(111) surface, and for TPD experiments with a

quadrupole mass spectrometer (Balzers QMS 422). The lower chamber contains an upgraded ELS 22 high resolution electron energy loss spectrometer and a double-pass CMA for Auger electron spectroscopy (Staib Instruments). The top and lower chambers are separated by a gate valve. The typical base pressure of the system is less than 1×10^{-10} mbar.

The Ni(111) single crystal, cut and polished to less than 0.1º of the low Miller-index plane (Surface Preparation Laboratories, Zaandam, the Netherlands), can be heated to 1200 K by electron bombardment and cooled to 85 K. The crystal temperature is measured by a chromel-alumel thermocouple spot-welded to the edge of the crystal. The crystal is cleaned by Ar^+ sputtering, annealing at 1100 K, followed by oxidation in 10^{-7} mbar of O_2 and reduction in 10^{-6} mbar of H_2. After cleaning, the surface cleanliness is verified by AES. The hydrogen coverage is estimated from the TPD integral taken for m/e=2. We convert the integral to an absolute coverage using the intergral determined after dosing $30{,}000\times10^{-6}$ mbar*s H_2 at 85 K as a reference for 1 ML [8-10]. All TPD measurements are performed with a heating rate of 1.0 K/s. The HREEL spectra are recorded at 5 to 9 meV resolution (FWHM) with typical 1×10^4 cps for the scattered elastic peak.

We use a thermal hydrogen cracker (H-Flux, Tectra) for dosing atomic hydrogen. In this source, a heated tungsten capillary is kept at 1800 K while hydrogen flows through its orifice toward the Ni(111) surface. This cracking temperature avoids formation of tungsten vapor and provides a small radiative load onto the crystal. The distance between source and crystal in combination with a heat shield ensures that the crystal temperature remains below 90 K during dosing. At the cracking temperature of 1800 K, the dissociation fraction is estimated to be ~90% when the capillary pressure is below 1×10^{-5} mbar. While the atomic hydrogen beam is therefore actually a mixture of atomic and molecular hydrogen, we refer to the mixture as the atomic hydrogen beam. As a feed for the hydrogen cracker we use 5N5 H_2 (Messer) and 99.8% isotopic purity D_2 (Linde).

6.3 Results

Figure 6.1 shows a series of H_2 TPD spectra measured after exposing Ni(111) to various amounts of atomic hydrogen at 85 K. For comparison, we also show the desorption

spectrum of surface hydrogen in curve a, in which only H_2 is dosed to the maximum surface coverage. Curve a clearly shows two desorption features at 325 and 365 K, which is typical for an associative desorption spectrum of 1 ML chemisorbed hydrogen [8,9,18]. The 40 K difference in peaks testifies to the cleanliness of the surface and the absence of significant corrugation or defects [17]. In curves b, c, and d, we observe additional desorption features. Two closely-spaced peaks appear at 180 and 190 K and a small desorption feature appears at 125 K. The peaks at 180 and 190 K appear prior to the 125 K feature (compare traces b and c). The latter feature does not increase significantly with increasing atomic hydrogen dose, while the features at 180 and 190 K do (compare traces c and d). The appearance of lower temperature peaks does not significantly affect the peak positions for surface recombination at 325 and 365 K.

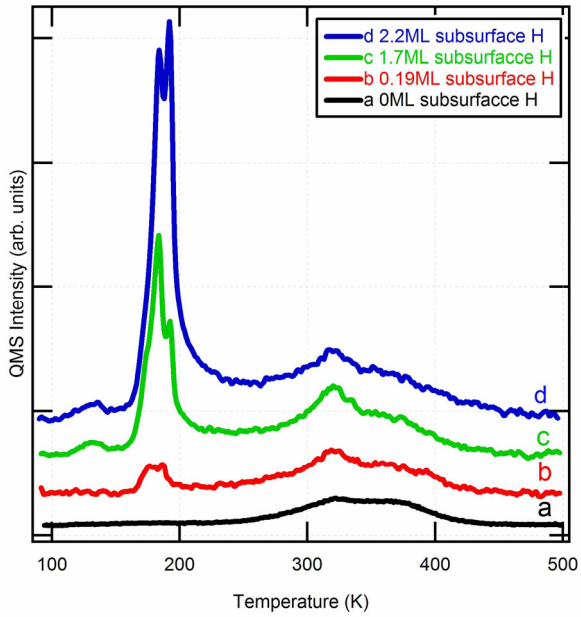

Figure 6.1 TPD spectra of m/e=2 measured after exposure of the Ni(111) crystal to various amounts of atomic hydrogen at 85 K.

Figure 6.2 shows two HREEL spectra measured after exposing Ni(111) at 85-90 K to atomic hydrogen (bottom trace) or atomic deuterium (top trace). The dotted line represents the

original HREELS spectra, while the solid line is a fit to this data using a summation of an exponential decay and three off-set Gaussian functions. The indicated amount of subsurface hydrogen (deuterium) is determined after the HREELS measurements from an integrated TPD spectrum. Both spectra are taken at 10º off-specular angle using an impact energy of the primary electron beam of 9.6 eV, since at this energy both surface and subsurface vibrations can be observed [18]. In the bottom trace, we distinguish four energy losses: a strong and sharp feature at 30 meV, a broader feature centered at 100 meV with peak appearing in the shoulder at 141 meV, and a broad feature centered at 420 meV. In the top trace, four energy losses appear at 24, 80, 100 and 305 meV. They show the same intensity and width variations as the features observed in the bottom trace. When repeating the experiment with atomic hydrogen, but flashing the crystal to 140 K prior to taking a HREEL spectrum, we observe the same spectrum as the bottom trace in figure 6.2 but without the 30 meV and 420 meV features.

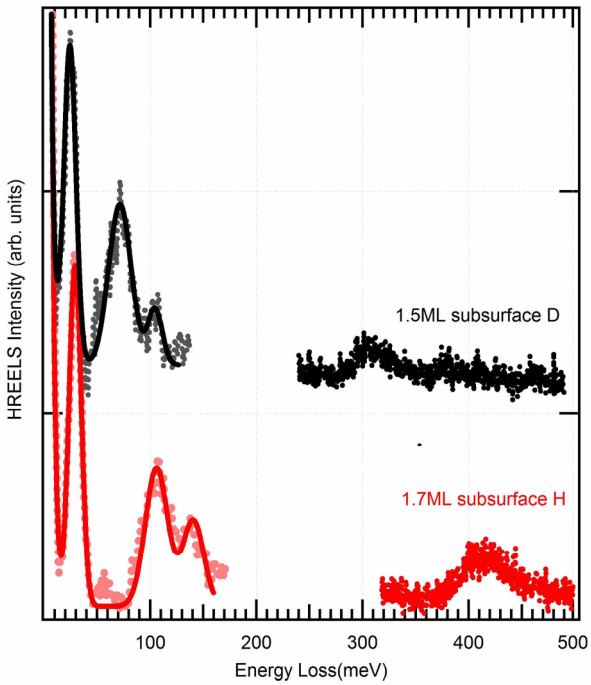

Figure 6.2 HREEL spectra collected at 85 K and at 10º off-specular angle with an impact energy of 9.6 eV. See text for details.

We have noted that preparation of the nickel hydride film at 85 K without any further treatment prior to collecting the HREEL spectrum leads to an almost complete loss of signal intensity for the elastically scattered beam. Signal intensity returns after flashing the crystal temperature to above 220 K. This suggests that formation of the nickel hydride layer at 85 K induces surface corrugation. Since the scattered intensity of the primary beam is diffuse, long signal averaging was required to collect each part of the spectra shown in figure 6.2. To minimize interfering contamination of the surface, we have therefore collected spectral information in the smaller energy regimes shown here with increased resolution. A single experiment using the H isotope and a lower resolution scanned the entire energy regime and showed no observable features in the energy window left out of the bottom trace.

Isotopic mixing of H_2 and D_2 in the feed of our thermal cracker allows us to dose H and D atoms simultaneously in combination with residual H_2, D_2 and HD. Figure 6.3 presents a HREEL spectrum taken at 85 K after dosing the clean Ni(111) surface with such a mixture. We focus here on energy regimes relevant to the interpretation of our data. Most prominently, we observe three energy losses in the higher energy regime at 305, 344 and 420 meV. Between 100 and 200 meV we observe no losses. The peak edge near 220 meV results from accumulating CO [35].

It may be suggested that the time required for signal averaging to obtain the spectra in figure 6.2 and 6.3 leads to contamination of the surface, especially by H_2O. Recently, we have studied water adsorption on (partially) hydrogen-covered Ni(111) in detail [36,37], also see Chapter 3 and 4. H_2O shows losses near 420, 200, 50-100 and 30 meV for stretching and bending vibrations, librations and frustrated translations, respectively. The relative intensities of these vibrations are such that when the O-H stretch is observed, the librations between 50-100 meV are more prominent in both specular and off-specular HREEL spectra [36]. Since in figure 6.2 the librations of water are not present, we conclude that the observed features are not due to H_2O. Also, flashing the crystal to 140 K prior to taking HREEL spectra should not lead to a loss of vibrational features of water, as any amount of water on (hydrogen-covered) Ni(111) does not desorb until >150 K [36]. Finally,

the presence of the 344 meV in figure 6.3 cannot be accounted for by a (deuterated) water isotope, and water contamination would have appeared by bending modes of (deuterated) water in the 100-220 meV window.

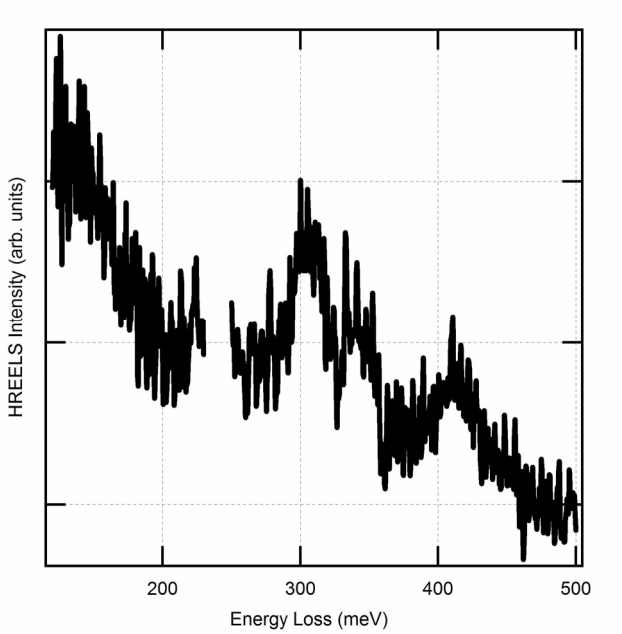

Figure 6.3 HREEL spectra region for H_2, D_2, and HD stretch region, as well as water bending mode region.

6.4 Discussion

First, we focus our attention on the TPD spectra in figure 6.1. As mentioned, in curve a only H_2 is dosed. The double peak feature at 325 K and 365 K is typical for desorption of 1 ML surface hydrogen. In curves b, c, and d atomic dosing is used and the same peaks appear, while additional maxima appear at 180 K and 190 K. The integral of the feature at 180-190 K reaches 1.7 and 2.2 surface monolayers in c and d, respectively. In previous publications, desorption of subsurface hydrogen from ultrathin nickel hydride layers was reported in similar temperature regimes [18,19,21-22]. Following this earlier assignment, we attribute these TPD maxima to 'resurfacing' hydrogen from interstitial sites with immediate reaction with surface-bound hydrogen to form $H_{2(g)}$. We note that the appearance

of H_2 in the gas phase at this temperature may also be interpreted as resulting from a phase transition of the ultrathin nickel hydride film to metallic nickel with a surface layer of atomically bound hydrogen. Since desorption of surface-bound hydrogen is sensitive to defects [17] the lack of changes in the 325 and 365 K features indicates that this reversible phase change does not lead to many defects at the Ni(111) surface.

When comparing our TPD spectra with the earliest report, we find that the width of the subsurface hydrogen features in our spectra is considerably narrower [18]. Although we cannot offer conclusive evidence at this point, we expect that it results from different procedures used to prepare the ultrathin nickel hydride film. Whereas the surface temperature remains below 90 K during exposure to atomic hydrogen in our experiments, other studies indicate that the crystal temperature increased to 130 K during dosing. This also explains why the 125 K TPD feature appearing in traces c and d was not observed in previous studies of this system.

Regarding the 125 K feature in our TPD traces, which amounts to ~0.15 ML in traces c and d and which does not increase noticeably in size when increasing the atomic hydrogen exposure, we note that such a low temperature peak for H_2 desorption has not been identified before for H_2/Ni(111). To our knowledge, only Andersson and coworkers observed a similar peak for hydrogen at 125 K when Ni(510) was exposed to molecular hydrogen [4]. On the basis of HREEL spectra, this TPD peak was attributed to desorption of molecular hydrogen bound to steps on the Ni(510) surface.

As mentioned in the introduction, two HREELS features at 145 meV and 119 meV are observed for the hydrogen-saturated Ni(111) surface. We also observe these features when we only dose H_2. Subsurface hydrogen yields an additional broad feature centered at 100 meV in HREEL spectra [18]. In figure 6.2, we ascribe the 100 and 141 meV features to subsurface and surface H, respectively. This assignment is in line with the expected isotope shift observed in the top trace in figure 6.2 when using D atoms. The broad feature centered at 80 meV is ascribed to subsurface D, while the small feature at 100 meV is ascribed to surface D.

In figure 6.2, we are left with two features at 30 (24) and 420 (305) meV for hydrogen (deuterium). The energy, shape and relative intensity of these losses compare well to those

observed for molecular hydrogen adsorbed on Ni(510) [30]. In that study, a broad feature centered at 398 meV (289 meV) was attributed to the stretch vibration of H_2 (D_2), while a sharp and intense peak at 28 (21) meV was assigned to the bending mode of Ni-H_2 (Ni-D_2) [4]. On Pd(210), molecular hydrogen adsorption has also been detected by TPD and HREELS [5]. Here, a feature near 420 (300) meV was suggested to result from the H-H (D-D) stretch vibration. Finally, ionic Ni_4^+ clusters created in a deuterium atmosphere bind molecular D_2 resulting in an IR active D-D stretch vibration at 305 meV [38]. The resemblance of all these observations to ours suggests that the 420 (305) meV feature in our spectra results from an internal H_2 (D_2) stretch of molecular hydrogen bound to the ultrathin nickel hydride (deuteride) film, while the 30 (24) meV feature results from a Ni-H_2 (Ni-D_2) bend. The disappearance of these peaks when flashing the crystal to 140 K prior to taking a HREEL spectrum connects the 125 K TPD feature to these particular energy losses and provides further evidence that H_2 is present at the surface after preparing the ultrathin nickel hydride layer at 85-90 K.

Finally, we turn to the HREEL spectrum in figure 6.3 which was taken after dosing a combination of H and D atoms. Of the three losses observed, the 305 and 420 meV features also occur when dosing only D or H (Figure 6.2) and likely result from the same vibrational modes and the same species. For the feature at 344 meV, a similar feature was observed when dosing HD on Ni(510) at 345 meV and the relative energies suggest that this experiment created H_2, HD and D_2 simultaneously at the ultrathin nickel hydride (deuteride) surface. Thus, we conclude that experiments in which the atomic hydrogen beam impinges on Ni(111) near 85 K produces molecularly bound hydrogen. This molecularly bound hydrogen desorbs at 125 K.

Finally, we are left to consider what changes the Ni(111) surface when forming an ultrathin nickel hydride layer such that it binds molecular hydrogen. The early studies on Ni(510) concluded that molecular hydrogen adsorbs at the steps of the nickel surface. We detect molecular hydrogen only when subsurface hydrogen is present in otherwise flat Ni(111). We also noted that exposing the crystal to atomic hydrogen at 85 K leads to an almost complete disappearance of signal intensity for the elastically scattered electron beam, which only reappears above 220 K, when all subsurface hydrogen has desorbed. The

combination of these observations suggests that formation of the ultrathin nickel hydride layer near 85 K induces corrugation and roughening that allows for molecular H_2 adsorption. As formation of nickel hydride from pure nickel expands the nickel lattice with 2.9 $Å^3$ per hydrogen atom up to x=0.7 in NiH_x [20], upward relaxation of surface nickel atoms is expected upon formation of a ultrathin nickel hydride layer on Ni(111). Such relaxation has been observed by STM for small quantities of subsurface hydrogen absorbed in Pd(111) [39]. Pd shows the same volume change per H atom in this regime of hydride formation [20]. A similar relaxation on Ni(111) would explain the loss of the elastically scattered electron beam intensity and provides adsorption sites for H_2 that resemble steps on Ni(510) and edge atoms in cationic Ni_4 clusters. Also, the recovery of the scattered elastic peak intensity above 220 K is in line with decomposition of a slightly corrugated ultrathin nickel hydride film, leading back to a smooth Ni(111) surface. Significant transport of Ni atoms (e.g. as NiH of NiH_2) along the surface in this reversible process of ultrathin hydride formation may be excluded as the reverse phase change to Ni(111) would have left the surface roughened with an accompanying change in the H_2 surface desorption features at 325 and 365 K in traces 1c and d. Also, the scattered elastic electron beam intensity would not have recovered.

6.5 Conclusions

We have demonstrated that dosing atomic hydrogen on Ni(111) at a surface temperature below 90 K leads to molecular hydrogen bound to an ultrathin nickel hydride layer. We suggest that the adsorption of molecular hydrogen is due to reversible roughening associated with formation of the NiH_x layer. However, the roughening is modest and likely consists only of relaxation of nickel atoms normal to the surface. The newly found molecular state of hydrogen persists to 125 K and may present an interesting case to study H_2 reaction and scattering dynamics.

6.6 References

[1] M. Lischka, and A. Groß, *Phys. Rev. B,* 2002, **65**, 075420.

[2] D. A. McCormack, R. A. Olsen, and E. J. Baerends, *J. Chem. Phys.,*2005, **122**, 194708.

[3] H. F. Busnengo, W. Dong, and A. Salin, *Phys. Rev. Lett.*, 2004, **93**, 236103.

[4] A.-S. Mårtensson, C. Nyberg, and S. Andersson. *Phys. Rev. Lett.*, 1986, **57**, 2045.

[5] P. K. Schmidt, K. Christmann, G. Kresse, J. Hafner, M. Lischka, and A. Groß, *Phys. Rev. Lett.*, 2001, **87**, 096103.

[6] I. M. N Groot, K. J. P. Schouten, A. W. Kleyn, and L. B. F. Juurlink, *J. Chem. Phys.,* 2008, **129**, 224707.

[7] K. Christmann, O. Schober, G. Ertl, and M. Neumann, *J. Chem. Phys.*, 1974, **60**, 4528.

[8] K. Christmann, R. J. Behm, G. Ertl, M. A. Van Hove, and W. H. Weinberg, *J. Chem. Phys.*, 1979, **70**, 4168.

[9] A. Winkler, and K. D. Rendulic, *Surf. Sci.*, 1982, **118**, 19.

[10] K. Mortensen, F. Besenbacher, I. Stensgaard, and W. R. Wampler, *Surf. Sci.*, 1988, **205**, 433.

[11] B. Bhatia, and D. S. Sholl, *J. Chem. Phys.*, 2005, **122**, 204707.

[12] J. Greeley, and M. Mavrikakis, *Surf. Sci.*, 2003, **540**, 215.

[13] R. Baer, Y. Zeiri, and R. Kosloff, *Phys. Rev. B*, 1997, **55**, 10952.

[14] H. Yanagita, J. Sakai, T. Aruga, N. Takagi, and M. Nishijima, *Phys. Rev. B*, 1997, **56**, 14952.

[15] A. C. Luntz, J. K. Brown, and M. D. Williams, *J. Chem. Phys.*, 1990, **93**, 5420.

[16] K. Christmann, *Surf. Sci. Rep.*, 1988, **9**, 1.

[17] K. D. Rendulic, A. Winkler, and H. P. Steinrück. *Surf. Sci.*, 1987, **185**, 469.

[18] A. D. Johnson, K. J. Maynard, S. P. Daley, Q. Y. Yang, and S. T. Ceyer, *Phys. Rev. Lett.*, 1991, **67**, 927.

[19] S. T. Ceyer, *Acc. Chem. Res.*, 2001, **34**, 737.

[20] Y. Fukai, The metal-hydrogen system, 1993, Springer-Verlag, Berlin.

[21] H. Premm, H. Pölzl, and A. Winkler, *Surf. Sci. Lett.*, 1998, **401**, L444.

[22] S. Wright, J. F. Skelly, and A. Hodgson, *Faraday Discuss.*, 2000, **117**, 133.

[23] A. T. Capitano, and J. L. Gland, *Langmuir*, 1998, **14**, 1345.

[24] H. Okuyama, T. Ueda, T. Aruga, and A, M. Nishijima, *Phys. Rev. B*, 2001, **63**, 233404.

[25] A. D. Johnson, S. P. Daley, A. L. Utz, and S. T. Ceyer, *Science*, 1992, **257**, 223.

[26] S. P.Daley, A. L. Utz, T. R. Trautman, and S. T. Ceyer, *J. Am. Chem. Soc.*, 1994, **116**, 6001.

[27] K. L. Haug, T. Bürgi, T. R. Trautman, and S. T. Ceyer, *J. Am. Chem. Soc.*, 1998, **120**, 8885.

[28] K. L. Haug, T. Bürgi, M. Gostein, T. R. Trautman, and S. T. Ceyer, *J. Phys. Chem. B.*, 2001, **105**, 11480.

[29] A. T. Capitano, K.-Ah. Son, and J. L. Gland, *J. Phys. Chem. B.*, 1999, **103**, 2223.

[30] D. R. Killelea, V. L. Campbell, N. S. Shumann, and A. L. Utz, *Science*, 2008, **319**, 790

[31] V. Ledentu, W. Dong, and P. Sautet, *J. Am. Chem. Soc.*, 2000, **122**, 1796.

[32] A. Michaelides, P. Hu, and A. Alavi, *J. Chem. Phys.*, 1999, **111**, 1343.

[33] G. Henkelman, A. Arnaldsson, and H. Jónsson. *J. Chem. Phys.*, 2006, **124**, 044706.

[34] S. Wright, J. F. Skelly, and A. Hodgson, *Chem. Phys. Lett.*, 2002, **364**, 522.

[35] W. Erley, H. Wagner, and H. Ibach, *Surf. Sci.*, 1979, **80**, 612.

[36] J. Shan, J. F. M. Aarts, A.W. Kleyn, and L. B. F. Juurlink, *Phys. Chem. Chem. Phys.*, 2008, **10**, 2227; this thesis chapter 3.

[37] J. Shan, J. F. M. Aarts, A.W. Kleyn, and L. B. F. Juurlink, *Phys. Chem. Chem. Phys.*, 2008, **10**, 4994; this thesis chapter 4.

[38] I. Swart, P. Gruene, A. Fielicke, G. Meijer, B. M. Weckhuysen, and F. M. de Groot, *Phys. Chem. Chem. Phys.*, 2008,**10**, 5743.

[39] E. C. H. Sykes, L. C. F-Torres, S. U. Nanayakkara, B. A. Mantooth, R. M. Nevin, and P. S. Weiss, *PNAS*, 2005, **102**, 17907.

Chapter 7

On the formation and decomposition of a thin NiH_x layer on Ni(111)

We have used temperature-programmed desorption in combination with high resolution electron energy loss spectroscopy to study the interaction of atomic hydrogen and deuterium with D or H-pre-covered Ni(111). Our results show a large isotopic effect when reversing the order of the isotopes used in preparing a thin nickel hydride (deuteride) layer, capped by a (nearly)-saturated surface hydrogen (deuterium) layer. Our results also show that atomic D atoms can "hammer" surface-bound H into the subsurface sites, whereas atomic H does not "hammer" surface-bound D into the subsurface sites. The large difference in collision-induced absorption cross-section for the two isotopes has various consequences. CO desorption traces and surface roughness probed using the elastically scattered intensity of an electron beam suggest that that NiH_x patches bulge upward relative to the remaining flat hydrogen or deuterium-covered Ni(111) surface. Decomposition of the NiH_x patches releases enough energy to desorb co-adsorbed CO.

7.1 Introduction

The development of metal hydrides as on-board hydrogen storage materials for mobile applications has undergone rapid development in recent years [1]. The kinetics of hydrogenating the metal hydride after its (partial) decomposition is one of several difficulties that still need to be overcome. For light metal hydrides, e.g. $NaAlH_4$, additives have been found to accelerate this process [2,3]. However, at the atomic level, the formation of a metal hydride from a pure metal and H_2, is poorly understood, let alone the action of catalysts. Although nickel hydride's gravimetric reversible hydrogen storage capacity limits its applicability for automotive applications, this material presents an interesting case, especially since the interaction of H_2 with various clean nickel surfaces is well studied. The latter is a consequence of the use of nickel as a catalyst for industrial hydrogenation reactions.

In general, metal hydrides are formed by simply exposing the metal to hydrogen gas. Hydrogen molecules dissociate at the metal surface and dissolve into the metal to form a solid solution of hydrogen atoms in the host metal lattice. This solid solution of hydrogen, commonly referred to as the α-phase of the metal-hydrogen system, exists only at low hydrogen concentrations. When a saturation level is reached, the α-phase undergoes a transition to a distinct solid hydride phase, also referred as the ß-phase. The two processes, which together constitute the total process of hydrogen uptake by the metal, are often expressed as:

$$M + \frac{1}{2} yH_2 \leftrightarrow MH_y \text{ (α-phase)}$$

$$MH_y + \frac{1}{2}(x-y)H_2 \leftrightarrow MH_x \text{ (ß-phase)}$$

Obviously, the first reaction may be separated into the dissociated adsorption of H_2 at the metal surface, and consecutive diffusion of H into the subsurface region. The reactions are reversible and their directions are determined by the pressure of hydrogen gas and the temperature of the metal. Nickel hydride is formed at 25 ºC above 6 kbar of gaseous hydrogen leading to a nearly stoichiometric hydride phase. The decomposition of nickel hydride takes place at approximately 3.4 kbar. Slightly higher values are observed for

formation and decomposition pressures at 65 ºC. Further details can be found in Ref 4 and 5.

Hydrogen dissociation on and desorption from clean low Miller index nickel surfaces, e.g. Ni(111), Ni(100) and Ni(110), have been studied in detail over the past decades. Experiments using ultrahigh vacuum (UHV) conditions and theoretical calculations have shown that the energy barrier to dissociate H_2 on Ni(111) is 46 kJ/mol, while for Ni(100) and Ni(110) it is 52 kJ/mol and 36kJ/mol respectively [6-10]. The desorption temperature for surface-bound hydrogen on Ni(111), Ni(100), and Ni(110) was observed between 320-380 K, 220-360 K, and 230-430 K respectively [8-11]. Under UHV conditions, nickel hydride can not be formed by dosing molecular H_2.

Absorption of atomic hydrogen into the subsurface sites has been studied in detail for Ni(111) [10,12-17]. Subsurface hydrogen was created by impinging atomic hydrogen from the gas phase onto the clean Ni(111) surface by Johnson *et al.*[13]. They used temperature-programmed desorption (TPD) and high resolution electron energy loss spectroscopy to detect and identify the subsurface hydrogen atoms. An additional double-peaked desorption feature appeared in TPD spectra near 185 and 215 K. An interstitial hydrogen vibration was observed near 100 meV, which compared favorably to the subsurface hydrogen vibrational mode observed with neutron scattering [18]. Other groups have observed similar TPD features, although the absolute desorption temperature for subsurface hydrogen appears to be strongly dependent on the exact procedure used to form a thin layer of nickel hydride on the nickel single crystal surface [14-16,19,20]. Subsurface hydrogen has been found to be extremely active in hydrogenation of simple hydrocarbons [10,19-21]. In addition, the deuterium isotope has been used as a titrant in experiments of bond-selectively controlled CHD_3 dissociation on Ni(111) [22].

Considering the dynamics of hydrogen absorption into subsurface sites, two mechanisms have been suggested [10]. First, collision-induced absorption is the dynamical process in which surface-bound hydrogen atoms are ‘hammered’ into subsurface sites by the impact of energetic inert gas atoms [10]. Second, in direct penetration hydrogen atoms penetrate the Ni(111) surface from the gas phase and equilibrate in a subsurface sites. While experimental evidence for the first mechanism is strong, direct absorption from the

gas phase is considerably more difficult to prove, as collision-induced absorption by impinging atomic hydrogen onto surface-bound atomic hydrogen may be mistaken for direct absorption.

Studies of hydrogen desorption where the H atoms originate from the subsurface region report inconsistent results. Early permeation experiments by van Willigen showed for polycrystalline nickel a distribution of emerging H_2 molecules that peaked strongly around the surface normal [23]. On the contrary, Wright *et al.* [15,16] found a cosine angular distribution of desorbing D_2 molecules in combined REMPI-TPD experiments where subsurface D atoms were created by implantation. In the latter studies, the authors suggest that their results indicate that D atoms resurface at vacant sites and diffuse on the surface before recombinatively desorbing as D_2. Several theoretical studies agree that this indirect reaction pathway, in which subsurface hydrogen (H_{subs}), absorbed directly below a surface-bound hydrogen atom (H_{surf}), first moves to an adjacent subsurface site before it emerges at an empty surface site and reacts to form H_2 [24,25]. However, in contrast to this indirect mechanism, Ceyer and co-workers have proposed a direct mechanism in which a hydrogen atom resurfaces from underneath a surface-bound species (e.g. CH_3 and C_2H_4) and reacts in a single step [10,21]. A theoretical study using density-functional theory (DFT) calculations has focused on H_{subs} + $CH_{3,surf}$ and finds support for such a direct reaction pathway [26]. However, other theoretical studies report that the pathway to form CH_4 in this manner is lowest when a hydrogen atom resurfaces at an empty threefold hollow site before reacting with CH_3 [25,27].

Recently, we preformed a study of the interaction of atomic H(D) with the bare Ni(111) surface (chapter 6). Our results confirm the absorption of hydrogen in subsurface sites when exposed to atomic hydrogen from the gas phase. We observed a double peak feature at 180 and 190 K in TPD spectra and our HREEL spectra show a broad feature centered at 100 meV. As a consequence of producing the nickel hydride thin layer at lower temperatures than previous studies, we also detected molecular H_2 at the nickel hydride surface that desorbed near 125 K. We have suggested that this molecular chemisorbed state results from an upward relaxation of surface nickel atoms when subsurface hydrogen atoms are present.

In this chapter, we use TPD in combination with HREELS to study the interaction of atomic hydrogen and deuterium with D or H-pre-covered Ni(111). Our results show a large isotopic effect when reversing the order of the used isotopes in preparing a thin nickel hydride (deuteride) layer, capped by a (nearly-)saturated surface hydrogen (deuterium) layer. Based on various TPD and HREELS experiments, we draw conclusions on the relative importance of various elementary reaction steps occurring when a H(D)-covered Ni(111) surface is exposed to D(H) atoms, the mechanism for consecutive recombinative desorption, and the uniformity with which NiH_x films form.

7.2 Experiment

Experiments are carried out in an UHV system, which consists of two chambers. The top chamber is equipped with an ion sputter gun, an atomic hydrogen source (H-flux, Tectra), a bakeable UHV leak valve, and a quadrupole mass spectrometer (Balzers QMS 422) used for TPD measurement and residual gas analysis. The lower chamber contains an upgraded ELS 22 high resolution electron energy loss spectrometer and a double-pass CMA Auger electron spectrometer (Staib Instruments). The top and lower chambers are separated by a gate valve. The typical base pressure of the system is less than 1×10^{-10} mbar.

The Ni(111) single crystal, cut and polished to less than 0.1° of the low Miller-index plane (Surface Preparation Laboratories, Zaandam, the Netherlands), can be heated to 1200 K by electron bombardment and cooled to 85 K. The crystal temperature is measured by a chromel-alumel thermocouple spot-welded to the edge of the crystal. The crystal is cleaned by Ar^+ sputtering, annealing at 1100 K, followed by oxidation in 10^{-7} mbar of O_2 and reduction in 10^{-6} mbar of H_2. After cleaning, the surface cleanliness is verified by AES. The hydrogen coverage is estimated from the TPD integral taken for m/e=2. We convert the integral to an absolute coverage using the integral determined after dosing $30{,}000 \times 10^{-6}$ mbar*s H_2 at 85 K as a reference for 1 ML. All TPD measurements were performed with a heating rate of 1.0 K/s. The HREEL spectra were recorded at 5 to 9 meV resolution (FWHM) with typical 1×10^4 cps for the scattered elastic peak.

The dosing of the atomic hydrogen is achieved by the atomic hydrogen source. A detailed description of the atomic hydrogen source is given in chapter 6. We have noted that in our experiments the atomic hydrogen beam is actually a mixture of H and H_2 (chapter 6), however to simplify, throughout the present study we refer to this mixture as the atomic hydrogen beam. During exposure of the atomic hydrogen beam, the crystal temperature is kept below 90 K.

We also performed experiments, in which H_2^+ is dosed onto the Ni(111) surface using a sputter gun. TPD spectra taken consecutively for m/e=2 show a single and broad peak at approximately 250 K in addition to the peaks resulting from associative desorption from the surface between 320 and 380 K. These spectra strongly resemble those published in previous studies using ionic implantation [12,14,15]. However, they are quite different from TPD spectra taking after dosing atomic hydrogen using our H-Flux. In the present study, we only use and compare data that employed atomic hydrogen absorption.

7.3 Results

In this chapter, our experiments start with dosing 1 ML D (H) on the Ni(111) surface by leaking D_2 (H_2) at 85 K, followed by HREELS measurements. Next, we expose this D-(H-) covered surface to impinging atomic H (D) atoms from our atomic hydrogen source below 90 K. After exposure to the atomic beam, we again dose the original molecular isotope at 85 K. This last step is necessary to refill empty sites left on the surface after exposure to the atomic hydrogen beam. Finally, we perform TPD experiments from 90 K to 500 K and monitor m/e=2, 3 and 4 with our QMS.

Figure 7.1 shows the HREEL spectra of the Ni(111) surface after forming 1 ML H_{surf} (7.1.a), or 1 ML D_{surf}(7.1.b) at 85 K from H_2 or D_2. Both spectra are taken at 10º off-specular angle using an impact energy of the primary electron beam of 9.6 eV. At this condition, hydrogen's surface vibrations can be well observed [13]. In figure 7.1.a, the spectrum exhibits two peaks at 141 meV, and 116 meV respectively. This spectrum is very similar to previously published HREEL spectra of 1ML surface hydrogen on Ni(111) and the two peaks have been assigned to the symmetric and antisymmetric stretch modes of

hydrogen atoms, respectively [13,28]. In our HREELS experiments, the same stretch modes for deuterium atoms are observed at 100 and 77 meV, as shown in figure 7.1.b.

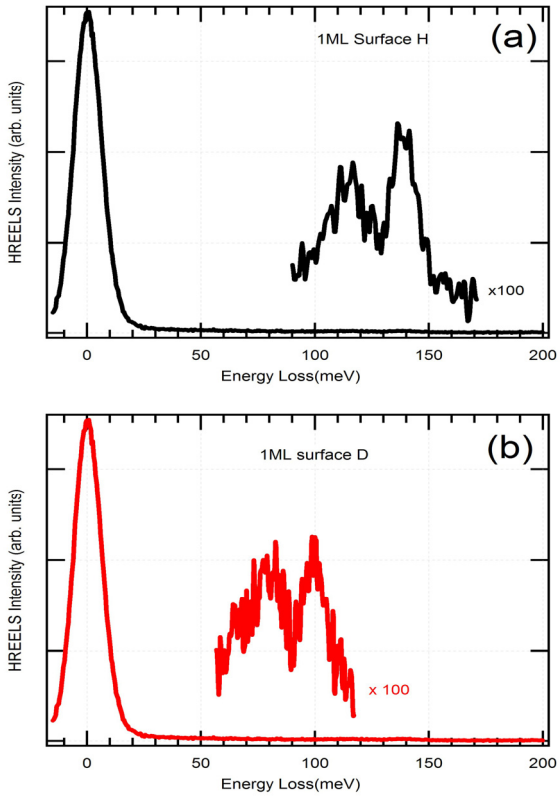

Figure 7.1 HREEL spectra of 1 ML H (a) or D (b) on Ni(111).

Figure 7.2 shows a HREEL spectrum after exposing H pre-covered Ni(111) to atomic D and finally re-dosing H_2. The spectrum shows three distinct features, a broad feature centered at 70 meV, a feature at 100 meV, and a feature at 148 meV. For comparison, figure 6.2 showed HREEL spectra for surface and subsurface H (figure 6.2 bottom trace) and surface and subsurface D (figure 6.2 top trace). The broad feature near 70 meV in figure 7.2 compares well with the 70 meV feature for subsurface deuterium in figure 6.2 (top trace). The 100 meV feature may be due to subsurface hydrogen and surface deuterium as both vibrations appear near this energy in figures 6.2 (bottom trace) and 7.1.b. The 148 meV may be assigned to surface H, although its vibrational frequency seems to have shifted

to slightly higher energy when compared to figure 7.1a. The vibrational features seem to indicate that bombarding a hydrogen-covered Ni(111) surface with D atoms leads to the formation of a thin, (mostly) hydrogen-terminated film of nickel hydride/deuteride.

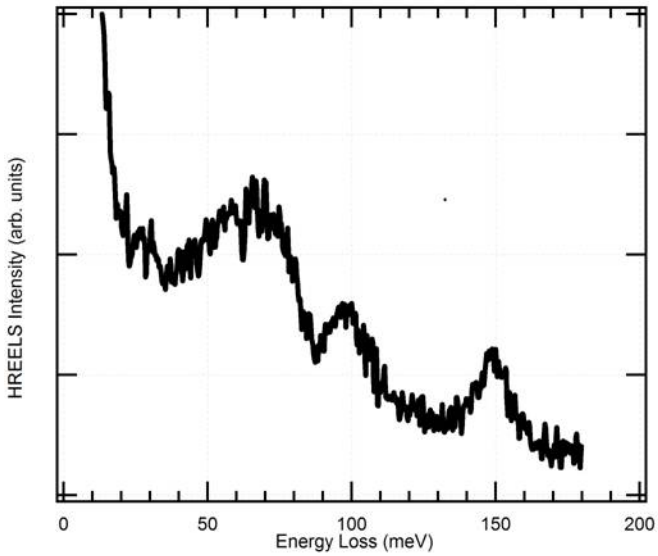

Figure 7.2 HREEL spectra taken after exposing Ni(111) to H_2, D and H_2 consecutively.

Figure 7.3 shows the variation of the HREELS elastic peak intensity after various sample treatments. The figure indicates that the intensity varies strongly after dosing molecular H_2 and atomic H or heating the crystal to different temperatures. First, the intensity increases after dosing H_2, which is expected since adsorption of hydrogen on metal surfaces increases the reflectivity of metals [29,30]. Next, the intensity decreases dramatically upon dosing atomic H to get 0.88 ML H in the subsurface region. As was mentioned in chapter 6, we suggested that the formation of this nickel hydride layer near 85 K induces surface corrugation. This corrugation is not restored after annealing the crystal at 120 and 165 K for 100 s. However, after annealing at 185 K for 100 s, half of the intensity returns. Finally, after annealing at 220 K, at which point all subsurface H has desorbed (see figures 6.1 and 7.4), the intensity returns to the value observed for (1×1)H/Ni(111). From figure 7.3 it is clear that surface corrugation is introduced when inserting hydrogen atoms

into the nickel lattice near 85 K. Surface reflectivity may be restored completely by increasing the crystal temperature temporarily to a value in between the decomposition temperature of the thin nickel hydride film and the desorption temperature of hydrogen from metallic Ni(111) surface.

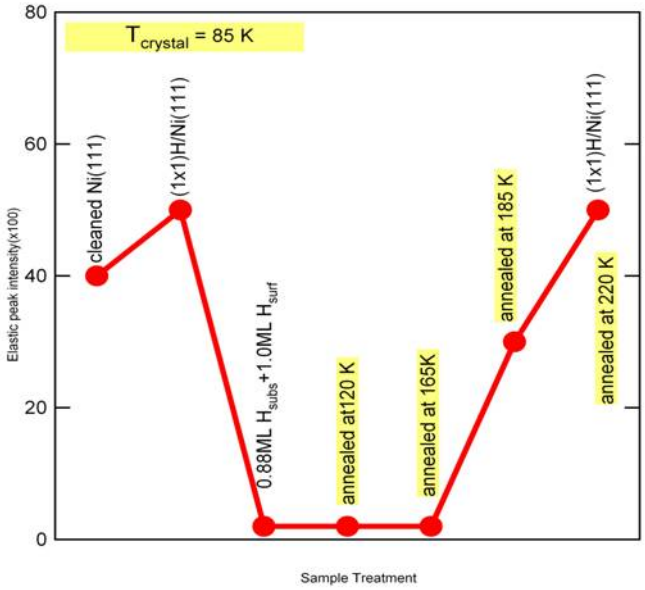

Figure 7.3 the variation of the HREELS elastic peak intensity after various sample treatments.

Six TPD spectra taken after various procedures of exposing the clean surface to atomic and molecular isotopes of hydrogen are shown in figure 7.4. There are two types of experimental variations and three different atomic doses. In figure 7.4a-c the surface was first covered with D using D_2, then exposed to atomic H, and finally re-exposed to 2×10^{-3} mbar*s D_2. In figure 7.4d-f, the isotopes were exchanged, but the order and exposures were maintained the same. The red curves represent the partial pressure of H_2 (m/e=2), the blue curves represent HD (m/e=3), and black curves represent D_2 (m/e=4). The amount of atomic exposures mentioned in figure 7.4 are rough estimates based on the atomic hydrogen source's filament temperature, H_2 (D_2) flow rates, and the distance between the atomic hydrogen source and the crystal [31]. We discuss desorption in terms of a low temperature regime (150-200 K) and a high temperature regime (300-400 K),

corresponding to decomposition of nickel hydride and associative desorption from Ni(111), respectively.

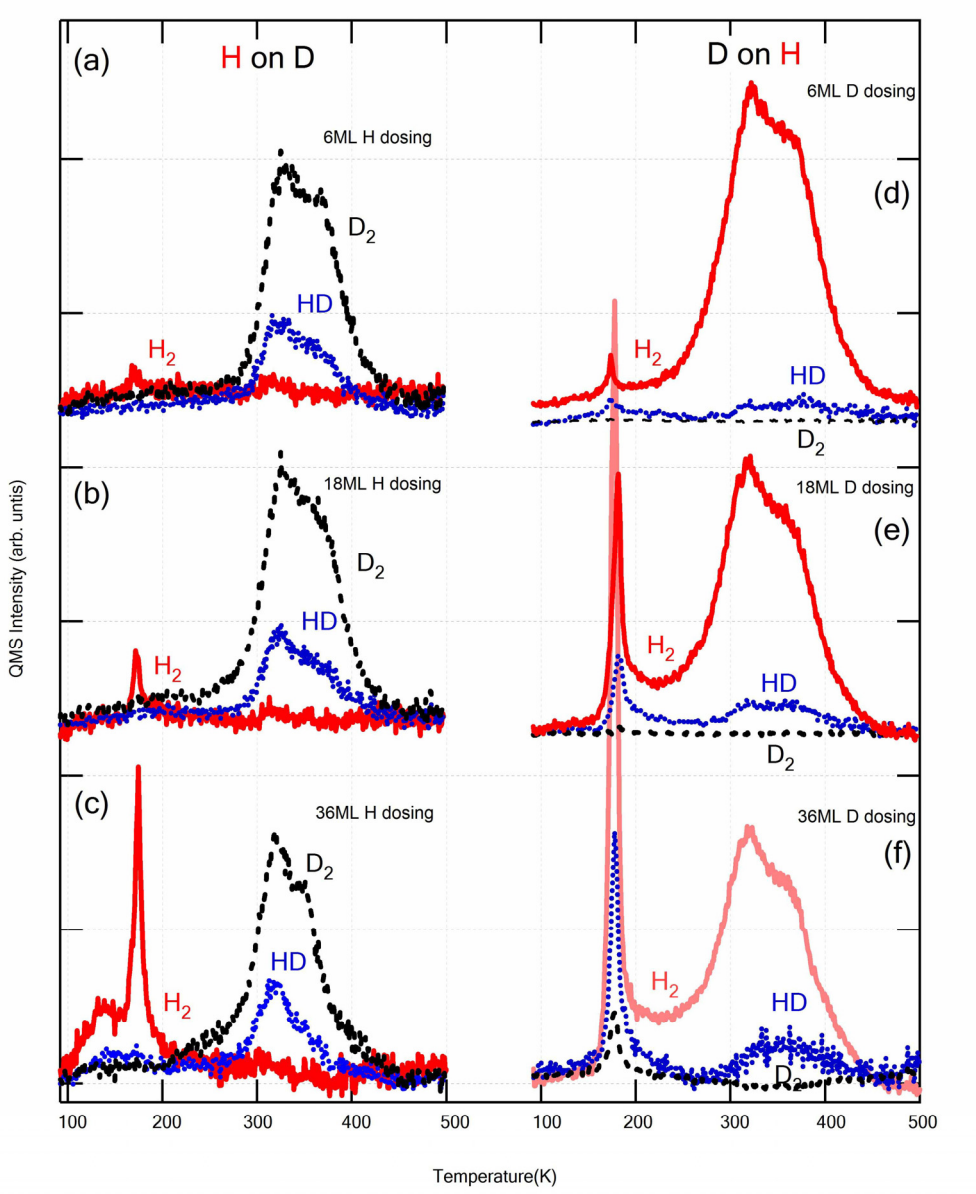

Figure 7.4 Six sets of TPD spectra of H_2, HD, and D_2 after two types of preparations. See text for detail.

Several features in figure 7.4 deserve attention. First, the rate at which desorption features in the low temperature regime appear varies with the order of employed isotopes. A surface covered initially by deuterium (7.4a-c) does not develop low temperature features nearly as fast as a hydrogen-covered surface (7.4d-f). Apparently, impinging $D_{(g)}$ on H_{surf} results in rapid build-up of interstitial species while this rate is much lower for $H_{(g)}$ impinging on D_{surf}.

Second, for $H_{(g)}$ impinging on D_{surf} (7.4a-c), only H_2 is observed in the low temperature desorption regime. The appearance of H_2 in the region of decomposition of a thin hydride film is not surprising as the surface was exposed to H atoms. However, it is noteworthy that the implanted H atoms apparently do not recombine with surface-bound D, which is plentiful judging from HD and D_2 desorption in the high temperature regime. For $D_{(g)}$ impinging on H_{surf} (7.4d-f), H_2 desorption in the low temperature regime dominates, but HD and D_2 are also observed to desorb at higher integrated D fluxes. Here, the appearance of H_2 in the low temperature regime is not obvious as the procedure to create the hydrogen terminated thin nickel hydride film involved only H_2 molecules and no H atoms.

Third, we notice in spectra where $H_{(g)}$ impinged on D_{surf}, that a significant amount of HD desorbs in the high temperature regime after the smallest integrated H flux (figure 7.4a). This amount of HD does not increase rapidly with larger H doses, while H_2 desorption in the low temperature regime increases significantly (figure 7.4b,c). Also, when comparing figure 7.4a to 7.4d, we notice that much less HD desorbs in the high temperature regime when the same amount of $D_{(g)}$ impinged on H_{surf}. In the series figure 7.4 d-f, the HD amount desorbing in the high temperature regime increases modestly with integrated D flux (figure 7.4d-f). However, even more noteworthy in these spectra is that increasing the dose of D atoms does significantly increase the amount of HD and D_2 appearing in the low temperature peak. To compare the amounts of H and D quantitatively, we have integrated the individual desorption features and, using the integral for the saturated H(D) Ni(111) surface as references, tabulated the desorbing amounts for various isotopes in table 7.1.

We note that the width of our low temperature desorption peak is much narrower than the width shown in TPD spectra for subsurface hydrogen obtained by other groups [12-14]. For example, the FWHM of the low temperature peak in figure 7.4.f is 13 K, while Ceyer

and co-workers reported approximately 50 K [13]. In chapter 6 we have suggested that this difference may be due to different preparation procedures for the thin nickel hydride layer.

Table 7.1
The list of coverages of all low temperature and high temperature peaks in figure 7.4.

dose H or D	H on D						D on H					
	Subsurface (ML)			Surface (ML)			Subsurface (ML)			Surface (ML)		
	H_2	HD	D_2	H_2	HD	D_2	H_2	HD	D_2	H_2	HD	D_2
6 ML	0.01	0	0	0	0.25	0.75	0.016	0.01	0	0.95	0.05	0
18 ML	0.025	0	0	0	0.27	0.72	0.12	0.05	0	0.9	0.1	0
36 ML	0.2	0	0	0	0.29	0.67	0.3	0.13	0.035	0.83	0.13	0.01

Finally, figure 7.5 shows two sets of TPD spectra for m/e=2 (bottom) and m/e=28 (top). In these experiments, CO is present in the chamber at low partial pressure of about ~ 5×10^{-9} mbar during exposure of the bare Ni(111) surface to atomic H below 90 K. In the H_2 desorption traces, we observe the expected desorption features in the low and high temperature regimes. In the experiment labeled "a", the exposure to atomic hydrogen was considerably higher than in the experiment labeled "b", leading to the equivalents of 4.5 and 1.5 ML of subsurface, respectively. In both CO TPD traces, desorption also occurs in a low and a high temperature regime. The desorption of CO in the low temperature regime strongly resembles the desorption of H_2 from the decomposition of nickel hydride thin layer and peaks at the same temperature. To our knowledge, such desorption of CO has not been previously observed. The high temperature CO desorption compares very well to previously published data [32,33] and to our own TPD studies of CO desorbing from the clean Ni(111) surface. Using the TPD trace for a saturated CO layer on Ni(111) as a

reference for the maximum coverage of 0.62 ML [33], we have quantified the total amount of CO desorbing in the experiments "a" and "b", and found that both reflect a nearly saturated CO layer. In experiment "b", 0.09 ML of CO desorbs in the low temperature regime, whereas the remaining CO desorbs in the high temperature regime. In the experiment "a", 0.15 ML CO desorbs below 200 K.

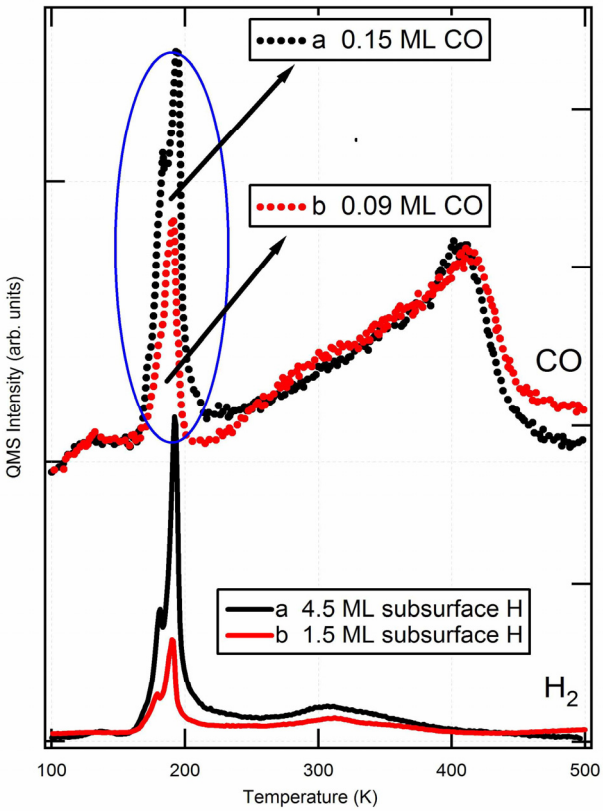

Figure 7.5 TPD spectra of m/e=2, and m/2=28, taken after impacting the bare Ni(111) surface to two different exposures of atomic H below 90 K with the presence of CO in the chamber. The numbers refer to the amounts of H and CO desorbed within the low temperature regime.

7.4 Discussions

We start the discussion with the established chemical reactions that may occur when a H(D) atom impinges on an D(H)-covered surface. The H(D) atom incident on an D(H)-covered

surface may simply reflect to the gas phase or abstract an adsorbed D_{surf}(H_{surf}) atom from the surface. This abstraction process is rreferred as the Eley-Rideal reaction:

$H_{(g)} + D_{surf} \rightarrow HD_{(g)} + *$ ("H on D",1a) and $D_{(g)} + H_{surf} \rightarrow HD_{(g)} + *$ ("D on H",1b)

This general chemical reaction may also occur through a "hot atom" mechanism [34]. A hot atom is an atom that has high translational energy. In "hot atom" mechanism, incident H(D) atoms move around on the surface as hot atoms until the excess energy is dissipated onto the surface and / or the adsorbed H(D) atoms. With the formation of $HD_{(g)}$, an empty site is created on the surface. This empty site can be filled by impacting H(D) atoms:

$H_{(g)} + * \rightarrow H_{surf}$ (2a) and $D_{(g)} + * \rightarrow D_{surf}$ (2b)

Such newly adsorbed H(D) atoms can consecutively be abstracted by the impacting H(D) atoms:

$H_{(g)} + H_{surf} \rightarrow H_{2(g)} + *$ (3a) and $D_{(g)} + D_{surf} \rightarrow D_{2(g)} + *$ (3b)

The impacting H(D) atoms may also, in parallel with the reaction 2, directly absorb into subsurface region via an empty surface site. The reaction can be expressed as:

$H_{(g)} + * \rightarrow H_{subs} + *$ (4a) and $D_{(g)} + * \rightarrow D_{subs} + *$ (4b)

Finally, impinging H(D) atoms may also lead to recombinative desorption of other atoms:

$H_{(g)} + D_{surf} + D_{surf} \rightarrow H_{surf} + D_{2(g)} + *$ (5a)

and $D_{(g)} + H_{surf} + H_{surf} \rightarrow D_{surf} + H_{2(g)} + *$ (5b)

Impacting H(D) atoms on an D(H)-covered surface can thus lead to creation of empty sites, exchange of D-H(H-D) on the surface, and absorption of H(D) in the subsurface in several parallel and consecutive reactions.

Now we consider the spectra shown in figures 7.4.d-f. As mentioned, in the experiments we only dosed molecular H_2 and atomic D. However, the H_2 TPD traces show a strong desorption feature around 180 K attributed previously to recombinative desorption of subsurface hydrogen atoms with surface-bound hydrogen atoms [13-15]. As at least half of the detected atoms in molecular H_2, HD, and D_2 observed in this temperature regime must originate from the subsurface region, subsurface H atoms must have been present after preparing the system in figures 7.4d-f. The TPD results therefore imply that exposing H-covered Ni(111) to atomic D leads to formation of H_{subs}. Apparently, in parallel with the previously mentioned reactions, reactions such as

$D_{(g)} + H_{surf} \rightarrow D_{surf} + H_{subs}$ (6) or $D_{(g)} + H_{surf} \rightarrow D_{(g)} + H_{subs}$ (7)
must also be considered.

There are two mechanisms possible for the dynamics of reactions (6) and (7). At first the surface species can be driven to a subsurface site by direct momentum transfer from an impacting atom: collision induced absorption (CIA). In addition, processes at the surface, for instance induced by hot D(H) atoms could drive atoms to a subsurface site. For instance, Ciobica *et al.* have demonstrated in DFT calculations for the H-Ru(0001) system, that a supersaturated H-overlayer is metastable and can lead to occupation of subsurface sites [35,36]. Ultimately, the supersaturated surface will relax by the ejection of molecular hydrogen to yield the saturated surface again. As we observe a very strong isotope effect in the absorption of H and D atoms and it is not clear how the relaxation of a supersaturated surface would lead to such an isotope effect, we infer that CIA is the most likely explanation of our observations.

The phenomenon of absorption through impacting species from the gas phase has been observed before for exposure of H-covered Ni(111) to various accelerated noble gas atoms from a supersonic expansion [10,37] and was referred to as CIA. The CIA process was also examined by a theoretical study, in which collisions of He, Ne, Ar, Kr, and Xe with the H-covered Ni(111) surface were simulated by molecular dynamics [38]. The simulation results show that direct collisions of noble gas atoms with adsorbed H atoms form the dominant mechanism of collision-induced absorption. The authors also suggested that there are two paths for efficient collision-induced absorption: the heavy collider path and the light collider path. The heavy collider path relies on decreasing the barrier to absorption by coupling of the impact energy to the substrate's phonons. This path dominates for collision of a heavy noble gas, e.g. Xe. The light collider path relies on transferring sufficient energy directly to an H atom so that it can overcome the energy barrier to absorb. This path dominates for collision of a light noble gas, e.g. He.

We return to considering the two types of collisions of atomic $D_{(g)}$ atoms with adsorbed H_{surf} atoms as expressed in reactions (6) and (7). Because of the small mass difference, energy transfer from impacting $D_{(g)}$ atoms to H_{surf} is even more efficient than for impacting He. Thus the light collider path is most likely to dominate this collision-induced absorption

process. In this case the required minimum energy transferred from $D_{(g)}$ to H_{surf} to absorb H_{surf} into a subsurface site equals the energy barrier for H between surface and subsurface sites. Various experimental and theoretical studies indicate that this value is close to 1 eV (100 kJ/mol) (see figure 1.1) [6,10,17,24,25]. This minimum transferred energy may be provided only by kinetic energy of $D_{(g)}$ atoms. When reaction (6) occurs, the impacting D atoms adsorb as D_{surf} after collision, so both kinetic energy of $D_{(g)}$ and potential energy released during adsorption can be transferred to H_{surf} atoms. However when reaction (7) occurs, the impacting D atoms are reflected back to gas phase after collision, so the transferred energy must only be provided by kinetic energy of $D_{(g)}$. For reaction (7), we prefer to present the simplest estimation here, in which we assume the energy transfer from $D_{(g)}$ to H_{surf} is nearly 100% and the kinetic energy of $D_{(g)}$ after collision is nearly zero. In this assumption, only the $D_{(g)}$ atoms with kinetic energy larger than 100 kJ/mol are able to "hammer" H_{surf} into subsurface sites. The velocity of such D(g) atoms should be larger than 1×10^4 m/s. According to the kinetic theory of gases, the fraction of $D_{(g)}$ atoms that have velocity larger than 1×10^4 m/s is obtained by evaluating the integral:

$$P = \int_{10^4}^{\infty} f(s)ds$$

in which $f(s)$ is the Maxwell distribution of speeds and is expressed as:

$$f(s) = 4\pi\left(\frac{M}{2\pi RT}\right)^{\frac{3}{2}} s^2 e^{-Ms^2/2RT}$$

As the cracking temperature of our H-Flux is 1800 K, such a rough estimate leads to $P \approx 0.01$ indicating that approximately 1% of $D_{(g)}$ atoms have a high enough velocity to "hammer" H_{surf} into subsurface sites. As the collision cross-section is likely small, the actual fraction of $D_{(g)}$ atoms that "hammer" H_{surf} into subsurface sites must be much smaller than 1% of the impinging flux. Comparing the fluxes in figures 7.4d-f, and the amount of H_{surf} having being "hammered" into subsurface sites in table 7.1 (0.016, 0.12, and 0.3 ML) it seems unlikely that reaction (7) dominates the creation of subsurface H atoms.

The transferred energy can also be provided by combination of kinetic energy and potential energy of $D_{(g)}$. When reaction (6) occurs, the impacting D atoms adsorb as D_{surf} after collision, so both kinetic energy of $D_{(g)}$ and potential energy released during adsorption can be transferred to H_{surf} atoms. The potential energy of a single D atom equals

the dissociation energy of ½ $D_{2(g)}$ plus the adsorption energy of a D atom on Ni(111). The dissociation energy of ½ $D_{2(g)}$ has been reported as 217 kJ/mol [39]. The adsorption energy of a H atom on Ni(111) is 46 kJ/mol. For a D atom, a minor isotope effect will change the adsorption energy. In the harmonic approximation, the difference in zero-point energies of H and D equals half of the difference between excitation frequencies, which are measured by HREELS at 141 and 100 meV for H and D, respectively, as shown in figure 7.1. Thus the zero-point energy of H is approximately 2 kJ/mol higher than D, which gives 48 kJ/mol for the adsorption energy of D. Therefore, for reaction (6), the total potential energy that may assist in CIA is 265 kJ/mol. For kinetic energy, we noted that the mean kinetic energy of $D_{(g)}$ equals $\frac{1}{2}Mc^2$, in which c is the root mean square speed of $D_{(g)}$ atoms at 1800 K. This root mean square speed is obtained by:

$$c = \left(\frac{3RT}{M} \right)^{\frac{1}{2}}$$

At 1800 K, the mean kinetic energy is 22 kJ/mol. Thus the combination of potential energy and average kinetic energy is 287 kJ/mol. This amount of energy is much larger than the energy barrier of ~100 kJ/mol for H between surface and subsurface sites. If the energy transfer efficiency from $D_{(g)}$ to H_{surf} is more than 35%, then H_{surf} can be very easily "hammered" into the subsurface site by CIA as reflected in reaction (6). A comparable study of the collision of $H_{(g)}(D_{(g)})$ with adsorbed D(H) on Pt(111) reported an energy transfer efficiency close to 50% [40]. As it does not seem unreasonable to expect a similar value for Ni(111), we conclude that reaction (6) best describes the CIA process that creates H_{subs}.

In the above discussion we have assumed that all potential energy due to the deep chemisorption well can be made available as kinetic energy to the impinging D atoms. Whether this is the case depends on the actual potential energy surface (PES). Although various theoretical studies have addressed H_{subs} + H_{surf} for Ni(111), dynamics studies performed for $H_{(g)}$ + H_{surf} on generic metal surfaces [41] and in particular on Ni(100) yield the best insight [42]. Here, attractive interaction between the gas phase H atom and H atom at the surface result in strong acceleration of the incoming H atom. Depending on the surface site for Ni(100) the acceleration is on the order of 1-2 eV. As the PES for Ni(111) is

likely comparable to that of Ni(100), we expect that CIA according to reaction (6) is likely the origin of absorbed H atoms in experiments of "D-on-H".

Based on absorption versus flux and the area of the (1×1)-H/Ni(111) unit cell we can estimate the CIA cross-section for H atoms in "D on H" experiments. As was mentioned before, table 7.1 shows that when we expose 18 and 36 ML $D_{(g)}$ on H-covered Ni(111), approximately 1% of $D_{(g)}$ atoms "hammer" H_{surf} into the subsurface sites. In combination, this value and the area of the (1×1)-H/Ni(111) unit cell yield a CIA cross-section for "D on H" of ~0.06Å^2. This is a very reasonable value considering the theoretical study of Tully *et al.* [38]. They reported a CIA cross-section of 0.04 Å^2 for impinging He atoms with 4.56 eV kinetic energy on H/Ni(111). It is noteworthy that these authors also suggest that the cross-section should increase with decreasing mass of the light collider.

For large D doses, D_2 desorption at 180 K starts appearing as shown in figure 7.4.f. This indicates that reactions:

$$D_{(g)} + * \rightarrow D_{subs} + * \quad (4b) \qquad \text{or} \qquad D_{(g)} + D_{surf} \rightarrow D_{surf} + D_{subs} \quad (8)$$

also take place when exposing the surface to atomic $D_{(g)}$ atoms. However, we can not distinguish or quantify these two reactions in the present study.

On the other hand, for "H on D", as shown in figures 7.2a-c, no desorption peaks resulting from the presence of subsurface deuterium (HD or D_2) are observed. This indicates that $H_{(g)}$ atoms do not "hammer" surface-bound D atoms into subsurface sites to a measurable extent at the conditions employed here. Therefore, the reactions

$$H_{(g)} + D_{surf} \rightarrow H_{surf} + D_{subs} \quad (9) \qquad \text{or} \qquad H_{(g)} + D_{surf} \rightarrow H_{(g)} + D_{subs} \quad (10)$$

which are the equivalent of the reactions that in the consecutive TPD experiments lead to H_2 desorption near 180 K in figures 7.4d-f, are not of significance in figures 7.4a-c. This also implies that the CIA cross-section for "H on D" must be much smaller than for "D on H". Kinetic energy transfer has been suggested to be similar for "H on D" and "D on H" resulting in similar Eley-Rideal cross-sections for "D on H" and "H on D" on Cu(111) [43]. The Eley-Rideal mechanism was proposed in 1938 by D. D. Eley and E. K. Rideal. In this mechanism, only one of the reactants adsorbs while the other reacts with it directly from the gas phase, without adsorbing. The Eley-Rideal cross section represents the surface area for this reaction to occur. Similarly, for Eley-Rideal studies on Ni(100), no large isotopic

effects were observed in any of the possible elementary reactions [42,44]. However, the authors state that they find that $D_{(g)}$ has a larger tendency to perturb H_{surf} than in the reverse case, in line with experimental observations of ER and HA reactions. Note that in this study CIA is not studied, although its occurrence is mentioned without detailed discussion [42]. Although the zero-point energy of H and D may influence the cross-sections, the energy difference is very small and should not result in significant changes [38]. We are left with two suggestions that may explain why absorption of D is not observed when using H as the 'hammer'. The first is the effect caused by coupling of the kinetic energy of impacting H(D) atoms and electronic friction prior to impact. An incoming particle towards the surface will experience an energy loss due to collision with and excitation of electrons. In a simple approximation, it can be described as a friction force acting on this particle to slow down its motion. Such friction force is also named as electronic friction. Because of a higher speed, $H_{(g)}$ experience more electronic friction prior to collision with D_{surf} than for the reverse case. $H_{(g)}$ may lose so much kinetic energy that it can not transfer enough energy to D_{surf} for CIA. The previously mentioned studies of energy loss in H(D) collision with D(H)-covered Ni(100) indicate that the average energy loss is in the order of 0.15 eV [44], which was supported by an independent theoretical study [45]. The second reason is the effect of coupling between the H_{surf}(D_{surf}) absorption dynamics and electronic friction in the substrate after collision. It has been shown that the heavier isotope D should be less affected by substrate electronic friction compared to H by Kindt *et al.* [38], resulting in more D atoms 'popping back out' after internal collisions in the subsurface cavity. Baer and coworkers include electronic friction in diffusion studies of H between surface and subsurface sites for Ni(111) and emphasize its importance in trapping the entering H atom [24]. In our experiments, such coupling effects may be the major contributor of large differences between CIA cross-sections for "H on D" and "D on H".

Upon further consideration of the H_2 formed at ~180 K in figure 7.4.a-c, we find two other noteworthy observations. First, we only observe H_2 desorption in the low temperature regime and no HD. Apparently, resurfacing H atoms do not recombine with surface-bound D even though surface-bound D atoms are the dominant species on the surface. The latter can be judged from HD and D_2 desorption in the high temperature regime. The observation

that we only find the H_2 isotope desorbing at 180 K indicates that H_{subs} formation goes in parallel with 'capping' the surface in the vicinity efficiently with H_{surf} and thus creating patches where only H is present both in the subsurface region and surface region. Recall that in our experiments we dose the original isotope molecularly after exposure to the other isotope as atoms. Had H_{subs} been created with many empty surface sites left over in the vicinity, than D_2 dissociative adsorption afterward would have resulted in HD desorption at 180 K.

The second noteworthy observation is that the absorption of H versus total H flux is initially slow but increases with exposure (see table 7.1). While dosing 6 ML H only leads to 0.01 ML H_2 desorbing at the low temperature regime, dosing 18 and 36 ML leads to 0.025 and 0.2 ML H_2 respectively. We explain the combination of this observation with the previous through a mechanism that combines reactions (1a) with consecutively (2a) and (4a). Here, an efficient CIA process of "H on H" may contribute as well. This combination of reactions yields the apparent autocatalytic effect, as 'H-isotope only reactions' can start as soon as some surface-bound D has been removed through the abstraction reaction (1a). The result of the "H-isotope only reactions" may lead to localized formation of subsurface H in patches (and thus sole H_2 desorption at 180 K) only when the rate of the consecutive reactions ((2a), (4a) and CIA of "H on H") far exceeds the rate of D-abstraction (1a). As the total amount of HD and D_2 desorbing in the high temperature regime does not increase rapidly with total H flux, this indeed seems to be the case. In addition, for the consecutive reactions, those leading to formation of empty sites are likely of less importance than those not leading to additional empty sites. For this reason it seems that reaction (2a), followed by "H on H" CIA dominates the process that induces formation of a local patch of NiH_x. In summary, as the distribution of subsurface H can not be uniform (it would have resulted in HD formation) our procedure for absorption of subsurface H in Ni(111) at 85 K must have lead to formation of patches of nickel hydride (NiH_x) in between a fairly pristine (1x1)-D/Ni(111) surface. "H on H" collision induced absorption likely played a dominant role in creation of these patches.

The results of CO experiments, as shown in figure 7.5 support our localized NiH_x hypothesis. Figure 7.5 shows that desorption of 1.5 ML subsurface H induces desorption of

0.09 ML CO at the same temperature, whereas desorption of 4.5 ML subsurface H induces desorption of 0.15 ML CO. Thus, when the amount of subsurface H increases three times, the amount of CO desorption only increases 60% in the temperature regime where subsurface H is removed. If the distribution of subsurface H were uniform, one would expect that the induced CO desorption at 180 K also increases approximately three times. However, if the formation of H_{subs} is localized as NiH_x with a capping layer of $CO_{(ads)}$, increasing of the concentration of H_{subs} (i.e. increasing x locally) does not require a proportional increase of CO desorption. Therefore, the induced CO desorption at 180 K is in agreement with our hypothesis that the formation of subsurface H is localized.

Another interesting point that we would like to note in these experiments is that the energy requirement for CO desorption is significantly larger than the energy released from a resurfacing H atom. A single resurfacing H atom has an excess energy on the order of 0.6 eV(~58 kJ/mol) to ~1 eV [15,16,24,46], while the adsorption energy of a single CO molecule at the saturation coverage and 85 K is ~1.5 eV(~145 kJ/mol) [33]. Previous studies reported that the adsorption energy of CO is not significantly affected when H is co-adsorbed on Ni(111) [47,48]. Thus, the desorption of a CO molecule at such low temperature cannot result from an individual resurfacing H atom. It seems more likely that CO desorption is due to the energy released in a phase transition of a local patch of NiH_x to (H-terminated) Ni(111). We suggest that the released energy from the phase transition leads to local heating of the surface and CO desorption.

The variation of the HREELS elastic peak intensity, as shown in figure 7.3, is also in line with our hypothesis that formation of subsurface H is localized. As was mentioned before, this variation is due to the surface corrugation at various conditions. In chapter 6, we concluded that the absorption of subsurface H in Ni(111) induces upward relaxation of surface nickel atoms. For a uniform distribution of subsurface H, one would expect that the surface is atomically smooth again when the subsurface H coverage is close to unity, e.g. 1 ML or 2 ML. However we observe that corrugation remains when the subsurface H coverage is ~ 1ML, as the HREELS elastic peak intensity drops as shown for a slightly lower subsurface concentration in figure 7.3. This observation therefore supports the suggestion regarding local formation of subsurface H in Ni(111) at 85 K. The return of the

reflectivity after annealing at 220 K, at which point all subsurface H has desorbed, indicates that in the patches of NiH_x, the Ni atoms only bulge upward. Local expansion of the nickel lattice by H absorption has also been reported in various theoretical studies [6,7,17]. Significant irreversible Ni atom transports along the surface would lead to surface roughening that would be visible through the distortion of the surface desorption features of H_2 between 300 and 400 K and a lowered final reflectivity of the elastically scattered intensity of the HREEL primary electron beam. This upward relaxation of certain patches may be difficult to detect or even invisible to LEED measurements, as the LEED image mostly reflects the structure of the (hydrogen of deuterium terminated) Ni(111) surface. For Pd(111), upward relaxation induced by absorption of H atoms has been shown using STM [49].

Finally, we note that our results also shed light on the recombinative desorption mechanism of subsurface hydrogen. In figure 7.4d-f, H_{surf} atoms are "hammered" into the subsurface sites by impacting $D_{(g)}$ atoms that stick to the surface after collision. In this case, each interstitial H atom at the octahedral subsurface site is accompanied by a surface-bound D atom right on top of it. Here, the distribution of subsurface hydrogen is expected to be fairly uniform. Now we consider the direct and indirect recombination mechanisms that may follow during the TPD ramp. In the direct recombination mechanism, a H atom directly attacks from underneath a surface-bound D atom and recombines with that D atom to form $HD_{(g)}$. This reaction is a single step and should result in HD formation in the low temperature regime. However, in figure 7.4d-f, H_2 dominates the low temperature desorption, while HD formation occurs as a minority pathway. Therefore, our data suggest that direct recombination is not dominant and the indirect recombination mechanism seems more favorable. In indirect recombination, subsurface H atoms resurface in adjacent hcp 3-fold hollow sites. For a resurfacing H atom that originally was "hammered" into subsurface by a D atom, it finds itself between two H atoms and a D atom in the adjacent fcc 3-fold hollow site. In this case, the ratio of two desorption products H_2 and HD is expected to be approximately 2:1. Table 7.1 shows that the ratios of H_2 and HD desorbing at the low temperature regime for three different $D_{(g)}$ dosing roughly reflect such a ratio. Therefore, our data supports the indirect recombination mechanism for the recombinative desorption

of subsurface hydrogen. This indirect mechanism is also favored by several experimental and theoretical studies [15, 16, 24, 25].

7.5 Conclusion

We have used TPD in combination with HREELS to study the interaction of atomic H and D with D or H-pre-covered Ni(111). Our results show that atomic D atoms can "hammer" surface-bound H into the subsurface sites, whereas atomic H does not "hammer" surface-bound D into the subsurface sites. The large difference in CIA cross-section for the two isotopes has various consequences. Experiments using "D on H" leads mostly to creation of H_{subs} through CIA, while consecutive TPD results indicate that resurfacing H atoms recombinatively desorb with surface-bound species in an indirect pathway. The CIA process dominates possible parallel reactions and has a cross-section of $0.06\,Å^2$. Experiments using "H on D" lead to formation of patches of NiH_x in an otherwise undisturbed D-covered Ni(111) surface. Here, CIA of "H on D" is absent and NiH_x patches are created by initial removal of some D_{surf} atoms, followed by more rapid H absorption processes. Here, CIA of "H on H" seems important and overtakes Eley-Rideal and other parallel reactions. CO desorption traces and surface roughness probed using the elastically scattered intensity of an electron beam suggest that that NiH_x patches bulge upward relative to the remaining flat hydrogen or deuterium-covered Ni(111) surface. Decomposition of the NiH_x patches releases enough energy to desorb co-adsorbed CO.

Finally, our observations that σ_{CIA}(D on H) >> σ_{CIA}(H on D) causes second thoughts about previously reported differences in Eley-Rideal cross-sections observed, for example, for "D on H" and "H on D" on Pt surfaces [50]. It is noteworthy that absorption of hydrogen in the first layer underneath the Pt(111) surface has recently been predicted from theoretical studies [51]. Therefore, for "D on H" the light collider CIA process may affect such studies on Pt surfaces. While for "D on H" two parallel reactions could occur (abstraction through Eley-Rideal or hot atom mechanisms and the light collider CIA), for "H on D" only abstraction reactions are likely. Thus, the Eley-Rideal cross-section for "H on D" may appear larger than for "D on H" due to a competing reaction in the latter case.

7.6 Reference

[1] L. Schlapbach, and A. Züttel, *Nature*, 2001,**414**, 353.

[2] B. Bogdanovic, and M. Schwickardi, *Appl. Phys. A,* **2001**, 72, 221.

[3] B. Sakintuna, F. L-Darkrim, and M. Hirscher, *Int. J. Hydrogen Energy,* **2007**, 32, 1121.

[4] M. V. C. Sastri, B. Viswanathan, and S. S. Murthy, *Metal Hydrides-Fundamentals and Applications*, 1998, Narosa Publishing House, New Delhi.

[5] G. Alefeld, and J. Völkl, *Hydrogen in Metals 116-Application-Oriented Properties*, 1978, Springer-Verlag, Berlin.

[6] B. Bhatia, and D. S. Sholl, *J. Chem. Phys.*, 2005, **122**, 204707.

[7] G. Kresse, and J. Hafner, *Surf. Sci.*, 2000, **459**, 287.

[8] K. Christmann, O. Schober, G. Ertl and M. Neumann, *J. Chem. Phys.*, 1974, **60**, 4528.

[9] A. Winkler, and K. D. Rendulic, *Surf. Sci.*, 1982, **118**, 19.

[10] S. T. Ceyer, *Acc. Chem. Res.,* 2001, **34**, 737.

[11] K.-Ah. Son, M. Marvikakis, and J. L. Gland, *J. Phys. Chem.*, 1995, **99**, 6270.

[12] I. Chorkendorff, J. N. Russell, and J. T. Yates, *Surf. Sci.*, 1987, **182**, 375.

[13] A. D. Johnson, K. J. Maynard, S. P. Daley, Q. Y. Yang, and S. T. Ceyer, *Phys. Rev. Lett.*, 1991, **67**, 927.

[14] H. Premm, H. Pölzl, and A. Winkler, *Surf. Sci. Lett.,* 1998, **401**, L444.

[15] S. Wright, J. F. Skelly, and A. Hodgson, *Faraday Discuss.,* 2000, **117,** 133.

[16] S. Wright, J. F. Skelly, and A. Hodgson, *Chem. Phys. Lett.*, 2002, **364,** 522.

[17] J. Greeley, and M. Mavrikakis, *Surf. Sci.*, 2003, **540**, 215.

[18] J. Eckert, C. F. Majkzrak, L. Passell, and W. B. Daniels, *Phys. Rev. B*, 1984, **29**, 3700.

[19] A. T. Capitano, K.-Ah. Son, and J. L. Gland, *J. Phys. Chem. B*. 1999, **103**, 2223.

[20] A. T. Capitano, and J. L. Gland, *Langmuir*, 1998, **14**, 1345.

[21] A. D. Johnson, S. P. Daley, A. L. Utz, and S. T. Ceyer, *Science*, 1992, **257**, 223.

[22] D. R. Killelea, V. L. Campbell, N. S. Shumann, and A.L. Utz, *Science*, 2008, **319**, 790.

[23] W. Van Willigen, *Phys. Letters,* 1968, **28A**,80.

[24] R. Baer, Y. Zeiri, and R. Kosloff, *Phys. Rev. B*, 1997, **55**, 10952.

[25] G. Henkelman, A. Arnaldsson, and H. Jónsson. *J. Chem. Phys.*, 2006, **124**, 044706.

[26] V. Ledentu, W. Dong, and P. Sautet, *J. Am. Chem. Soc.*, 2000, **122**, 1796.

[27] A. Michaelides, P. Hu, and A. Alavi, *J. Chem. Phys.*, 1999, **111**, 1343.

[28] H. Yanagita, J. Sakai, T. Aruga, N. Takagi, and M. Nishijima, *Phys. Rev. B*, 1997, **56**, 14952.

[29] L. J. Richter, B. A. Gurney, and W. Ho, *J. Chem. Phys.*, 1987, **86**, 477.

[30] G. Pauer, A. Eichler, M. Sock, M. G. Ramsey, F. Netzer, and A. Winkler, *J. Chem. Phys.*, 2003, **119**, 5253.

[31] G. Eibl, G. Lackner, and A. Winkler, *J. Vac. Sci. Technol.* A, 1998, **16**, 2979.

[32] F. P. Netzer, and T. E. Madey, *J. Chem. Phys.*, 1982, **76**, 710.

[33] G. Held, J. Schuler, W. Sklarek, and H.-P. Steinrück, *Surf. Sci.*, 1998, **398**, 154.

[34] C. T. Rettner, and D. J. Auerbach, *J. Chem. Phys.*, 1996, **104**, 2732.

[35] I. M. Ciobica, A. W. Kleyn, and R. A. Van Santen, *J. Phys. Chem.* B, 2003, **107** 164.

[36] B. Riedmüller, I. M. Ciobîcã, D. C. Papageorgopoulos, F. Frechard, B. Berenbak, A. W. Kleyn, and R. A. van Santen, *J. Chem. Phys.,* 2001, **115**, 5244.

[37] J. K. Maynard, A. D. Johnson, S. P. Daley, and S. T. Ceyer, *Faraday Discuss.,* 1991, **91,** 437.

[38] J. Kindt, and J. C. Tully, *J. Chem. Phys.*, 1999, **111**, 11060.

[39] A. Balakrishnan, and B. P. Stoicheff, J. Mol. Spectrosc, 1992, **156**, 517.

[40] J.-Y. Kim, and J. Lee, *Phys. Rev. Lett.*, 1999, **82**, 1325.

[41] B. Jackson, and D. Lemoine, *J. Chem. Phys.*, 2001, **114**, 474.

[42] Z. B. Guvenc, X. W. Sha, and B. Jackson, *J. Chem. Phys.*, 2001, **115**, 9018.

[43] D. V. Shalashilin, B. Jackson, and M. Persson, *J. Chem. Phys.*, 1999, **110**, 11038.

[44] Z. B. Guvenc, X. W. Sha, and B. Jackson, *J. Phys. Chem. B*. 2002, **106**, 8342.

[45] R. Martinazzo, S. Assoni, G. Marinoni, and G. F. Tantardini, *J. Chem. Phys.*, 2004, **120**, 8761.

[46] X. W. Sha, and B. Jackson, *Chem. Phys. Lett.*, 2002, **357,** 389.

[47] G. E. Mitchell, J. L. Gland, and J. M. White, *Surf. Sci.*, 1983, **559**, 167.

[48] W. Braun, H.-P. Steinrück, and G. Held, *Surf. Sci.*, 2005, **574**, 193.

[49] E. C. H. Sykes, L. C. F-Torres, S. U. Nanayakkara, B. A. Mantooth, R. M. Nevin, and P. S. Weiss, *PNAS*, 2005, **102**, 17907.

[50] H. Busse, M. R. Voss, D. Jerdev, B. E. Koel, and M. T. Paffett, *Surf. Sci.*, 2001, **490**, 133.

[51] P. Legare, *Surf. Sci.*, 2004, **559**, 169.

Summary

As nickel and platinum are in the same group of the periodic table, the Ni(111) and Pt(111) surfaces may be expected to show similar interaction with water and hydrogen. However in this thesis, we show these interactions for Ni(111) are quite different from those of Pt(111). Moreover, our results show that the Ni(111) surface is a unique surface with regards to its chemistry of water and hydrogen.

The experiments described in this thesis were carried out under ultra-high vacuum (UHV) conditions. We used a nickel single crystal surface, Ni(111), as a substrate in our experiments. Two main techniques employed in our study are temperature-programmed desorption (TPD) and high resolution electron energy loss spectroscopy (HREELS).

The interaction of H_2O and D_2O with a bare and hydrogen-saturated Ni(111) surface is studied and compared to Pt(111) in chapter 3. We reported that hydrogen, atomically bound to Ni(111), affects the interaction between this metal surface and water significantly. Whereas a hydrogen-bonded network of water multilayers shows isotopic scrambling without water dissociation at 85 K on the surface, the H-Ni bond is too strong to allow isotope exchange with co-adsorbed water. We expect that the same H-Ni bond strength prevents formation of H_3O^+ or similar species, which have been suggested for Pt(111). In contrast, our data actually suggest that saturating the Ni(111) surface with hydrogen makes the surface hydrophobic, and that multilayered islands of water molecules form at submonolayer coverages.

In chapter 4 we described the surface coverage dependence of the co-adsorption of D and D_2O on the Ni(111) surface. This co-adsorption behavior on Ni(111) shows big differences compared to Pt(111). We show how pre-covering the surface with various amounts of D under UHV conditions affects adsorption and desorption of D_2O. We suggest that the effects of co-adsorption are strongly dependent on D-coverage. In the deuterium pre-coverage range of 0 - 0.3 ML, adsorption of deuterium leaves a fraction of the available surface area bare for D_2O adsorption, which shows no significant changes compared to adsorption on the bare surface. Our data indicates phase segregation of hydrogen and water into islands. At low post-coverages, D_2O forms a two-phase system on the remaining bare surface that shows zero-order desorption kinetics. This two phase system likely consists of

a two-dimensional (2D) solid phase of extended islands of hexamer rings and a 2D water gas phase. Increasing the water post-dose leads at first to 'freezing' of the 2D gas and is followed by formation of ordered, multilayered water islands in between the deuterium islands. For deuterium pre-coverages between 0.3 and 0.5 ML, our data may be interpreted that the water hexamer ring structure, $(D_2O)_6$, required for formation of an ordered multilayer, no longer forms. Instead, more disordered linear and branched chains of water molecules grow in between the extended, hydrophobic deuterium islands. These deuterium islands have a D-atom density in agreement with a (2x2)-2D structure. The disordered water structures adsorbed in between form nucleation sites for growth of 3D water structures, which (partially) spill over the deuterium islands. Loss of regular lateral hydrogen bonding and weakened interaction with the substrate reduces the binding energy of water significantly in this regime and results in lowering of the desorption temperature. At deuterium pre-coverages greater than 0.5 ML, the saturated (2x2)-2D structure mixes with (1x1)-1D patches. The mixed structures are also hydrophobic. On such surfaces, submonolayer doses of water lead to formation of 3D water structures well before wetting the entire hydrogen-covered surface. From the literatures, we find that the Pt(111) surface has not been studied in the same detail for co-adsorption of hydrogen and water. However, the few studies that have investigated this system show no evidence for such complex behavior as we observe on Ni(111).

The identification and characterization of hydroxyl (OH) on the Ni(111) surface is described in chapter 5. We find clear evidence of stretching, bending and translational modes in HREEL spectra that differ significantly from modes observed for H_2O and O on Ni(111). Hydroxyl may be produced from water using two different methods. Annealing of water co-adsorbed with atomic oxygen at 85 K to above 170 K leads to creation of OH with simultaneous desorption of excess water. Pure water layers treated in the same fashion show no dissociation. However, exposure of pure water to 20 eV electrons below 120 K produces OH in the presence of adsorbed H_2O. In combination with temperature-programmed desorption studies, we show that OH groups recombine between 180 and 240 K to form O and immediately desorbing H_2O. The lack of influence of co-adsorbed H_2O at 85 K on hydroxyl's O-H stretching mode indicates that OH does not participate in a

hydrogen-bond network. This is in agreement with the theoretical prediction of an almost vertically bound OH on Ni(111). In comparison to Pt(111), again we observe very different behavior as OH, formed by similar methods, is incorporated in hydrogen-bonded networks of OH and H_2O on Pt(111).

The second part of this thesis starts in chapter 6 with the investigation of the interaction of atomic hydrogen with bare Ni(111). We have demonstrated that dosing atomic hydrogen on Ni(111) at a surface temperature below 90 K leads to molecular hydrogen bound to an ultrathin nickel hydride layer. We suggest that the adsorption of molecular hydrogen is due to reversible roughening associated with formation of the NiH_x layer. However, the roughening is modest and likely consists only of relaxation of nickel atoms normal to the surface. The newly found molecular state of hydrogen persists to 125 K and may present an interesting case to study H_2 reaction and scattering dynamics. Atomic adsorption of hydrogen finds no undisputed equivalent for Pt(111), and the absorption behavior on Pd is also quite different due its exothermicity. For Pd however, the molecularly-bound state and upward surface relaxation have been observed.

In the last chapter of this thesis, chapter 7, the interaction of atomic hydrogen and deuterium with D or H-pre-covered Ni(111) is studied. Our results show a large isotopic effect when reversing the order of the isotopes used in preparing a thin nickel hydride (deuteride) layer, capped by a (nearly-)saturated surface hydrogen (deuterium) layer. Our results also show that atomic D atoms can “hammer” surface-bound H into the subsurface sites, whereas atomic H does not “hammer” surface-bound D into the subsurface sites. The large difference in CIA cross-section for the two isotopes has various consequences. CO desorption traces and surface roughness probed using the elastically scattered intensity of an electron beam suggest that that NiH_x patches bulge upward relative to the remaining flat hydrogen or deuterium-covered Ni(111) surface. Decomposition of the NiH_x patches releases enough energy to desorb co-adsorbed CO.

Samenvatting

Aangezien nikkel en platina in dezelfde groep van het periodiek systeem staan zou verwacht kunnen worden dat het Ni(111) en Pt(111) oppervlak een vergelijkbare interactie vertonen met water en waterstof. In dit proefschrift wordt echter aangetoond dat voor Ni(111) deze interacties significant anders zijn dan voor Pt(111). Bovendien laten onze resultaten zien dat het Ni(111) oppervlak uniek is als het gaat om water en waterstof chemie.

De experimenten die beschreven worden in dit proefschrift zijn uitgevoerd onder ultrahoog vacuüm (UHV) condities. We hebben een nikkel éénkristal, Ni(111), gebruikt als substraat bij onze experimenten. De twee belangrijkste technieken die hierbij gebruikt zijn zijn temperatuur geprogrammeerde desorptie (TPD) en hoge resolutie elektron energieverlies spectroscopie (HREELS).

De interactie van H_2O en D_2O met een kaal en een waterstofverzadigd Ni(111) oppervlak is bestudeerd in hoofdstuk 3. We laten zien dat waterstof de interactie tussen dit metaaloppervlak en water aanzienlijk beïnvloedt. De H-Ni binding is te sterk om isotoop uitwisseling met het gecoadsorbeerde water toe te laten. We verwachten dat dezelfde H-Ni bindingssterkte de vorming van H_3O^+ of een vergelijkbare soort, zoals voorgesteld voor Pt(111), verhindert. Daartegenover suggereert onze data juist dat het verzadigen van het Ni(111) oppervlak met waterstof het oppervlak hydrofoob maakt, waarbij meerlagige eilandjes van watermoleculen gevormd worden bij bedekkingsgraden van minder dan een monolaag.

In hoofdstuk 4 hebben we de bedekkingsgraad (θ) afhankelijkheid van de coadsorptie van D en D_2O op het Ni(111) oppervlak beschreven. We laten zien dat de effecten van coadsorptie sterk afhangen van de D-bedekkingsgraad. Onze data suggereert dat voor $0 < \theta_D < 0.3$ ML en lage θ_D D en D_2O in eilandjes segregeren en dat D_2O een twee fasen systeem in evenwicht vormt: een roostergas en een goed geordende 2D vaste stof. Het watergas “bevriest” als zijn ruimte beperkt wordt door het gepreadsorbeerde D. Als de totale hoeveelheid D en D_2O groter is dan de hoeveelheid die interactie met het metaal aan kan gaan, loopt het extra D_2O over op D-eilandjes waarbij meer ongeordende structuren

en/of multilagen gevormd worden. Wanneer θ_D tussen de 0.3 en 0.5 ML ligt, vormen D_2O clusters nucleatie plaatsen tussen D eilandjes voor de groei van ongeordende 3D structuren.

De identificatie en karakterisatie van hydroxyl (OH) op het Ni(111) oppervlak is beschreven in hoofdstuk 5. We vinden duidelijk bewijs voor strek- en buigvibraties en translatiebewegingen in HREEL spectra die significant verschillen van de vibraties en bewegingen die worden waargenomen voor H_2O en O op Ni(111). Hydroxyl kan op twee verschillende manieren van water gemaakt worden. Het gebrek aan invloed van gecoadsorbeerd H_2O op de O-H strekvibratie van hydroxyl bij 85 K geeft aan dat OH niet deelneemt aan een netwerk van waterstofbruggen. Opnieuw zien we significant ander gedrag dan op Pt(111) waar OH, dat op een vergelijkbare manier is gevormd, wordt geïncorporeerd in een netwerk van waterstofbruggen tussen OH en H_2O.

Het tweede gedeelte van dit proefschrift begint in hoofdstuk 6 met onderzoek naar de interactie tussen atomair waterstof en kaal Ni(111). We laten zien dat het doseren van atomair waterstof op Ni(111) bij oppervlakte temperaturen onder de 90 K leidt tot moleculair waterstof dat gebonden is aan een ultradunne nikkelhydride laag. We suggereren dat de adsorptie van moleculair waterstof veroorzaakt wordt door een reversibele verruwing van het oppervlak welke geassocieerd is met de vorming van de NiH_x laag. De verruwing is echter gering en bestaat waarschijnlijk alleen uit de relaxatie van nikkel atomen haaks op het oppervlak.

In het laatste hoofdstuk van dit proefschrift, hoofdstuk 7, is de interactie van atomair waterstof en deuterium met een met D of H voorbedekt Ni(111) oppervlak bestudeerd. Onze resultaten tonen een groot isotoop effect als de doseervolgorde van de isotopen wordt omgedraaid. Onze resultaten laten ook zien dat D-atomen oppervlaktegebonden H-atomen naar bindingsplaatsen onder het oppervlak kunnen “hameren”, terwijl H-atomen oppervlaktegebonden D-atomen niet onder het oppervlak “hameren”. CO desorptie spectra en de ruwheid van het oppervlak, bepaald door middel van de intensiteit van een elastisch verstrooide elektronen bundel, suggereren dat NiH_x plekjes opbollen ten opzichte van het overgebleven vlakke met waterstof of deuterium bedekte Ni(111) oppervlak.

List of publications

This thesis is based on the following publications:

Chapter 3

Junjun Shan, Jacques F. M. Aarts, Aart W. Kleyn, and Ludo B. F. Juurlink
The interaction of water with Ni(111) and H/Ni(111) studied by TPD and HREELS
Phys. Chem. Chem. Phys., 2008, **10**, 2227.

Chapter 4

Junjun Shan, Jacques F. M. Aarts, Aart W. Kleyn, and Ludo B. F. Juurlink
Co-adsorption of water and hydrogen on Ni(111)
Phys. Chem. Chem. Phys., 2008, **10**, 4994.

Chapter 5

Junjun Shan, Aart W. Kleyn, and Ludo B. F. Juurlink
Identification of Hydroxyl on Ni(111)
Chemphyschem., 2009, **10**, 275.

Chapter 6

Junjun Shan, Aart W. Kleyn, and Ludo B. F. Juurlink
Adsorption of molecular hydrogen on an ultrathin layer of Ni(111) hydride
Chem. Phys. Lett., 2009, **474**, 107.

Chapter 7

Junjun Shan, Aart W. Kleyn, and Ludo B. F. Juurlink
On the formation and decomposition of a thin NiH_x layer on Ni(111)
To be submitted.

In addition, the author has participated in the following articles:

Roberto Macovez, Michael R. C. Hunt, Junjun Shan, Andrea Goldoni, Thomas Pichler, Maddalena Pedio, Paolo Moras, Carla Castellarin-Cudia, Joachim Schiessling, Luc Venema, and Petra Rudolf
Metal-to-insulator transition in thin-film polymeric AC_{60}
New J. Phys., 2009, **11,** 023035.

Christine Hann, Junjun Shan, Irene M. N. Groot, Aart W. Kleyn, and Ludo B. F. Juurlink
Selective poisoning of active sites for D_2 dissociation on Pt
To be submitted

Junjun Shan, Christine Hann, Yin Liu, Otto T. Berg, and Ludo B. F. Juurlink
Employing a cylindrical single crystal to study step effects in gas-surface dynamics
In preparation

Curriculum Vitae

Junjun Shan was born in the city of Hangzhou, China, on September 21, 1979. After obtaining his bachelor degree and master degree in physics in 2002 and 2004, he decided to continue his education in chemistry. In September 2004, he started his chemistry study as a PhD student at the Leiden Institute of Chemistry under the supervision of Prof. Dr. Aart W. Kleyn and Dr. Ludo B. F. Juurlink in the Catalysis and Surface Chemistry group. This group is currently headed by Prof. Dr. Marc T. M. Koper. His studies focused the interaction of water and hydrogen with nickel surfaces. The results of these studies are described in this thesis. Several studies have been presented at a number of national and international scientific conferences. During his PhD study, Junjun supervised one bachelor student during a three-month research project, and taught several 1st and 2nd year practical courses.

Acknowledgements

At the end of this thesis I would like to say that this thesis would have not been possible without the help and encouragement of many people to whom I am very grateful.

Firstly, I would like to express my gratitude to Ludo Juurlink and Aart Kleyn for providing me the opportunity to study for a PhD degree in Leiden and for their continuous help and support. I would also like to thank Wim Roeterdink and Jacques Aarts for initiating me into the secrets of the UHV system and the high-resolution electron energy loss spectrometer.

I am very grateful to all other colleagues for the fantastic working atmosphere created in our group: Marc Koper, Ben Nieuwenhuys, Johan Bakker, Alex Yanson, Irene Groot, Christine Hahn, Janneke van der Niet, Klaas Jan Schouten, Aart Gieske, Andrea Gluhoi, Andrey Koverga, Dima Bashlakov, Francois Devred, Gonzalo García, José Dijkzeul, Matteo Duca, Para Rodríguez-Pérez, Steven Kleijn, Stanley Lai, and Thijs Hoogenboom.

I kept the last words for my family. I would like to thank my wife Haiyan Liu, and my parents for their love and total support during my study. I would also like to thank my little daughter Elaine Shan for the happiness that she gives to the whole family.

To those whom I forgot to mention, I beg that person's pardon in advance.